RADAR LAND CLUTTER MEASUREMENTS AT FREQUENCIES OF 9.5, 16, 35, AND 95 GHz

N. C. Currie, et al

Georgia Institute of Technology

Prepared for:

Frankford Arsenal

2 April 1975

TECHNICAL REPORT NO. 3

RADAR LAND CLUTTER MEASUREMENTS AT FREQUENCIES OF 8.5, 16, 35, and 95 GHz

EES/GIT PROJECT A-1486

Prepared for

UNITED STATES ARMY
FRANKFORD ARSENAL
PHILADELPHIA, PA. 19137
UNDER
CONTRACT DAAA 25-73-C-0256

By

N. C. Currie, F. B. Dyer, and R. D. Hayes

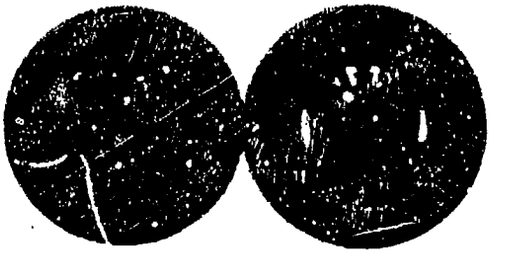

2 April 1975

ENGINEERING EXPERIMENT STATION
Georgia Institute of Technology
Atlanta, Georgia 30332

Unclassified

SECURITY CLASSIFICATION OF THIS PAGE (When Data Entered)

REPORT DOCUMENTATION PAGE		READ INSTRUCTIONS BEFORE COMPLETING FORM
1. REPORT NUMBER	2. GOVT ACCESSION NO.	3. RECIPIENT'S CATALOG NUMBER
4. TITLE (and Subtitle) Radar Land Clutter Measurements at Frequencies of 9.5, 16, 35 and 95 GHz.		5. TYPE OF REPORT & PERIOD COVERED Technical Report 6. PERFORMING ORG. REPORT NUMBER A-1485-003
7. AUTHOR(s) N. C. Currie, F. B. Dyer, and R. D. Hayes		8. CONTRACT OR GRANT NUMBER(s) DAAA25-73-C-0256
9. PERFORMING ORGANIZATION NAME AND ADDRESS Sensor Systems Division, Engineering Experiment Station, Georgia Institute of Technology Atlanta, Georgia 30332		10. PROGRAM ELEMENT, PROJECT, TASK AREA & WORK UNIT NUMBERS Mod. P-00004
11. CONTROLLING OFFICE NAME AND ADDRESS Frankford Arsenal United States Army Philadelphia, Pennsylvania 19137		12. REPORT DATE 2 April 1975 13. NUMBER OF PAGES ~~107~~ 105
14. MONITORING AGENCY NAME & ADDRESS(if different from Controlling Office)		15. SECURITY CLASS. (of this report) Unclassified 15a. DECLASSIFICATION DOWNGRADING SCHEDULE
16. DISTRIBUTION STATEMENT (of this Report)		
17. DISTRIBUTION STATEMENT (of the abstract entered in Block 20, if different from Report)		
18. SUPPLEMENTARY NOTES Georgia Tech Project A-1485-003		
19. KEY WORDS (Continue on reverse side if necessary and identify by block number) Radar Backscatter Land Clutter Millimeter Spectrum Correlation		

20. ABSTRACT (Continue on reverse side if necessary and identify by block number)

A series of measurements of radar backscatter from foliage and other natural objects have been made at frequencies of 9.5, 16.5, 35, and 95 GHz. The geometry of the experiments and the equipment were chosen such as to provide data useful to the equipment designer in the choice of operating frequency for his particular mission. Amplitude statistics for both horizontal and vertical polarizations were obtained. Non-coherent spectral measurements and correlation properties were investigated in detail as functions of frequency, incident angle, and windspeed. Limited comparisons are made between previous measurements and

DD FORM 1473 EDITION OF 1 NOV 65 IS OBSOLETE

Unclassified

SECURITY CLASSIFICATION OF THIS PAGE (When Data Entered)

20. continued

analyses and the current experimental results, and certain properties of the results are discussed in relation to the phenomenology of land clutter. Extensive summaries of the data obtained are included as a part of the report.

ENGINEERING EXPERIMENT STATION
Georgia Institute of Technology
Atlanta, Georgia 30332

RADAR LAND CLUTTER MEASUREMENTS AT FREQUENCIES OF 9.5, 16, 35, and 95 GHz

Technical Report No. 3
EES/GIT Project A-1485

by
N. C. Currie, F. B. Dyer, and R. D. Hayes

Prepared for

United States Army
Frankford Arsenal
Philadelphia, Pennsylvania 19137

under
Contract DAAA 25-73-C-0256

2 April 1975

Contract DAAA-25-73-C-0256
Frankford Arsenal
United States Army
Philadelphia, Pennsylvania 19137

A-1485-TR-3
Engineering Experiment Station
Georgia Institute of Technology
Atlanta, Georgia 30332

RADAR LAND CLUTTER MEASUREMENTS AT FREQUENCIES OF 9.5, 16, 35, and 95 GHz

by

N. C. Currie, F. B. Dyer, and R. D. Hayes

ABSTRACT

A series of measurements of radar backscatter from foliage and other natural objects have been made at frequencies of 9.5, 16.5, 35, and 95 GHz. The geometry of the experiments and the equipment were chosen so as to provide data useful to the equipment designer in the choice of operating frequency for his particular mission. Amplitude statistics for both horizontal and vertical polarizations were obtained. Noncoherent spectral measurements and correlation properties were investigated in detail as functions of frequency, incident angle, and windspeed. Limited comparisons are made between previous measurements and analyses and the current experimental results, and certain properties of the results are discussed in relation to the phenomenology of land clutter. Extensive summaries of the data obtained are included as a part of the report.

ACKNOWLEDGMENTS

In addition to the authors, several individuals within the U.S. Government and at Georgia Tech have provided assistance in completing the studies described herein. Mr. Joe Miller, Superintendent of Kennesaw National Battlefield Park, and his staff were very understanding in allowing the use of Kennesaw Mountain as a test site, and were very helpful in several instances where equipment problems arose during the tests. Mr. Conrad Shore of Frankford Arsenal, U.S. Army, provided valuable guidence and technical support throughout the program. At Georgia Tech Messrs. William Dunn, Fred Durham, Sam Formby, and Ms. Ellen Robertson participated in the data analysis or aided in the report preparation associated with this work. Our appreciation is due Mr. Steve Zehner who provided valuable insight in the interpretation of the data, especially the spectral distributions. Ms. Ann Evans and Ms. Darenda Rakestraw were responsible for final preparation and typing of the report.

TABLE OF CONTENTS

LIST OF FIGURES

List of Figures (continued)

List of Figures (continued)

List of Figures (continued)

List of Figures

List of Figures (continued)

List of Figures (continued)

LIST OF TABLES

I. INTRODUCTION

This report summarizes the results of a measurement program to determine the characteristics of radar backscatter from land clutter at millimeter wavelengths which was conducted at Kennesaw National Battlefield Monument, Georgia, over the period June to October 1975. Emphasis in the report is placed on determining the backscatter properties of trees and other vegetation for summer and fall foliage conditions and for grazing angles between 1° and 25°.

A. Background

Under Contract DAAA25-73-C-0256 with the U. S. Army, Frankford Arsenal, the Engineering Experiment Station (EES) at Georgia Tech undertook to develop suitable mathematical models of radar target and clutter characteristics to allow computer simulation of fire-control radar systems in the millimeter frequency region. As a first step in this program, a literature search was conducted to determine what data were available at the millimeter wavelengths on clutter and target characteristics which could affect system performance. A summary of these data and the empirical models which were developed were presented in Technical Report No. 1.

The results of that study brought to light a number of deficiencies in the available data. It was determined that (1) few data were available on the radar cross-section (RCS) characteristics of ground clutter above X-band, particularly below 10° grazing angle; (2) only limited data were available above X-band to describe the spectral and polarization behavior of ground clutter; (3) very limited data were available on the effects of atmospheric conditions, especially precipitation, in the millimeter region; and (4) there was a scarcity of data on the radar cross-section properties of hard targets at these frequencies. EES then proposed to Frankford Arsenal a program of investigation designed to fill in the gaps in available

clutter data in the millimeter region, to be followed by an analysis program aimed at tying the data results together in a unified model for millimeter radar systems.

Frankford Arsenal, in response to the proposed program, undertook to fund specific studies of the backscatter from precipitation and from land clutter at millimeter frequencies.

Ballistic Research Laboratories was funded in part by Frankford to conduct an experiment to measure backscatter from rain at millimeter frequencies at McCoy A.F.B., Florida; and EES was tasked, in a modification (Mod. P-00002) to the original contract, to assist in experiment planning and to act as on-site observers during the actual tests. In addition, under this program, EES constructed and delivered to BRL a range-gated boxcar sampler unit which would allow recording of backscatter data on magnetic tape during the tests. The services and activities performed were detailed in a letter report at the end of the McCoy tests [2].

After the termination of the rain backscatter radar field tests, EES was tasked by Frankford Arsenal (Mod. P-00003) to reduce and analyze the data contained on the magnetic tapes in order to obtain amplitude distribution characteristics and spectral and correlation properties of the radar backscatter from rain which could not be determined by the photographic methods of data reduction used by BRL. Later on, in another addition to the contract (Mod. P-00005), EES was tasked to complete the analysis of rain drop-size distribution tapes that were recorded during the McCoy tests and which were partially reduced by the Illinois Water Survey. The results of the analysis of the radar backscatter and rain drop-size magnetic tapes are summarized in Technical Report No. 2 on the contract [3].

In addition to the rain backscatter study, Frankford Arsenal funded a measurement program designed to provide certain of the data needed to correct the deficiencies in understanding of land clutter in the millimeter region. Specifically EES, under contract Mod. P-00004, undertook a measurement program to determine the backscatter properties from trees and other vegetation for summer and fall foliage conditions and for small depression angles as a function

of transmitted frequency, polarization, and transmitted-received polarization sense. As in the case of the rain backscatter study, data on the received signals from land clutter were recorded on magnetic tape so that the amplitude distribution properties and spectral and correlation characteristics could be determined in addition to the average backscatter characteristics. This report will summarize the results of that land clutter measurements program.

B. Description of Radar Field Measurements

1. Radar Test Site

In order to obtain the desired measurements a test site was required which would allow look angles of 10° or more down to grazing and yet provide an area in which the M-109 van that houses the test radars and data-gathering equipment could be positioned so as to provide an unobstructed view of tree-covered areas. Furthermore, due to the limited funds available for the measurement program, the test site had to be located within commuting distance of EES.

A test site which met all of the necessary conditions was located at Kennesaw Mountain situated in the Kennesaw Mountain National Monument about 20 miles northwest of Atlanta, Georgia. This area contains numerous overlooks where the trees on the mountainside have been cut back to allow a clear view of the surrounding countryside. Two such overlooks were selected as test sites for the measurement program. Site 1 was located near the summit of the mountain and provided look angles from 10° to 1°. Areas of both coniferous and deciduous trees as well as large grassy fields were visible from this site. Site 2 was chosen because it faced nearby Little Kennesaw Mountain. Little Kennesaw is heavily wooded and has a slope of approximately 15°. By recording radar returns from its slopes, depression angles of as much as 25° could be simulated (except for the fact that the trees on its slopes stand vertically). Figures 1 and 2 show the fields of view from the two test sites. Site 1 faced due north while Site 2 faced southwest.

Figure 1. Field of view from the top of the radar van located at test site 1 near the summit of Kennesaw Mountain.

Figure 2. Field of view from the radar van located at test site 2 overlooking Little Kennesaw Mountain.

2. Description of Test Radars

The four test radars used for this experiment were mounted on a single test vehicle along with integrated controls and data acquisition equipment as shown in Figure 3. The 9.5 GHz, 16.5 GHz, and 35 GHz radars are permanently mounted to the test vehicle and have removable antennas on the roof while the receivers and controls are inside the vehicle. The 95 GHz radar has the antenna and receiver integrated into one package (to minimize waveguide losses) and sits on a platform on the van roof which can be positioned in both azimuth and elevation. The parameters of the four radars are given in Tables 1 through 4. Although the X-band and K_u-band systems can tune over a range of frequencies, they were set for these tests at 9.5 and 16.5 GHz, respectively.

While differing in detail, the 9.5, 16.5, and 35 GHz radars are similar. They are all short-pulse systems and are dual-polarized; that is, they receive both horizontal and vertical polarizations simultaneously while transmitting either horizontal or vertical polarization. These three systems may be operated in either the scanning or nonscanning mode. The 9.5 GHz radar, has both a 3 ft-diameter scanning parabolic cylinder and a 5-ft diameter nonscanning dish, both of which were used for these experiments. Each dish can be boresighted by means of a removable rifle scope. All three of these systems incorporate logarithmic receivers of wide dynamic range (approximately 80 dB) to permit accurate measurement of returns from targets having a widely varying signal strength. Each system incorporates provisions for injection of known calibration signals into both parallel- and cross-polarized channels. A common prf reference of 2000 Hz was used for all systems during the tests described here.

The 95 GHz system is somewhat different from the other three systems in that the antenna is a nonscanning Cassegrain type and all controls are mounted in one package containing antenna, transmitter, and receiver. The antenna can also be boresighted by means of a rifle scope, as can the other antennas. The radar does not currently have dual-polarized capability, although either vertical or horizontal polarization is available.

The antenna sizes of the four radars resulted in beamwidths ranging be-

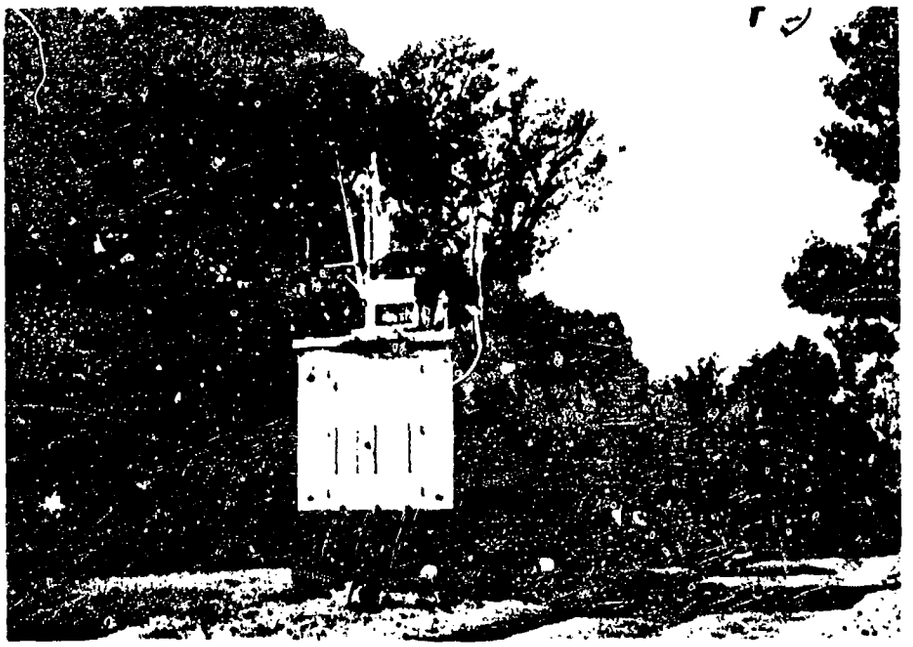

Figure 3. View of radar van in position for data gathering at test site 1 on Kennesaw Mountain.

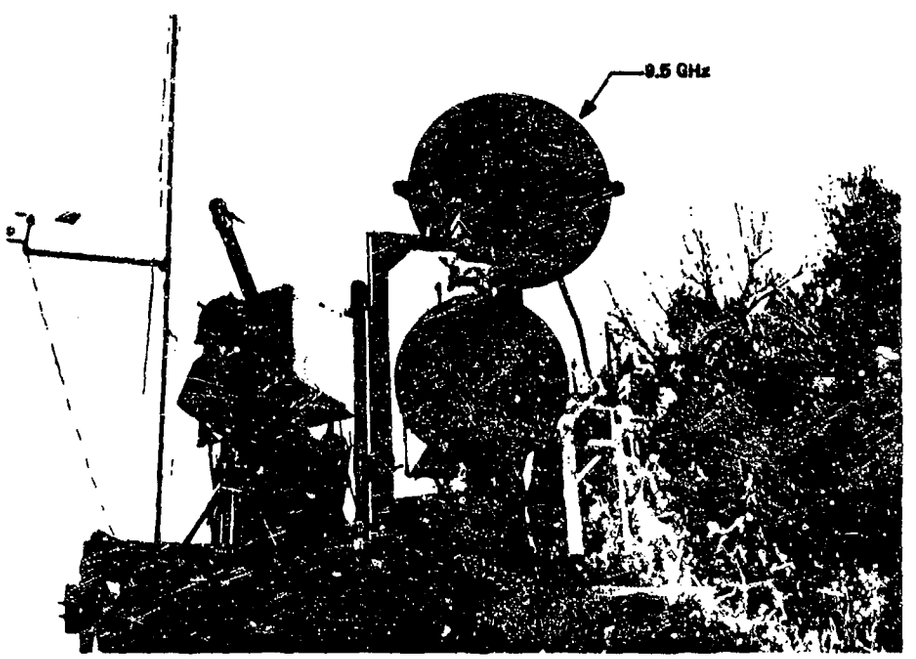

Figure 4. Close-up view of the radar antennas located on top of the radar van.

TABLE 1

PARAMETERS OF GEORGIA TECH GT-I EXPERIMENTAL RADAR

Parameter	Description
Frequency	8.5-9.6 GHz
Peak Power	40 kW
Pulse Width	50 ns
PRF	0-4000 pps
Antenna Type	Nonscanning Paraboloid
Azimuth Beamwidth	1.5°
Elevation Beamwidth	1.65°
Antenna Gain	Vertical Polarization 41.4 dB
	Horizontal Polarization 41.6 dB
Antenna Type	Scanning Parabolic Cylinder
Scan Rate	0-100 RPM
Azimuth Beamwidth	2°
Elevation Beamwidth	5°
Antenna Gain	Vertical Polarization 30 dB
	Horizontal Polarization 31 dB
Polarization	H or V transmitted
	H and V received simultaneously
IF Center Frequency	60 MHz
IF Bandwidth	20 MHz
IF Response	Logarithmic (linear available)
Noise Figure	12 dB
Dynamic Range	80 dB
Display Type	A-scope

TABLE 2

PARAMETERS OF GEORGIA TECH GT-J EXPERIMENTAL RADAR

Parameter	Description
Frequency	16-17 GHz
Peak Power	50 kW
Pulse Width	50 ns
PRF	0 - 4000 pps
Antenna Type	Scanning Paraboloid
Scan Rate	0-120 rpm
Azimuth Beamwidth	1.5^{o}
Elevation Beamwidth	1.5^{o}
Antenna Gain	Vertical Polarization 41.5 dB
	Horizontal Polarization 41.4 dB
Polarization	H or V transmitted
	H and V received simultaneously
IF Center Frequency	60 MHz
IF Bandwidth	20 MHz
IF Response	Logarithmic (linear available)
Noise Figure	13 dB
Dynamic Range	70 dB
Display Type	A-scope, B-scope, PPI

TABLE 3

PARAMETERS OF GEORGIA TECH GT-K EXPERIMENTAL RADAR

Parameter	Description
Frequency	35 GHz
Peak Power	40 kW
Pulse Width	50 ns
PRF	0-4000 pps
Antenna Type	Scanning Paraboloid
Scan Rate	0-120 rpm
Azimuth Beamwidth	1^{o}
Elevation Beamwidth	1^{o}
Antenna Gain	Vertical Polarization 43 dB
	Horizontal Polarization 43 dB
Polarization	H or V transmitted
	H and V received simultaneously
IF Center Frequency	60 MHz
IF Bandwidth	20 MHz
IF Response	Logarithmic
Noise Figure	14 dB
Dynamic Range	70 dB
Display Type	A-scope, B-scope, PPI

TABLE 4

PARAMETERS OF GEORGIA TECH GT-M EXPERIMENTAL RADAR

Parameter	Description
Frequency	95 GHz (Nom)
Peak Power	6 kW
Pulse Width	50 ns or 10 ns
PRF	0-4000 pps
Antenna Type	Paraboloid (Cassegrain)
Azimuth Beamwidth	$.70^{o}$
Elevation Beamwidth	$.65^{o}$
Antenna Gain	Vertical Polarization 46.3 dB
	Horizontal Polarization 46.3 dB
Polarization	H or V
IF Center Frequency	60 MHz or 160 MHz
IF Bandwidth	20 MHz or 100 MHz
IF Response	Logarithmic (linear available)
Noise Figure	15 dB
Dynamic Range	70 dB
Display Type	A-scope

tween 1.5° for the 9.5 GHz radar (2.0° with the scanning parabolic cylinder) to 0.7° for the 95 GHz radar, a factor of only two to one. This allows returns from clutter to be measured at the four frequencies for approximately the same size clutter patches so that meaningful comparisons can be made. Figure 4 gives a close-up view of the four antennas on the top of the radar van.

3. Data Gathering Equipment

For purposes of data gathering, the RF from the 9.5, 16.5, and 35 GHz radars and the IF from the 95 GHz radar are piped from the roof of the radar van to logarithmic IF amplifiers located in the operating console. The resulting logarithmic videos are fed through video line drivers so that various displays and equipment can be connected to the appropriate video outputs without loading the video signals. Also located at the console are a six-channel narrow-aperture sampler which stretches the video samples at a particular time so that it can be recorded on an fm tape recorder, two A-scope displays, a B-scope display (for displaying scanning data), a frequency counter, and the timer control unit for the radars. Figure 5 gives a view of the radar console.

The radar transmitter controls and rf signal generators (for calibration purposes) for the 9.5, 16.5, and 35 GHz systems are located in a rack to the left of the operating-console as shown in Figure 6. Figure 7 gives a simplified block diagram of the equipment configuration of one of the radar systems for calibration and measurement of received power from targets and clutter. For calibration purposes a signal generator pulse is injected into the receiver input through a coupler with the transmitter off, and the power level of the signal generator is stepped from 0 dBm to the receiver noise level in equal steps (usually 5 or 10 dB) while the receiver video response is sampled, stretched, and recorded on magnetic tape.

When measuring the return from targets (nonscanning), the antennas are boresighted on the targets, and an adjustable range gate is used to vary the range at which the received signal is sampled and recorded.

View of the operating console inside the radar van showing the "A and B-scope" displays and the data acquisition instrumentation.

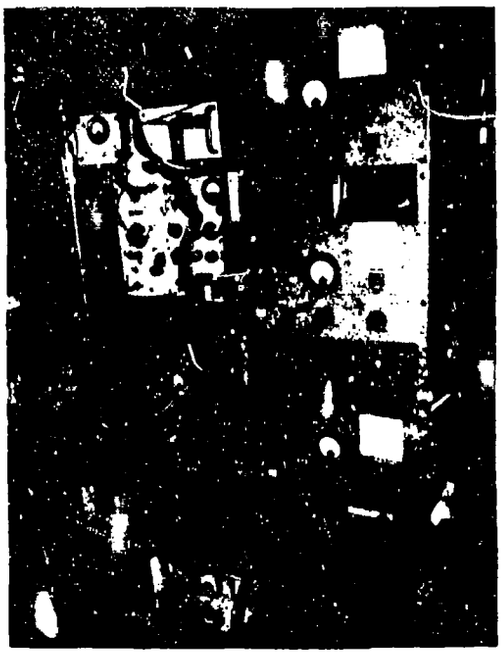

Close-up of the radar transmitter controls and the rf calibration equipment.

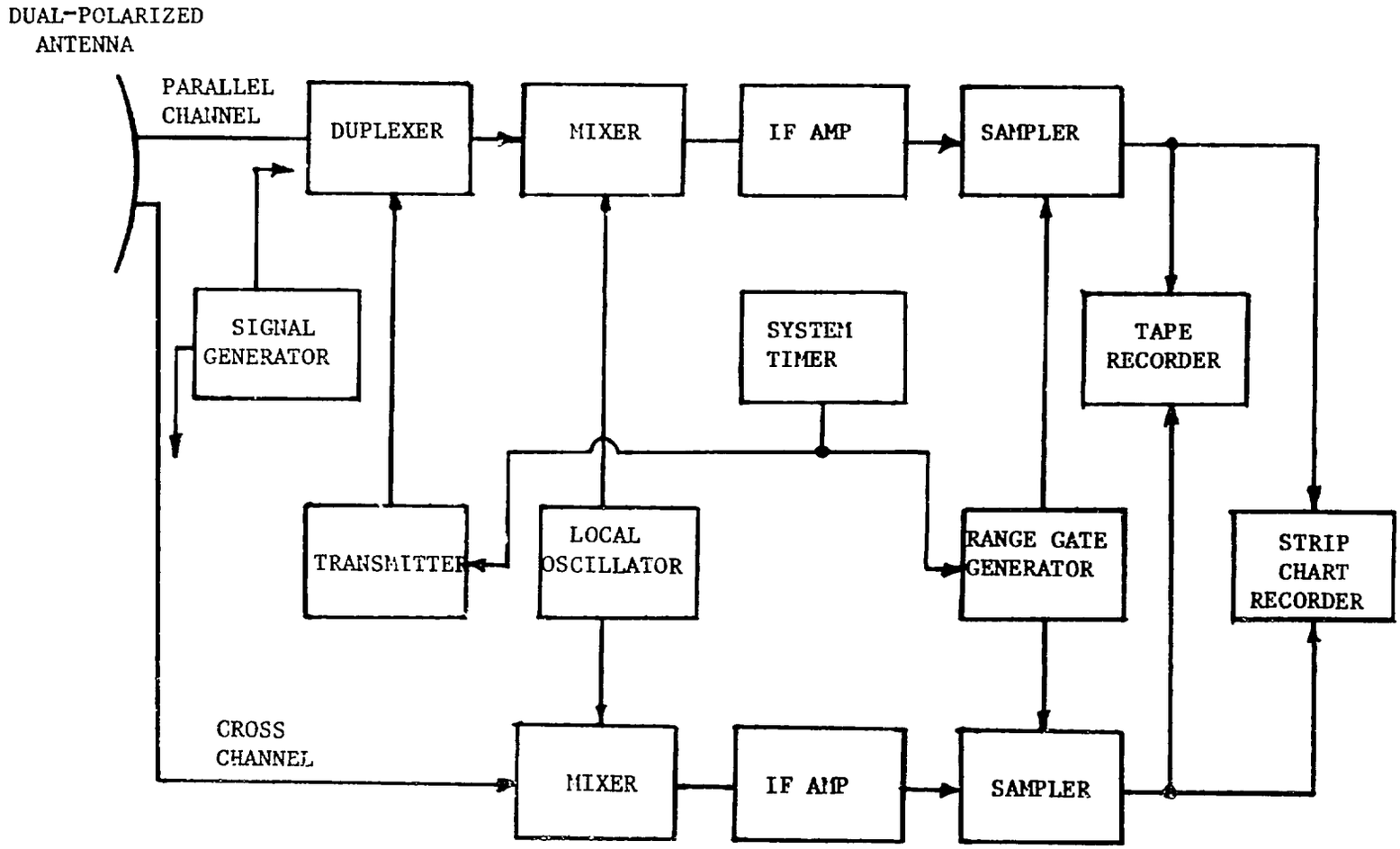

Figure 7. Simplified block diagram of equipment configuration for measuring received power from targets and clutter.

No signal generator is available for calibration purposes with the 95 GHz radar so that calibration is achieved by boresighting the radar antenna on a corner reflector of known radar cross-section, varying a precision RF attenuator in the received power path until receiver noise is reached, and recording the resulting transfer function on magnetic tape. This procedure relates the received signals directly to effective radar cross-section, which is the quantity to be measured. This method can be made to yield rather high accuracy if sufficient attention is directed to mapping the effects of multipath and other site-dependent factors.

For the 9.5, 16.5, and 35 GHz radars, the calibration of received power must be related to RCS, the desired quantity to be measured. This is achieved by solving the radar equation and carefully measuring the transmitted power, antenna gain, and waveguide losses.

The RCS of a target as a function of received power for a given radar system is given by: [4]

$$\sigma\ (m^2) = \frac{Pr\ (4\pi)^3 R^4}{Pt\ G^2 \lambda^2} \qquad (1)$$

where: Pr is the received power in milliwatts
Pt is the transmitted power in milliwatts
G is the antenna gain
λ is the wavelength in meters
R is the range in meters

As a further check on the calculations, measurements were performed on several corner reflectors of known RCS. The configuration shown in Figure 8 is an example of the technique used, and shows a 22-inch corner reflector deployed on a 16-ft mast.

Figure 8. View of one of the radar corner reflectors used for calibration mounted on a 16 ft. mast.

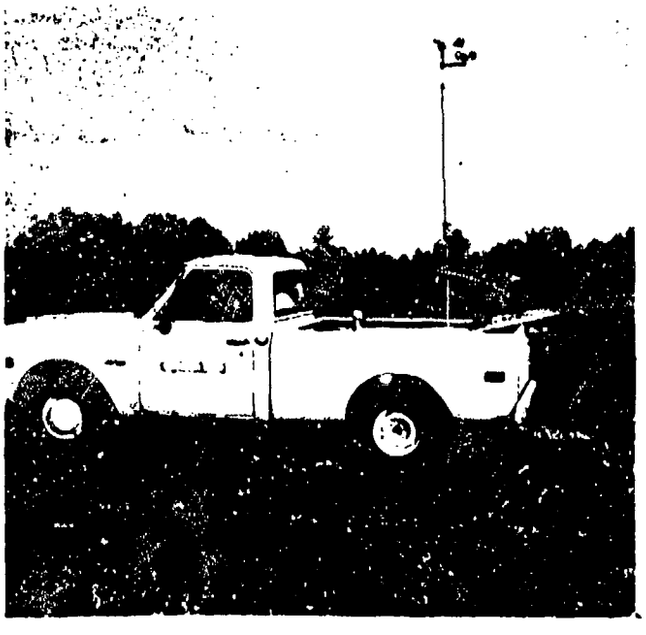

Figure 9. Truck mounted wind speed-and-direction instrumentation deployed in a large grassy field.

It was desired to attempt to correlate wind speed and direction with the amplitude and spectral properties of the clutter returns being recorded. However, wind measurements made at the radar van could not be expected to simulate wind conditions several km away. Accordingly, a portable anemometer was mounted in the back of a pick-up truck as shown in Figure 9 in order to allow measurement of wind conditions near each clutter patch under test. Attempts were made to position the truck downwind from the area tested whenever the appropriate access was available. For those few areas where the truck could not be so positioned, representative measurements were made in the general area. Citizen band radios were used to inform personnel in the pickup truck when data were being recorded, and wind speed and direction were recorded at 30-second intervals during these periods.

4. Measurement Procedure

The measurement procedure followed in taking land clutter backscatter data typically consisted of the following steps:

(1) After a suitable warm-up period, a calibration was performed on the 9.5, 16.5, and 35 GHz radars utilizing signal generators to input known power levels to the radar receivers as stated previously.

(2) The four radars were boresighted on one of several corner reflectors located in a cleared area and the received power levels were recorded. A 95 GHz calibration was generated by changing the rf attenuator in 5 dB steps until the receiver noise level was reached as explained above.

(3) The pick-up truck was dispatched to a position downwind from the clutter patch to be measured.

(4) A characteristic target such as an unusually shaped tree was used to align the boresight position (using the rifle scopes) of each antenna so that all the antennas were pointing at the same clutter patch. The depression angle to the boresight target from the top of the radar van was measured with a theodolite.

(5) The returns from the clutter patch were recorded simultaneously for several minutes for both horizontal and vertical polarizations.

(6) The antennas were repositioned to a new clutter area, and the measurement procedure was repeated.

(7) Calibrations were recorded at the beginning and end of each magnetic tape as a check against drift in the radars or the recording equipment.

(8) From time to time A-scope photos were taken to document the video characteristics.

The data obtained as a result of the tests represent the amplitude fluctuations of the power received by each of the radars from a specific clutter patch defined by the radar pulse lengths and the azimuthal antenna beamwidths.

The recorded signals were processed by computer to yield average values for the received power, the distribution shapes of the fluctuations, and the spectral properties.

II. DATA ANALYSIS

A. Data Analysis Techniques

The data obtained from the radar backscatter measurements consisted mainly of fm magnetic tape recordings of amplitude fluctuations of the received signals from land clutter. Strip chart recordings, A-scope photographs, and other miscellaneous data such as log sheets of wind-speed and direction, provided background information to supplement the magnetic tapes, but were not analyzed directly.

1. Data-Reduction Facility

The PDP-8/F based data-reduction facility of the Sensor Systems Division of EES was used to process all the magnetic tapes from the radar backscatter tests. Figure 10 gives a view of the basic computer components. These include the following: (1) An analog signal-conditioner unit which provides variable gain and offset to allow the interface of varied types of signals to the data-reduction facility. (2) A Fabri-Tek Model 1072 Instrument Computer which serves as an A/D and D/A interface, and also computes real-time pulse-height distributions and cross-correlation functions. The D/A output from the Fabri-Tek computer can be displayed on a CRT display or can be plotted on an x-y plotter. (3) A PDP-8/F computer which can exchange information directly with the Fabri-Tek computer. (4) A teletype. (5) A Sykes Compucorp Digital Cassette Recorder for program development and storage.

The PDP-8/F contains 16K of memory, of which 8K is magnetic core. An extended version of FOCAL$_{TM}$ has been developed for use with the PDP-8/F and is designated FOCL/F [5]. This language is interactive and greatly facilitates program correction and modification. Also available is a machine language software package for calculating fast Fourier transforms (FFT), and a set of software commands for Fabri-Tek control. These two machine language software packages along with the extended FOCAL$_{TM}$ software make this system a very powerful and flexible data-reduction facility.

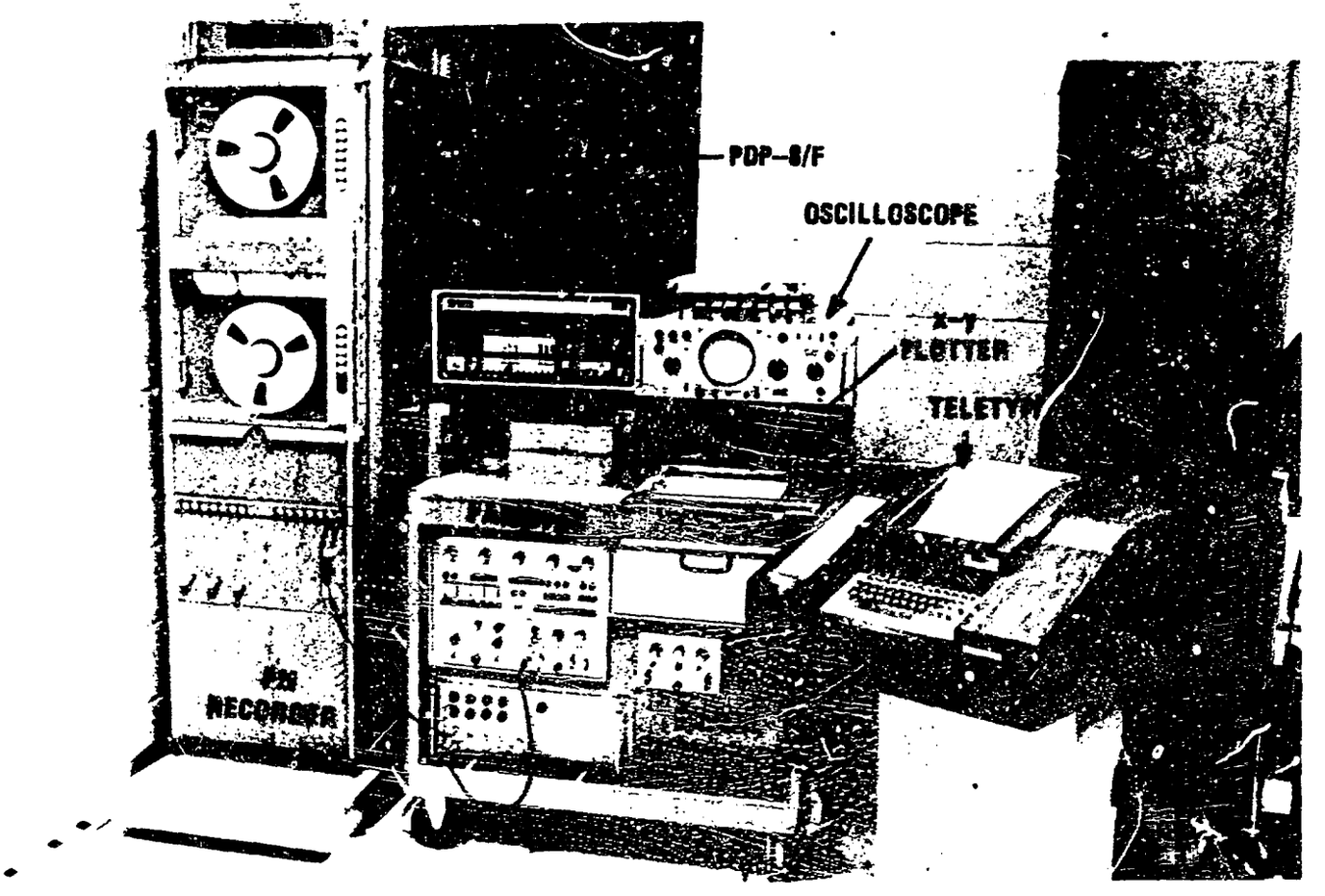

Figure 10. View of the Sensor Systems Division's PDP-8/F based data reduction facility.

2. Data Analysis Procedure

The types of analyses which are normally obtained from the data facility include: (1) pulse-height amplitude (PHA) distributions, (2) frequency spectra, and (3) auto- and cross-correlation functions. The methods for obtaining these three classes of results are sufficiently different as to require entirely different FOCAL$_{TM}$ programs for their calculation. Taken as a whole, results from these three types of analysis have been used to characterize the recorded data.

a. Pulse-Height Amplitude Distributions

Pulse-height amplitude distributions calculated by the data facility are displayed in two forms: as probability density plots and as probability distribution functions. The probability density plots are generated from data time histories from the magnetic records. The analyzer samples the input analog time history, A/D converts the samples, determines into which of 1024 amplitude bins the sample belongs, and increments a stored variable corresponding to the number of samples which have fallen in that amplitude window. When repeated a large number of times, this process generates a voltage amplitude distribution which is then calibrated and divided by the total number of samples to achieve a normalized probability density function.

The voltage amplitude distributions are calibrated by reference to a known comb (amplitude) signal. The peak of the distribution for each voltage step in the calibration comb is assigned the dB value corresponding to that calibration step. The PHA program in the PDP-8/F then does a cubic fit to the calibration and generates a table relating dB value and amplitude bin number. The cubic fit program was developed to "linearize" nonuniform calibration steps so that the output density functions can be plotted on a linear scale.

The probability distributions are calculated by point-by-point numerical integration of the probability density functions. The functional values of these distributions are then multiplied by a nonlinear transfer function so that they can be plotted on probability paper.

The resultant probability distributions are useful in determining the median values of the distributions and also their shapes. In addition, for certain classes of functions, the average values can be determined from the distributions using a simple formula [6].

b. Frequency Spectra

The frequency spectra data-reduction program uses the fast Fourier transform subroutines available for the PDP-8/F to transform input time histories to the frequency domain. The program has several options which allow the spectral data to be presented in different forms including: (1) voltage amplitude in dB versus frequency, (2) normalized voltage amplitude in dB versus frequency, and (3) normalized power spectral density in dB versus frequency.

The voltage amplitude program in the PDP-8/F computer processes an input time history which has been sampled, A/D converted, and stored by the Fabri-Tek. The program computes the fast Fourier transform for that time history, and calculates the square root of the sum of the squares of the real and imaginary parts of each element in the transform. Since a time history typically represents the voltage out of a logarithmic receiver, which is proportional to the logarithm of the received power, the amplitude of the spectrum corresponding to the time history is measured in dB relative to a milliwatt (dBm). Thus, to calibrate the spectral amplitude in dB, a calibration is stored in memory which relates dB values to input voltage amplitudes, and each time history is converted to dB values as it is read in. Since the Fourier transform is a linear process, the spectrum amplitude will be proportional to dB if the time history is calibrated in dBm and the proportionality constant is set equal to one in the program.

Figures 11 and 12 give typical time histories for 95 GHz and 9.5 GHz. The vertical scales represent radar cross-section in units of dBsm. (Received power can be related to cross-section if the appropriate radar constants are known.) A time history is limited in duration to the number of Fabri-Tek memory bits times the sample period. For this case,

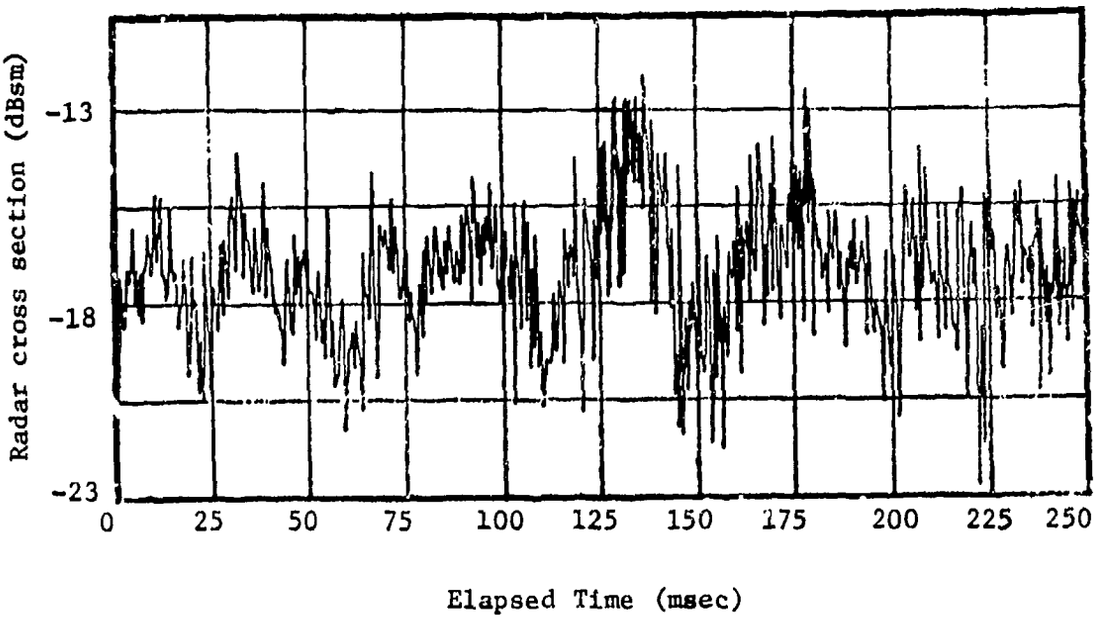

Figure 11. Time history of the recorded backscatter from deciduous trees; 95 GHz, vertical polarization.

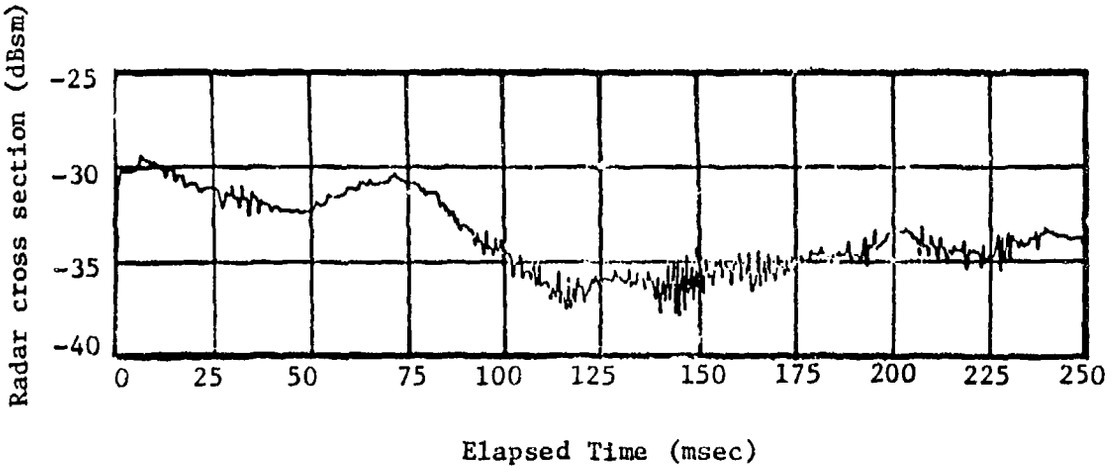

Figure 12. Time history of the recorded backscatter from deciduous trees; 9.5 GHz, vertical polarization.

the sample rate equals the prf used in taking the data (2000 Hz), so that a time history is given by: 1/2000 x 1024 = 0.512 seconds. To achieve the equivalent of a longer time history, the Fourier transforms of 8 adjacent time histories are averaged together. The actual number of time histories averaged is arbitrary; however, previous experience has shown that eight to ten are sufficient to establish a reasonable short term average.

In calculating the FFT, the dc term has been set to zero because its amplitude is normally so much larger than the rest of the spectrum that dynamic range problems are encountered in the computer due to the form of the FFT algorithm. Thus, the zero frequency point is zeroed in all the plots. However, this dc point can still be determined independently from the amplitude distribution functions.

A second method of displaying the log amplitude spectrum is to normalize the spectrum by dividing all the elements by the peak element value. The spectrum is then plotted in dB relative to the peak voltage amplitude, which is normally the lowest frequency point. This type of plot is very useful for comparing frequency roll-off characteristics of spectral plots with different amplitudes.

Although the data recorded on the magnetic tapes represent the voltage output from a logarithmic receiver, it was deemed desirable to plot the equivalent spectrum for a linear receiver. Therefore a modification was developed to the spectrum program which allowed the "delogging" of the input data prior to calculation of the Fourier transform. When normalized, this program results in the calculation of the normalized linear frequency spectrum. [7] For certain classes of functions, to which all the data processed here belong, this power spectrum is equivalent to the power spectral density. The unnormalized calibrated power spectrum cannot be determined by this method since the dc term is thrown away, as previously described.

c. Auto- and Cross-Correlation Functions

The auto-correlation functions and cross-correlation functions for input time histories are determined by two different methods in the data analysis. Auto-correlation functions are computed from the inverse transform of the magnitude of the Fourier transform squared in the PDP-8/F

computer, while cross-correlation functions are measured using an SD-75 plug-in in the Fabri-Tek computer. The SD-75 plug-in samples two separate input signals, A/D converts them, and calculates partial products between samples as a function of time to generate the correlation function between the signals. This computation is given by

$$\phi_{AB}(n\Delta\tau) = \frac{1}{k} \sum_{i=1}^{k} A(t_i)\ B(t_i + n\Delta\tau);\ n = 0,\ 1,2\ldots,k-1 \qquad (2)$$

where k = number of discrete points for which the correlation function is to be determined,

$k\Delta\tau$ = total sample length,

$A(t_i)$ = amplitude of first function sampled at time t_i,

$B(t_i)$ = amplitude of second function sampled at time t_i.

This method could have been used to generate auto-correlation functions by connecting the same signal to both plug-in inputs, but this was not done because of several limitations in the plug-in. First, the set-up and calibration of the auto-correlation plug-in is difficult, and requires considerable manual handling of the data. In addition, due to the limited memory available in the Fabri-Tek, the lowest frequency that that can be accurately measured is approximately one-tenth the total sampling period while the highest frequency is, from the sampling theorem, about one-half the sampling rate. Thus to measure the auto-correlation function of a signal with 1000-Hz bandwidth, the sample rate would be 2000 Hz and the lowest frequency would be:

$$F_{low} = \frac{\text{Sample Rate}}{\text{Total Memory}} = \frac{2000\ \text{Hz}}{1024\ \frac{\text{Memory}}{\text{Bits}}} = 1.95\ \text{Hz}. \qquad (3)$$

Utilizing the fast Fourier transform in the PDP-8/F to perform auto-correlation calculations solves the problems inherent in using the SD-75 plug-in in the Fabri-Tek, except for the lower frequency limitation. Since the Fabri-Tek memory is used to store the time histories, the same low frequency limitations apply. However, a partial solution to this problem is to calculate the auto-correlation function using a lower sample rate to pick up lower frequencies at the expense of higher frequencies. A family of curves can thus be generated at different sampling rates which describe the auto-correlation function over any desired band of frequencies.

In the case of cross-correlation function computation, the current FFT program used in the PDP-8/F computer is not suitable, and the SD-75 plug-in in the Fabri-Tek must be used even with its limitations. Calibration is obtained with the plug-in by using signals with known correlation functions, such as a sine wave or Gaussian noise. The results from an unknown signal are then compared with those of the known signals.

B. Summary of Results

1. Interpretation of the Data

The goal of this test program was to obtain information on the properties of backscatter from land clutter at frequencies above 10 GHz and at the lower grazing angles which would be useful to the radar system designer. In particular, the experiment was structured to allow direct determination of the transmitted frequency dependence of the backscatter to aid in system frequency choice. To achieve this goal, dependence of the test results on the measurement system parameters must be reduced as much as practical, so that the data can be applied to the general case. The radar system factors which affect the magnitude of the received power from a radar cell include: (1) range, (2) antenna beamwidths, (3) transmitted pulse length, (4) transmitter power, (5) antenna gain, (6) system losses, and (7) transmitted frequency. The most commonly accepted way to present data on reflectivity

of surfaces so as to remove the dependence on the above parameters has been to calculate the quantity σ^o (the radar cross-section per unit area). The received power from a given surface area can be related to the return from an equivalent metal plate of given area by using the radar equation as discussed in Section I-B. This equivalent reflectivity area is divided by the actual area illuminated by the "footprint" of the radar beam on the ground to obtain σ^o, the reflectivity ratio.

The solid angle within a radar beam, assuming a Gaussian antenna pattern*, is given by: [8]

$$\psi_b = \frac{\pi \theta_a \theta_e}{4} \qquad (4)$$

where:

ψ_b = solid angle of the beam,
θ_a = azimuth 3 dB beamwidth in radians,
θ_e = elevation 3 dB beamwidth in radians.

For large depression angles, the area of the "footprint" of the beam on the ground is given by:

$$A_b = \frac{\pi}{8} \times \theta_a \theta_e R^2 \times \frac{1}{\sin E} \qquad (5)$$

where:

θ_a = azimuth beamwidth in radians,
θ_e = elevation beamwidth in radians,
R = slant range in meters,
E = depression angle in radians.

*The antenna patterns obtained from measurements made on the antenna range at Georgia Tech show these antenna to have a A_1 far-field distribution. A Gaussian distribution is an excellent approximation to a A_1 distribution within the half power beamwidth.

For a pulsed radar at low depression angles the area illuminated on the surface is a function of the azimuth beamwidth and the pulse length, and is given by:

$$A\tau = \frac{\theta_a R}{\sqrt{2}} \times \frac{\tau C}{2} \times \frac{1}{\cos E}$$

where: θ_a = antenna beamwidth in radians,
R = range in meters,
τ = pulse length in seconds,
C = speed of light in meters/second,
E = depression angle ($\cos E \simeq 1$ for small angles).

The angle of transition from Equation 5 to Equation 6 is given by:

$$\text{Tan } E_T = \frac{\sqrt{2}\ \theta_e\ R}{\tau C}$$

where:

θ_e = is elevation beamwidth in radians,
R = range in meters,
τ = pulse length in seconds,
C = speed of light in meters/second.

This transition angle E_T is equal to 51^o for the 9.5 GHz and 16.5 GHz radars, 39^o for the 35 GHz radars, and 30^o for the 95 GHz radar at a range of 500 meters (the minimum range at which data were recorded), and becomes larger as the range increases. Since the largest depression angle encountered during the tests was 25^o, Equation 6 was used to calculate the area of the beam "footprint" on the surface for each of the radars in order to determine σ^o. (It should be noted that a maximum depression angle of 25^o was encountered when the radars were pointed at Little Kennesaw Mountain which has a slope of approximately 15^o.)

Figure 13 gives the area calculated for the "footprint" of the beams for each of the test radars as a function of range. Since land clutter is typically nonuniform in nature, it is desirable that the beam areas of all test radars be as nearly equal as possible, so that the same areas are illuminated. This allows any difference in the reflectivity characteristics of the clutter to be attributed to frequency effects alone. The differences in beam areas among the four test radars are no more than 6 dB and should therefore allow direct comparison of the results.

One problem with obtaining measurements at extremely low angles (less than two degrees) is that the area illuminated by the beam becomes quite large due to the long ranges typically encountered. Thus the likelihood of having uniform clutter in the radar cell is greatly reduced, and the chances of having man-made targets of large radar cross-section present in the radar cells are increased. Also the signal-to-noise ratio becomes a problem at long ranges, particularly for the relatively low powered radars used in these tests. For these reasons, no data are presented below 2^{o} depression angle.

One of the primary differences between millimeter radars and those of lower frequency bands is the much smaller beamwidth for an antenna of given size, which results in a much greater angular resolution. Generally short pulse lengths (50-100 nanosec) are also utilized in order to enhance the resolution. The effect of this increased resolution on returns from land clutter is to make the clutter appear much less uniform than for lower resolution radars, since in many cases individual trees or other relatively large stationary targets are individually resolved.

This is also true for the case of the radars used in the test program. Figures 14 and 15 give views of patches of deciduous and pine trees on which measurements were made at a range of about 1.1 km. The circles on the figure give the coverage of the 9.5 GHz radar beam (3 dB points) which had the largest beamwidth of the test radars (1.5 degrees). It is obvious that at this short range, at most only two or three trees are included in the beam "footprint"

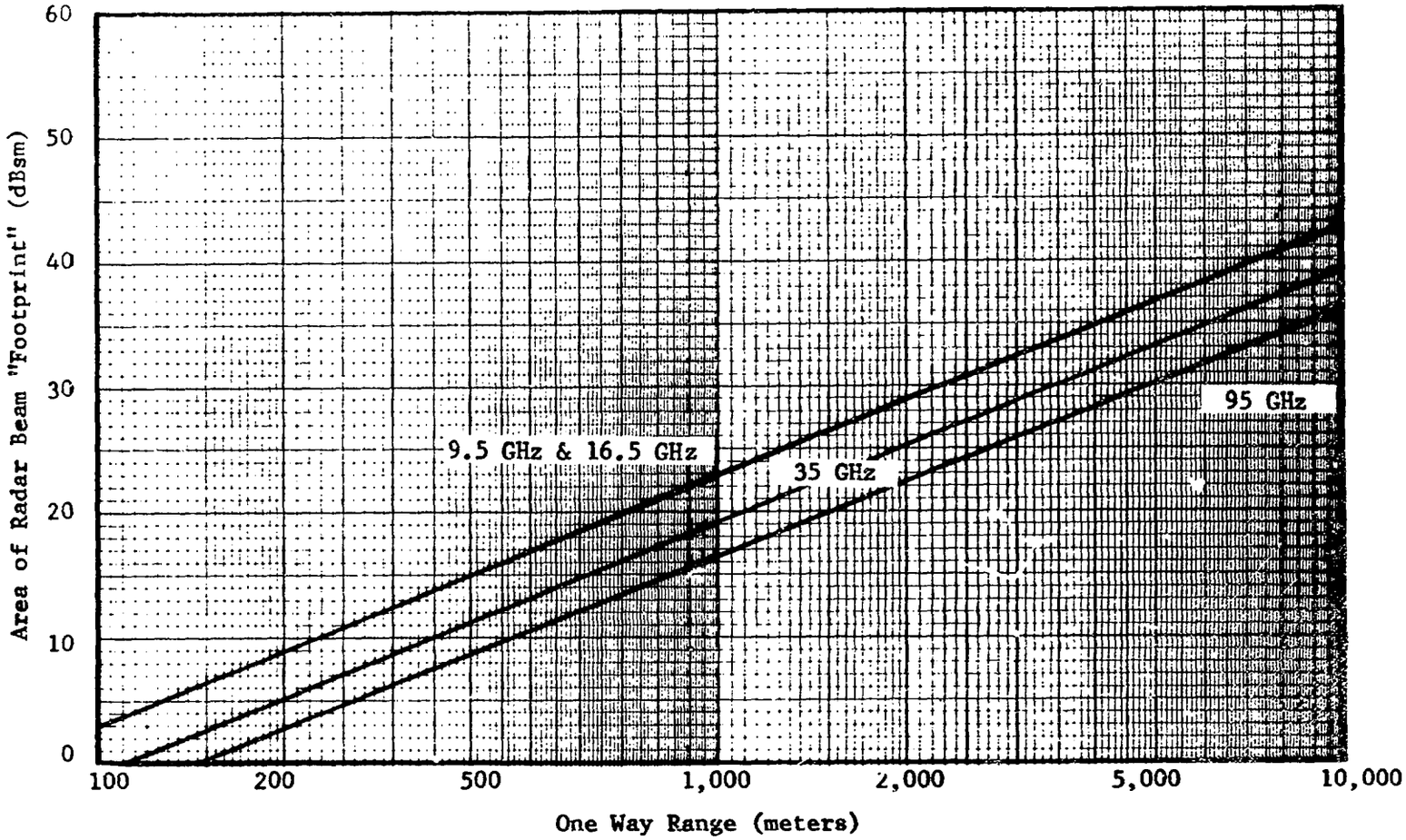

Figure 13. Calculated area for the "footprint" on the ground for each of the radars used in the measurement program as a function of range.

Figure 14. View of a deciduous tree area from test site 1 showing the 3dB antenna pattern for the 9.5 GHz radar (circle) superimposed on the trees. The depression angle is 8°; the range is 1.1 km.

Figure 15. View of a pine tree area from test site 1 showing the 3dB antenna pattern for the 9.5 GHz radar (circle) superimposed on the trees. The depression angle is 8°; the range is 1.1 km.

at one time. In addition, the vertical coverage is limited by the transmitted pulse length rather than the elevation beamwidth, so that the "footprint" is even smaller than shown in the figures. This fact helps to account for the spread in the backscatter data (of about 10 dB) for return from different tree patches at about the same range and look angle. However, since these measurements simulate the results that would be obtained for an operational high resolution radar, they are thus a valid measure of the problem facing the system designer in specifying the performance of such a system.

At longer ranges a number of trees are included in the cell so that the return should be more uniform. Figure 16 shows the 3 dB beam pattern on a large field at a range of about 4 km. The antenna pattern just fills the field vertically, although once again the vertical extent of the beam is limited by the pulse length rather than the vertical beamwidth.

Data taken at Site 2 on the side of Little Kennesaw Mountain were intended to simulate higher angles than could be obtained at Site 1, since the angular slope of the mountain adds to the effective depression angle with respect to the ground surface from the radar. However due to the short range involved ($\sim$ 0.5 km) and the narrow beamwidths and pulse lengths of the test radars, individual trees were resolved on the mountainside. Figure 17 shows the 3 dB pattern on the mountain for the 9.5 GHz radar. Since the trees on a mountainside grow vertically, the slope of the mountain becomes unimportant in its effects on the backscatter. For this reason the data taken on the side of Little Kennesaw Mountain are listed as a special case; however, they are compared directly with the other data in those situations where it is appropriate. For wider beamwidths and pulse lengths than used here, the extrapolation of the mountainside data to the case of data on flat ground at a higher look angle could be made correctly on a more general basis.

Four types of land clutter were studied based on their availability to the test sites. These include: pine trees, deciduous trees, mixed pine

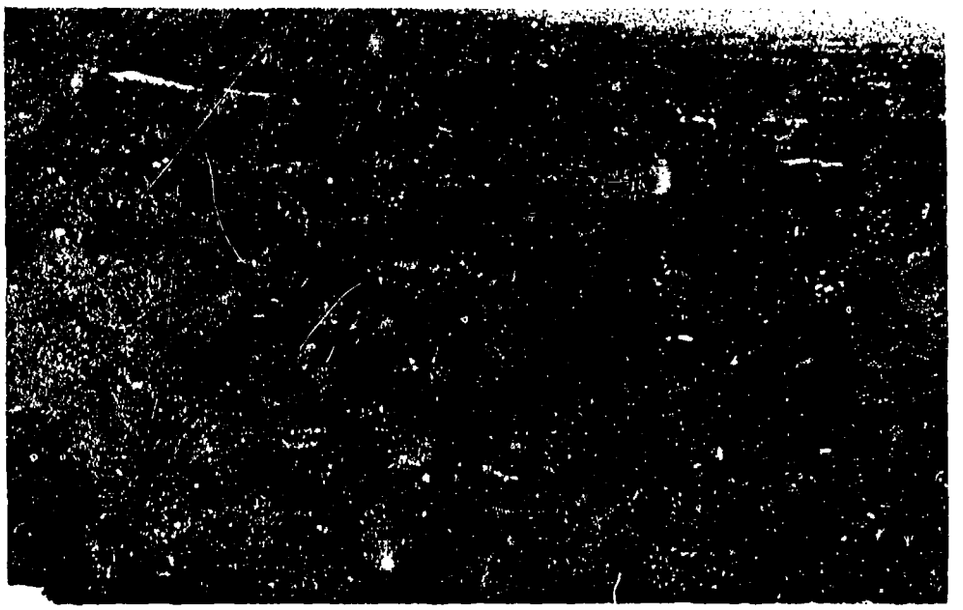

Figure 16. View of a large field from test site 1 showing the 3dB antenna pattern for the 9.5 GHz radar (circle) superimposed on the field. The depression angle is 3°; the range is 4.1 km.

Figure 17. View of the deciduous tree area on Little Kennesaw Mountain from test site 2 showing the 3dB antenna pattern for the 9.5 GHz radar (circle) superimposed on the trees. The depression angle is 0.4°; the range is 0.5 km.

and deciduous trees and a grassy field. For the reasons given above, it was not possible to distinguish types of clutter at low angles because of the large antenna beam areas which resulted. However, for depression angles between 5° and 10° it was possible not only to illuminate uniform clutter patches but to explicitly identify the scatterers so that differences in the return characteristics could be determined fairly accurately.

2. Average Backscatter Data

The measured backscatter per unit area for the various types of ground clutter studied are given in Figures 18 through 24. Figures 18 through 20 compare data measured during the summer with data obtained in the fall at 9.5 GHz, 35 GHz, and 95 GHz (no 16.5 GHz data were taken in the summer). Figures 21 through 24 compare data obtained for vertical and horizontal polarizations at 9.5 GHz, 16.5 GHz, 35 GHz, and 95 GHz.

No marked differences between the summer and fall data appeared in general; however, at 35 GHz, the summer data were slightly higher than those taken in the fall. Review of the available data suggests that this trend does not appear to hold at 95 GHz. (No summer data were obtained at this frequency for small depression angles because of equipment problems.)

It should be noted that all of the data plotted at or above 15° depression angle were measured on the side of Little Kennesaw Mountain at Test Site 2. The angles plotted were obtained by the addition of the actual depression angles from the radars to the average slope of Little Kennesaw which is 15° to obtain the equivalent depression angles. As discussed in the previous section (i.e., the relatively small antenna beam patterns on the mountainside) and because the trees grow vertically, the measurement geometry is not exactly equivalent to a true, larger depression angle. That the data appear to be a few dB lower than might be expected for the plateau region tends to confirm this conclusion.

The polarization dependence of the data is shown in Figures 21-24. In general vertical polarization appears to give 3-5 dB higher backscatter than

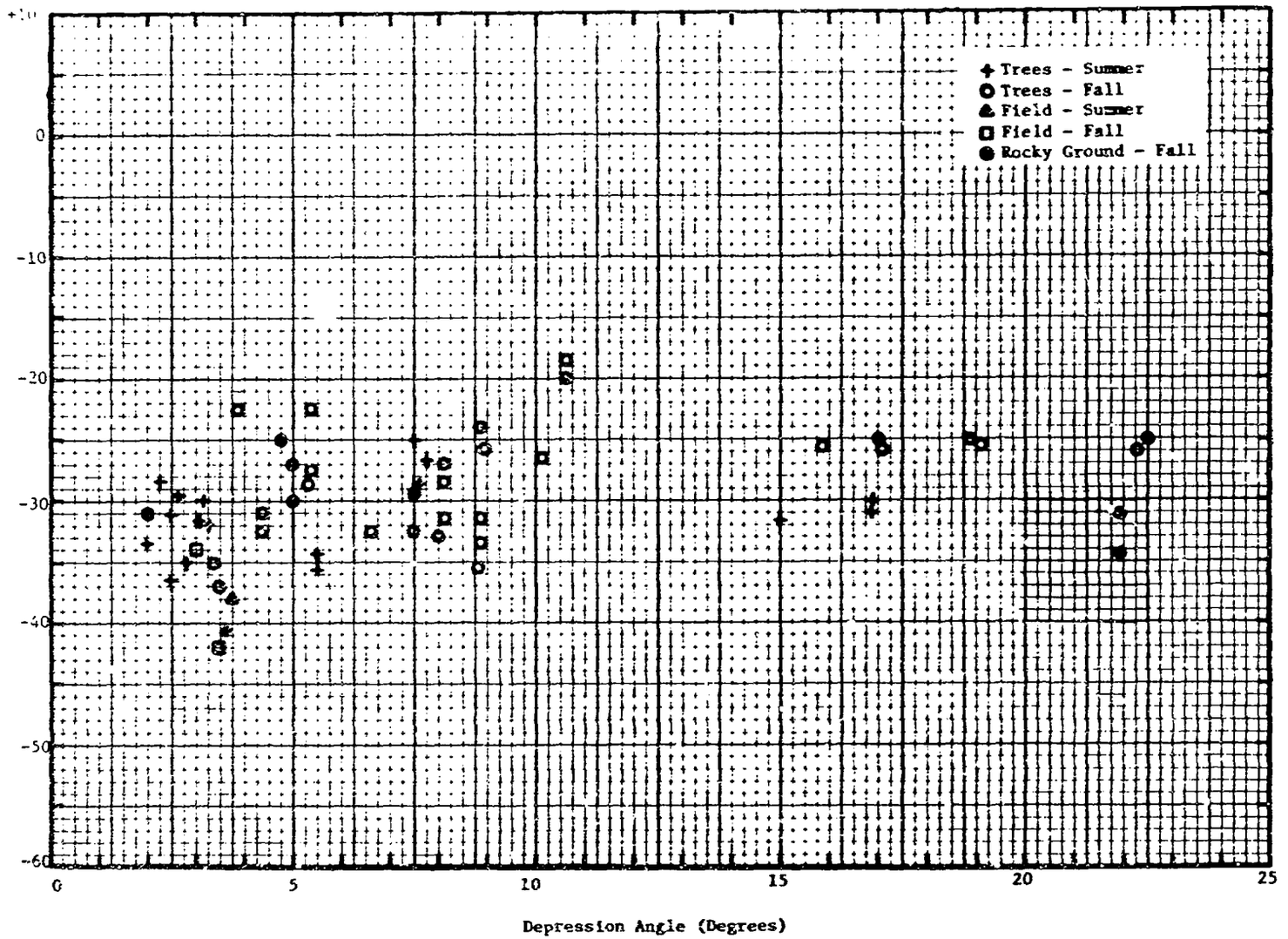

Figure 18. Comparison of the average backscatter per unit area measured in the summer and in the fall; 9.5 GHz.

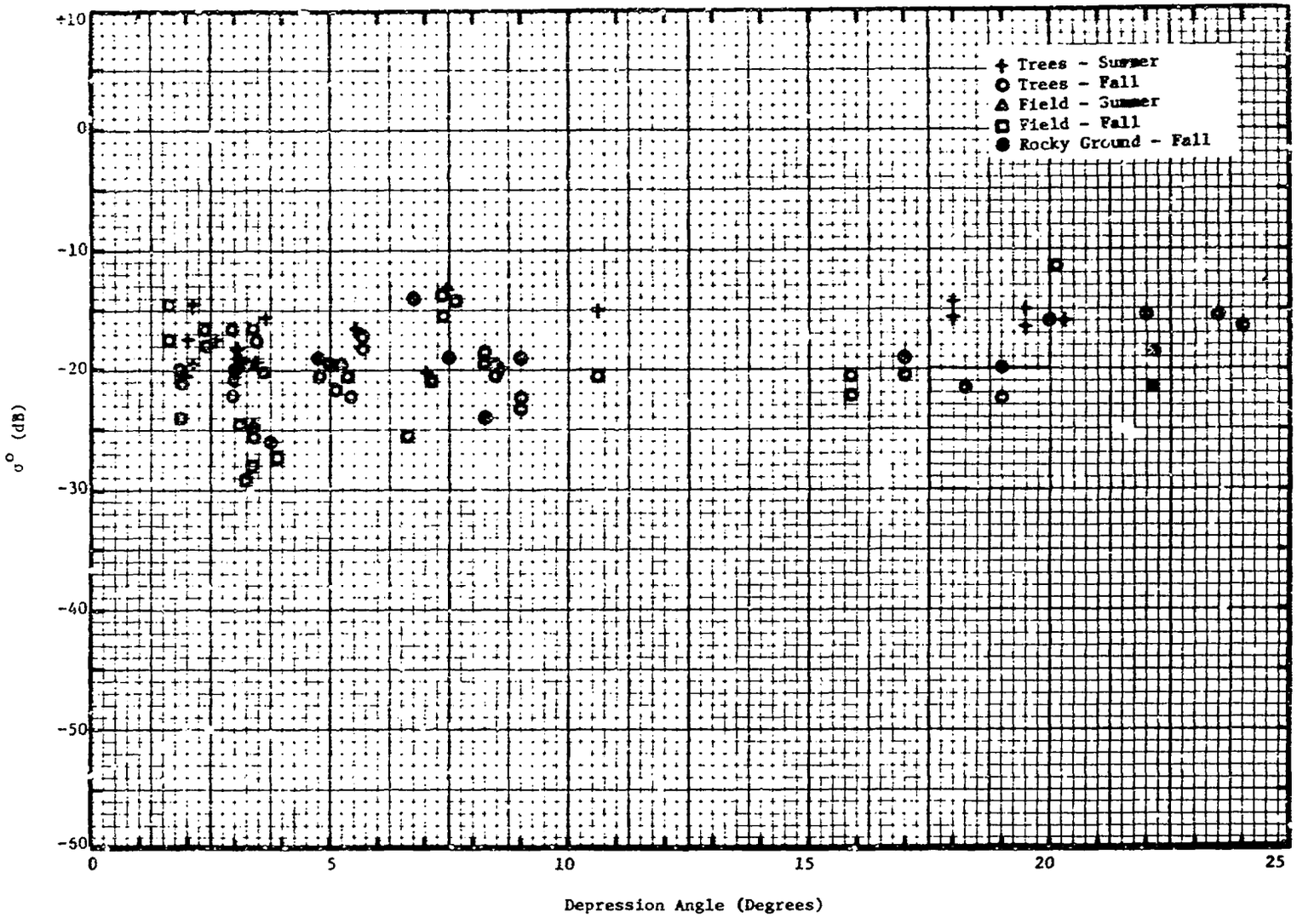

Figure 19. Comparison of the average backscatter per unit area measure in the summer and in the fall; 35 GHz.

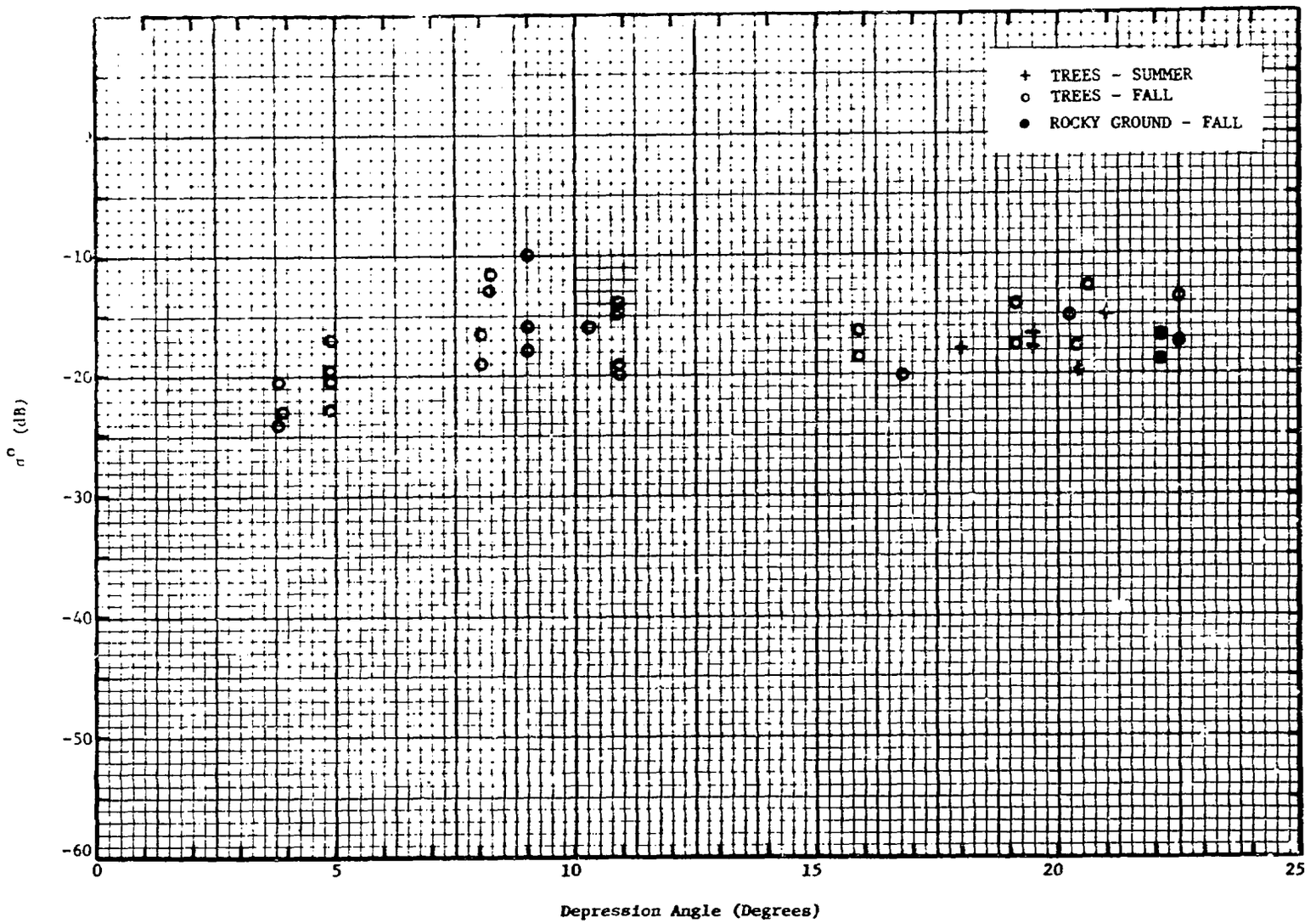

Figure 20. Comparison of the average backscatter per unit area measured in the summer and in the fall; 95 GHz.

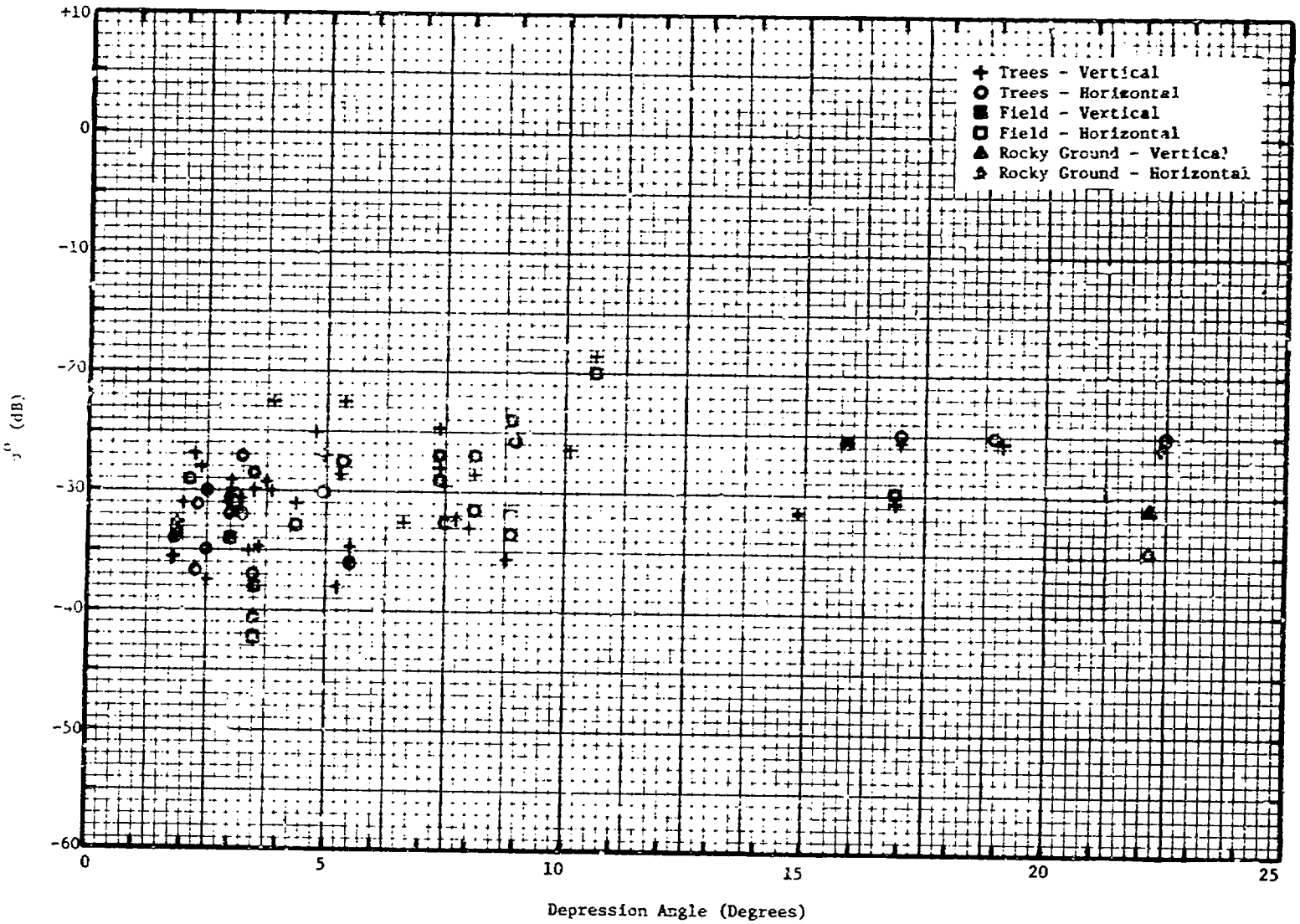

Figure 21. Comparison of the average backscatter per unit area for vertical and horizontal polarizations; 9.5 GHz.

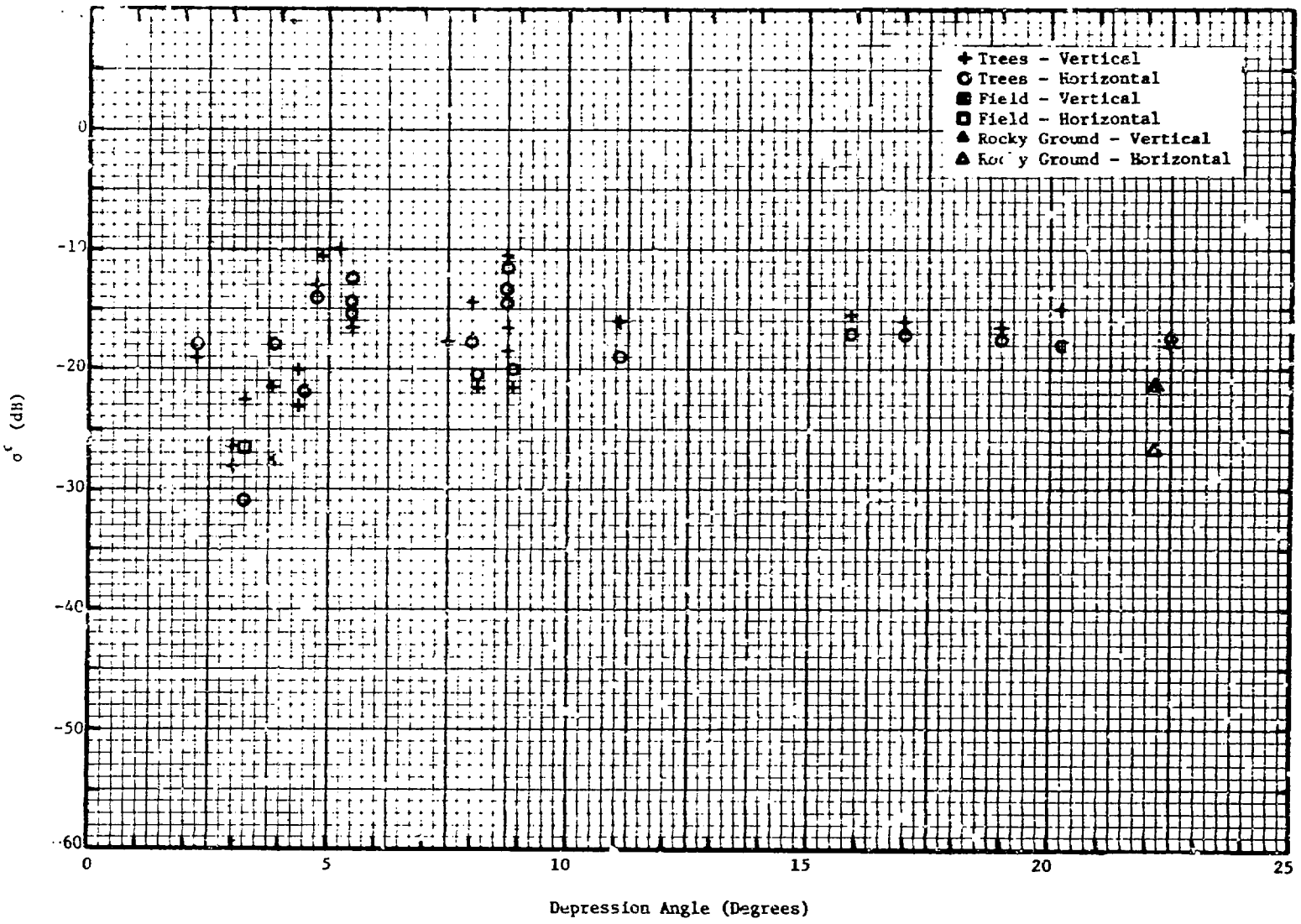

Figure 22. Comparison of the average backscatter per unit area for vertical and horizontal polarizations; 16.5 GHz.

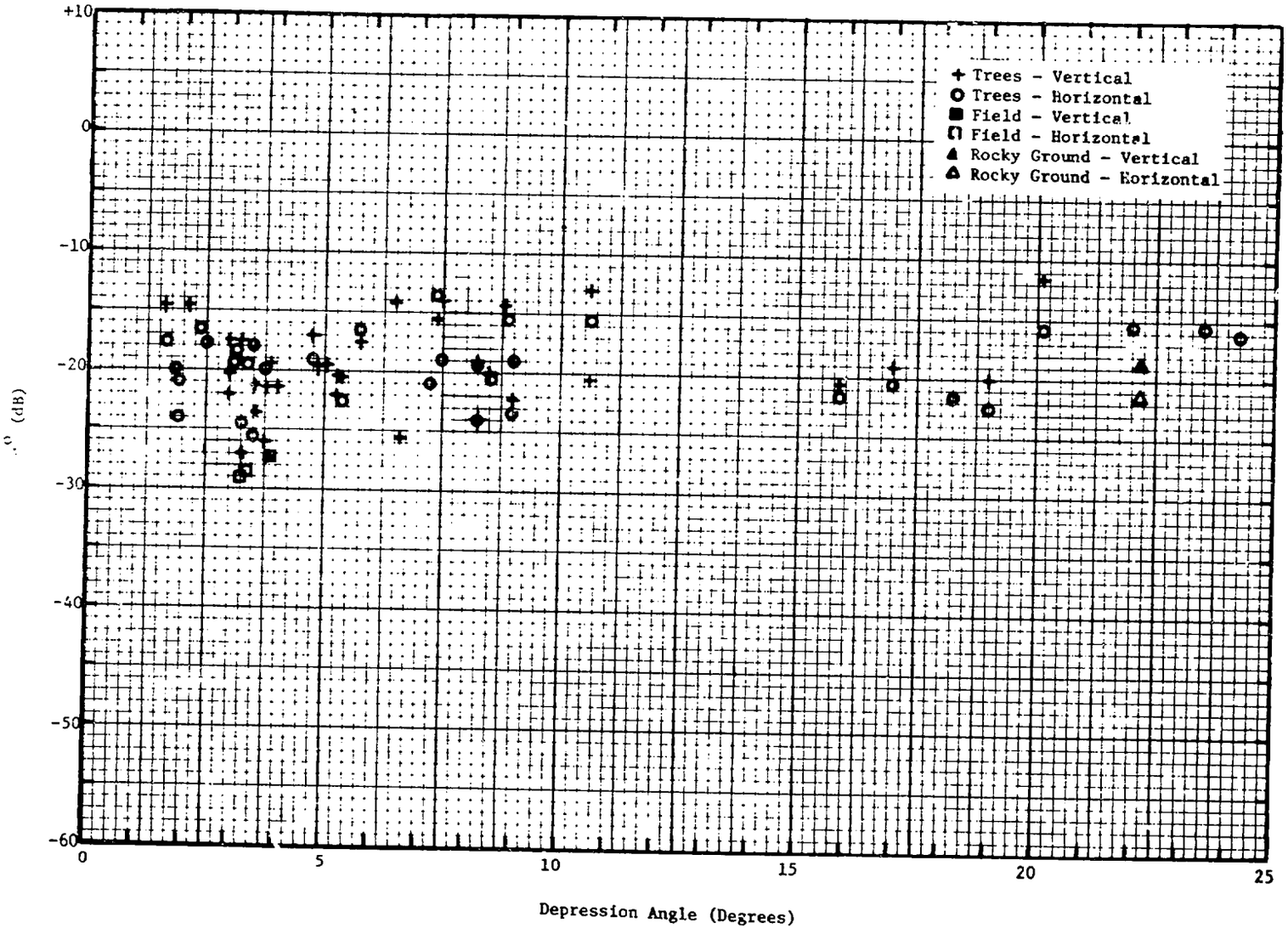

Figure 23. Comparison of the average backscatter per unit area for vertical and horizontal polarizations; 35 GHz.

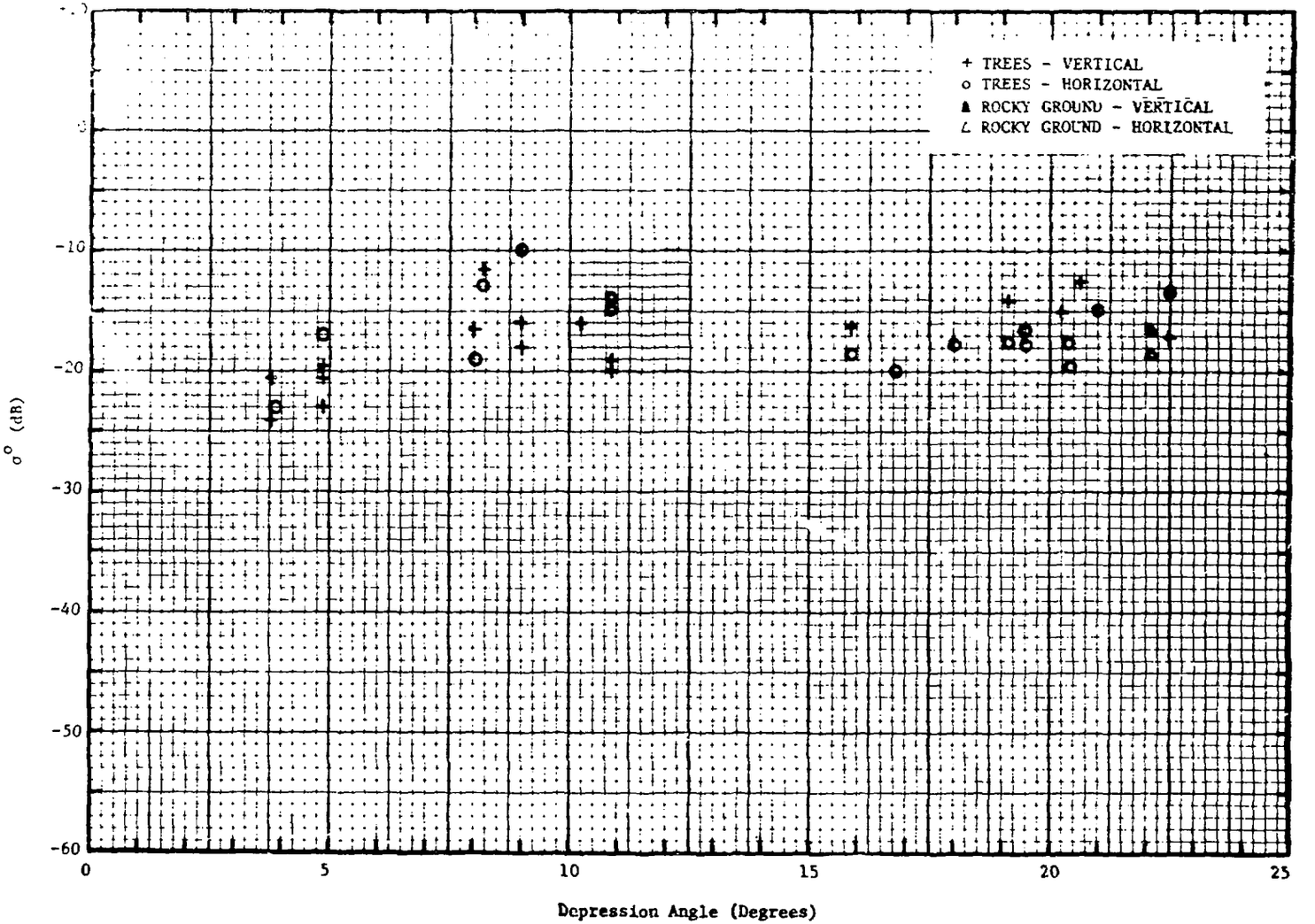

Figure 24. Comparison of the average backscatter per unit area for vertical and horizontal polarizations; 95 GHz.

horizontal polarization; however, the polarization dependence in backscatter is less than the scatter in the data (about 12 dB average.) The average value of the backscatter from trees was approximately independent of angle above about 5° depression angle, and equaled -27 dB at 9.5 GHz, - 18 dB at 16.5 GHz and 35 GHz, and -16 dB for 95 GHz. The average value for the grassy field was -37 dB at 9.5 GHz, -27 dB at 16.5 GHz and 35 GHz; no data on the field were obtained at 95 GHz. because the range was too great. The average values of the return from the rocky area were -33 dB at 9.5 GHz, -24 dB at 16.5 GHz, -20 dB at 35 GHz and 95 GHz.

The data appear to have a change in slope between 3 and 5° depression angle where σ° drops off rapidly. This has been reported by other experimenters at frequencies of X-band and below, and is thus consistent with previous results although the break is not as pronounced as previously reported. This is probably due to the extremely short pulse lengths used for this experiment which result in the illuminated beam area at low grazing angles being limited by the pulse length rather than the vertical beamwidth. Thus the equivalent illuminated ground area does not increase as fast at low angles as would otherwise be the case.

3. Amplitude Fluctuations

As discussed in a previous section, the methods of recording data on received signals from targets during these tests utilizing a range-gated sampler and a magnetic tape recorder, allowed the statistics of signal fluctuations to be computed with the data facility. Thus the cumulative probabilities of the amplitude fluctuations of the return from a radar cell defined by the antenna azimuth beamwidth and the transmitted pulse length were obtained.

Figures 25 through 28 give typical cumulative distributions for the returns from deciduous trees at 9.5, 16,5, 35, and 95 GHz. The most important conclusion to be drawn from the figures is that all the distributions are nearly log normal. (Log normal plots as a straight line on these figures.) While this was not true for every run made, it was true for the majority of

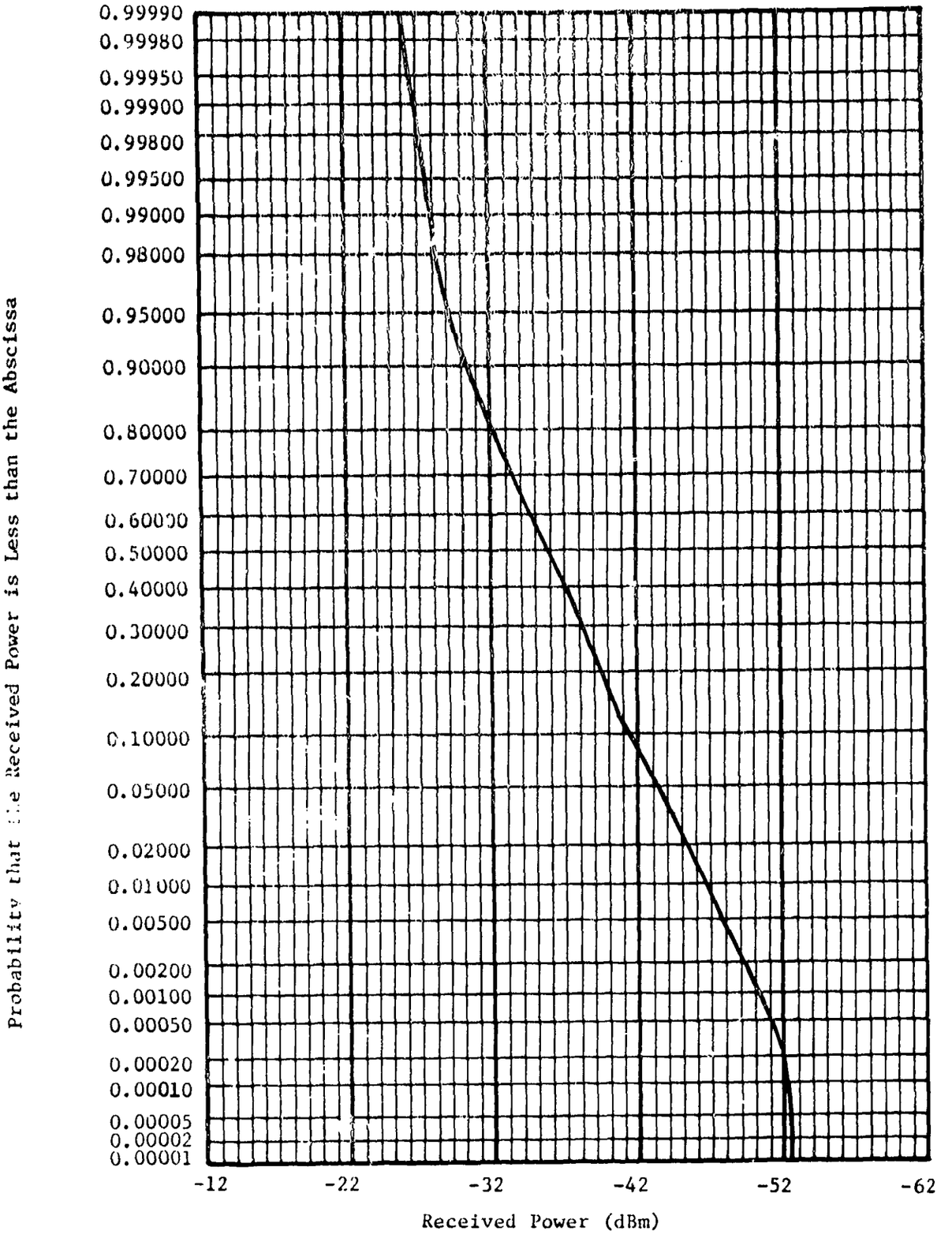

Figure 25. Cumulative probability distribution of the received power from deciduous trees; 9.5 GHz, horizontal polarization, and 4.1° depression angle.

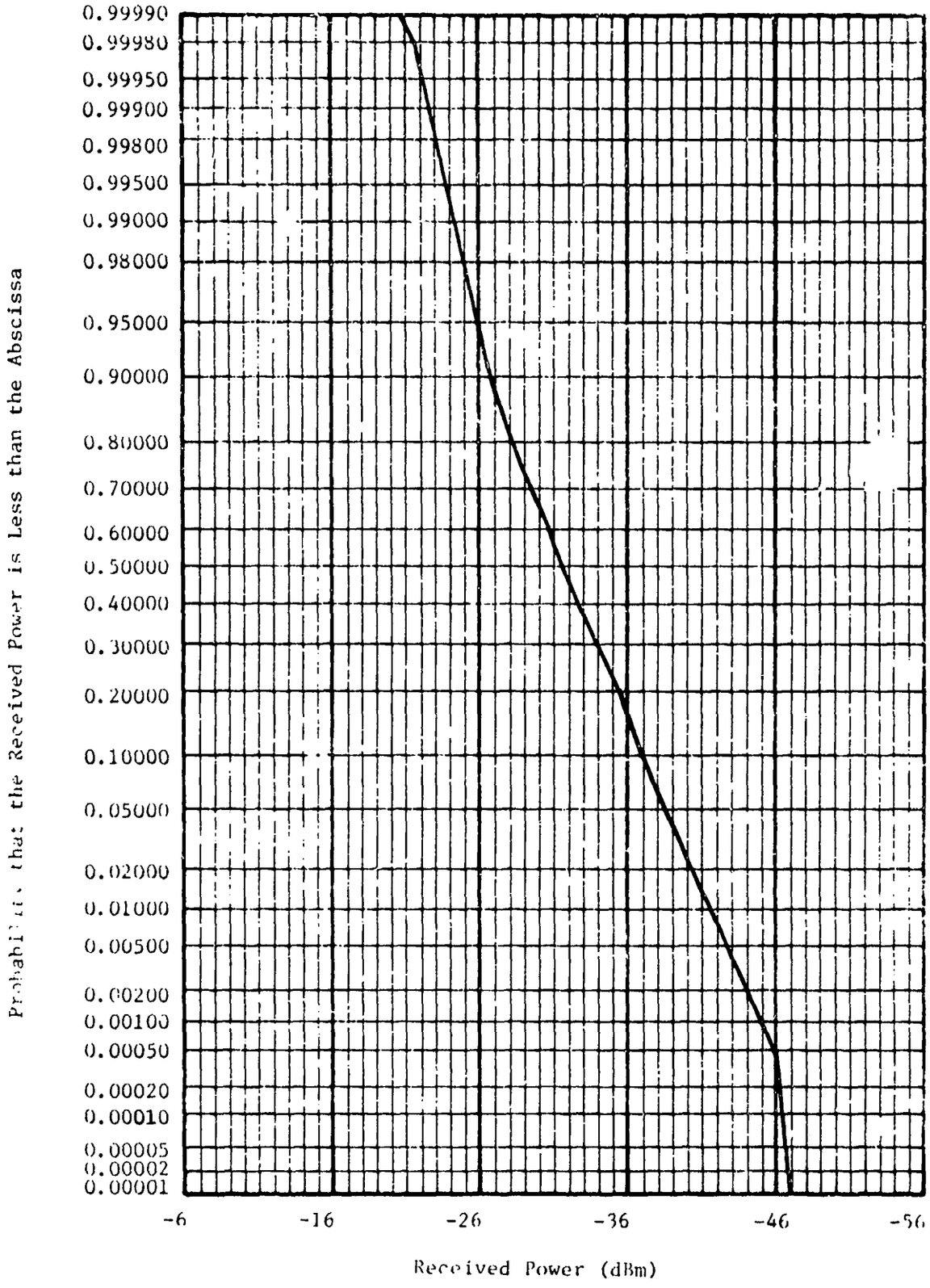

Figure 26. Cumulative probability distribution of the received power from deciduous trees; 16.5 GHz, horizontal polarization, and 4.1° depression angle.

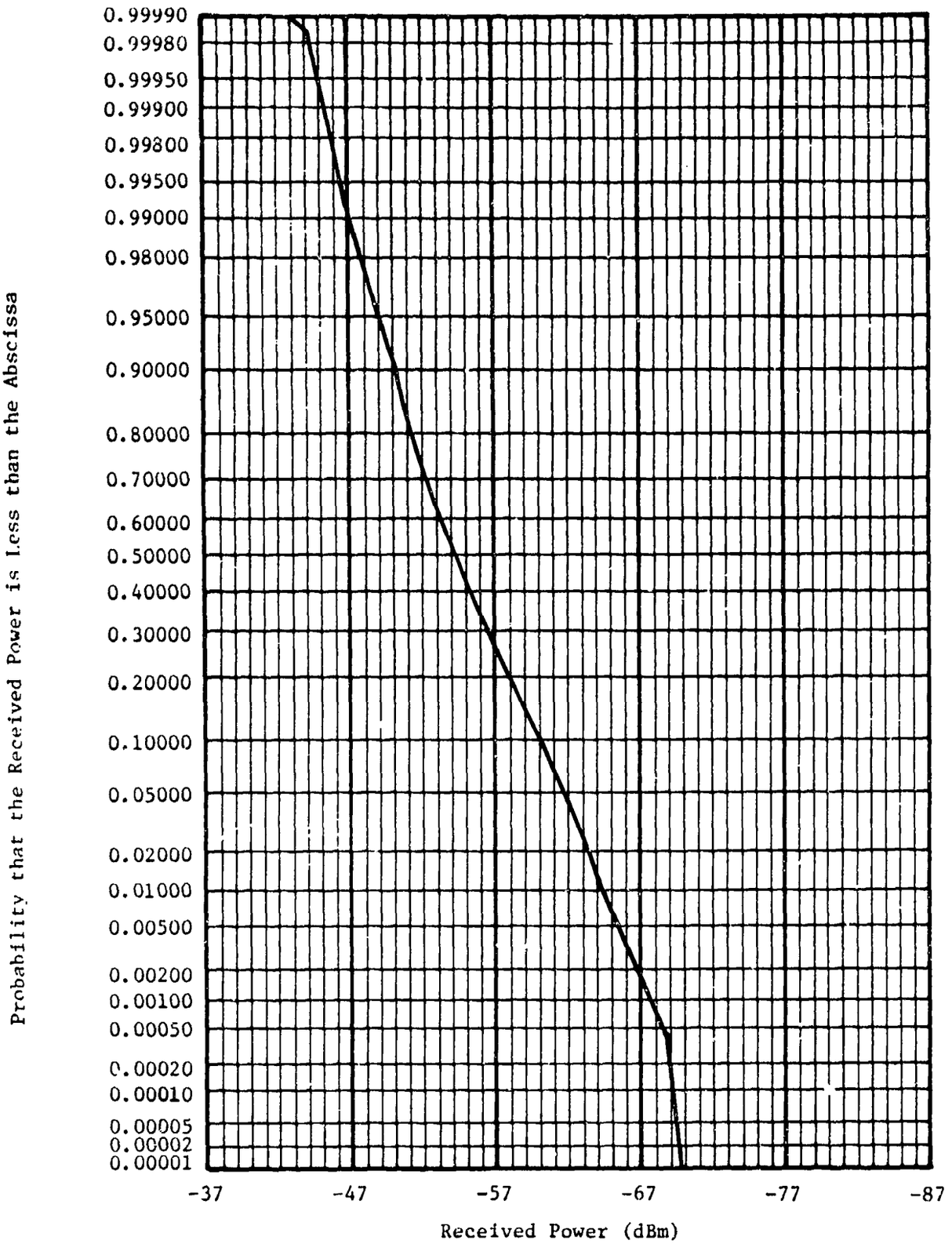

Figure 27. Cumulative probability distribution of the received power from deciduous trees; 35 GHz, horizontal polarization, and 4.1° depression angle.

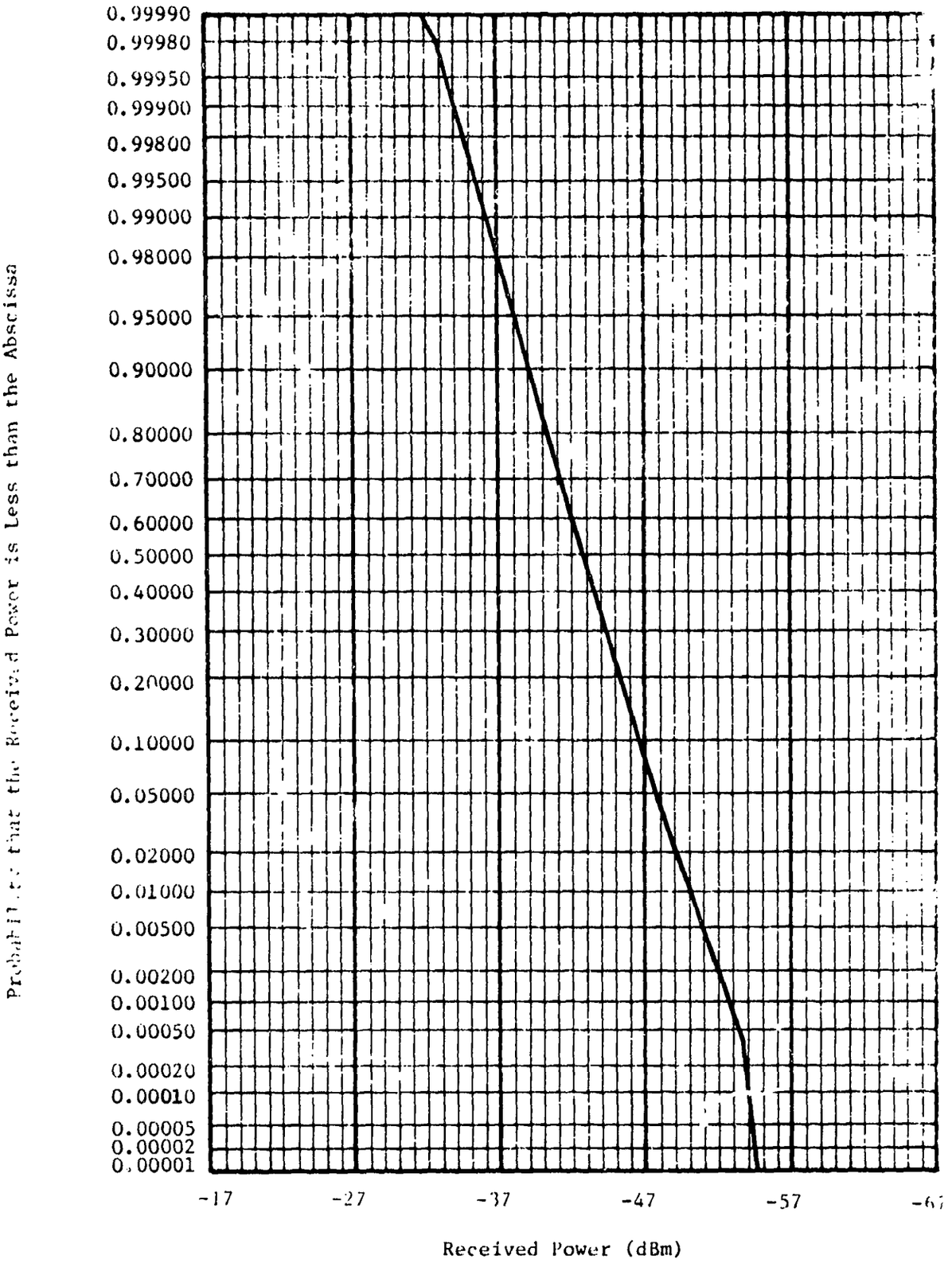

Figure 28. Cumulative probability distribution of the received power from deciduous trees; 95 GHz, horizontal polarization, and 4.1° depression angle.

the data. This, of course, allows the data to be modeled very easily when computing target-to-clutter ratios for radar system design.

If the clutter distributions are log normal, then one can talk about the widths of the distributions in terms of the standard deviations of the distributions. Table 5 gives the averages of the calculated standard deviations for each type of clutter measured during the tests. As can be seen from the table the standard deviations for trees increase slightly with transmitted frequency, although for pine trees the standard deviations appear much larger at 95 GHz than at the other frequencies. The standard deviations appear independent of frequency and are much lower for the grassy field and rocky area than for trees, which is to be expected since these areas have a relatively constant return. The standard deviations for trees range about 3-5 dB higher than for a corner reflector, which represents a large stationary target.

Figures 29 through 32 give the probability densities for the standard deviations for deciduous trees, pine trees, and mixed trees at 9.5, 16.5, 35, and 95 GHz. Few differences in the frequency of occurrence of a given value of the standard deviation exist for a given tree type except at 95 GHz. At 95 GHz both the deciduous and pine tree distributions are bimodal, although the values from deciduous trees appear to have a wider spread over the range of 2 dB to 12 dB.

The large standard deviations (greater than 6 dB) appear to correlate well with wind speeds greater than 10 mph and in a direction parallel to line-of-sight from radar to target area. This trend probably exists at the lower frequencies but did not show up in these data.

Figures 33 through 36 show the polarization dependence of the probability density functions for the standard deviations. As can be seen, there is little polarization dependence although vertical appears to have slightly higher values.

TABLE 5.

SUMMARY OF THE STANDARD DEVIATION
FOR VARIOUS CLASSES OF CLUTTER

Clutter Type	Polarization	9.5 GHz	16.5 GHz	35 GHz	95 GHz
		Average Value of Standard Deviation (dB)			
Deciduous Trees-	Vertical	3.9	-	4.7	-
Summer	Horizontal	4.0	-	4.0	5.4
	Average	4.0	-	4.3	5.4
Deciduous Trees -	Vertical	3.9	4.2	4.4	6.4
Fall	Horizontal	3.9	4.3	4.3	5.3
	Average	3.9	4.2	4.3	5.0
Pine Trees	Vertical	3.5	3.7	3.7	6.8
	Horizontal	3.3	3.8	4.2	6.3
	Average	3.4	3.7	3.9	6.5
Mixed Trees-	Vertical	4.3	-	4.0	-
Summer	Horizontal	4.6	-	4.2	-
	Average	4.4	-	4.1	-
Mixed Trees -	Vertical	4.1	4.1	4.7	6.3
Fall	Horizontal	4.5	4.3	4.6	5.0
	Average	4.4	4.2	4.6	5.4
Grassy Field	Vertical	1.5	-	1.7	2.0
	Horizontal	1.0	1.2	1.3	-
	Average	1.3	1.2	1.4	2.0
Rocky Area	Vertical	1.1	2.2	1.8	1.6
	Horizontal	1.2	1.7	1.7	1.7
	Average	1.1	1.9	1.8	1.7
10" Corner Reflector - (Located in Grassy Field)		1.0	1.0	1.2	1.2

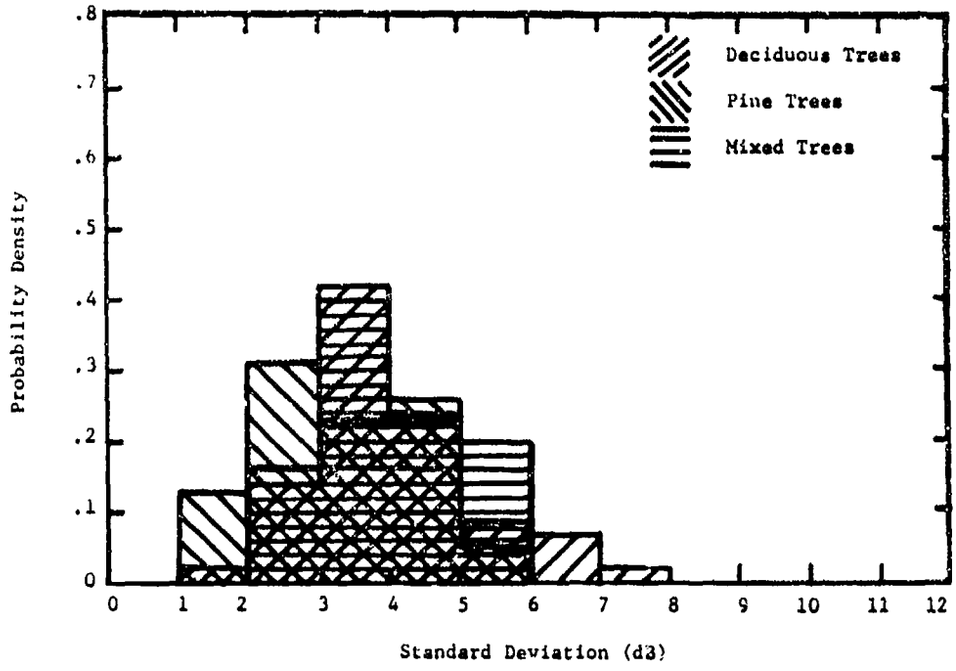

Figure 29. Probability density function for the measured standard deviations of the amplitude distributions as a function of tree type; 9.5 GHz.

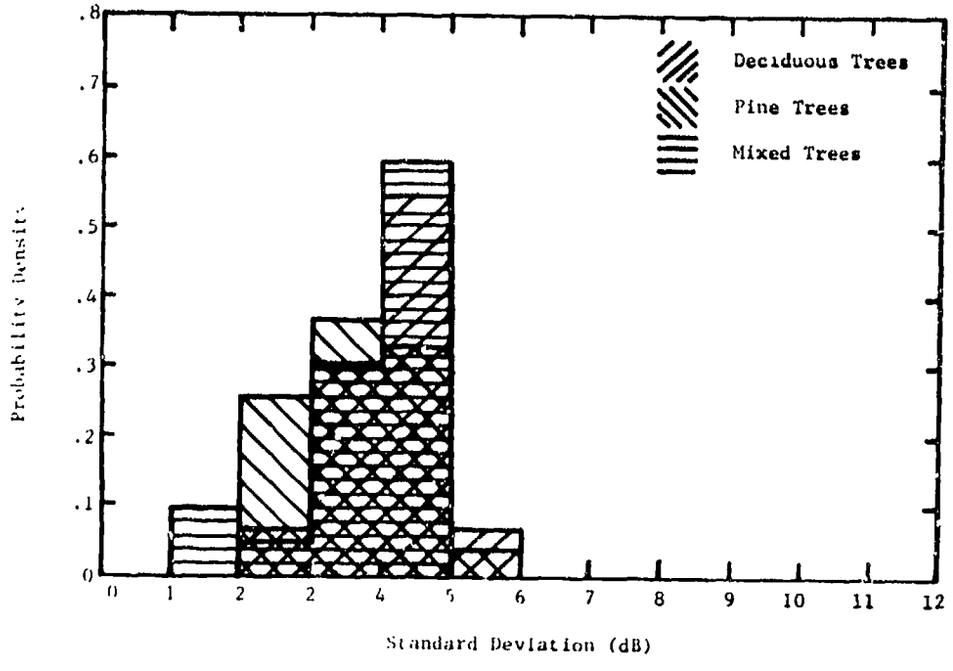

Figure 30. Probability density functions for the measured standard deviations of the amplitude distributions as a function of tree type; 16.5 GHz.

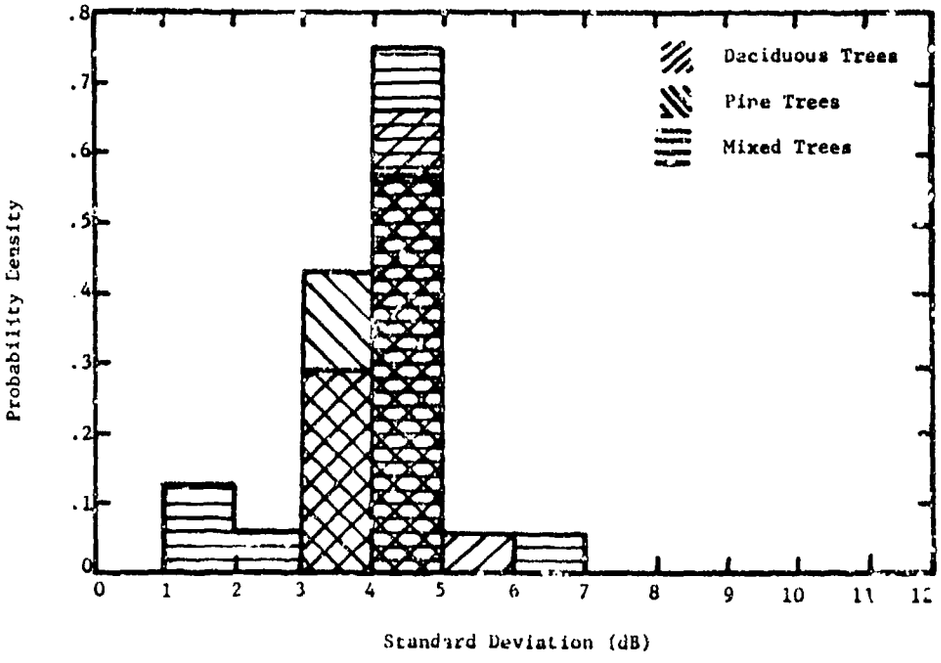

Figure 31. Probability density functions for the measured standard deviations of the amplitude distributions as a function of tree type; 35 GHz.

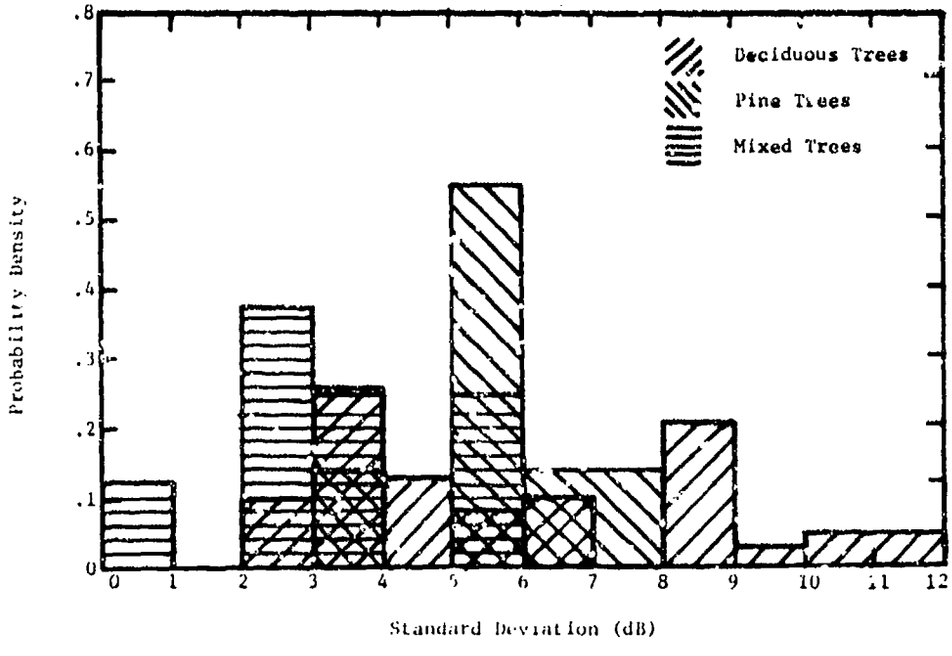

Figure 32. Probability density functions for the measured standard deviations of the amplitude distributions as a function of tree type; 95 GHz.

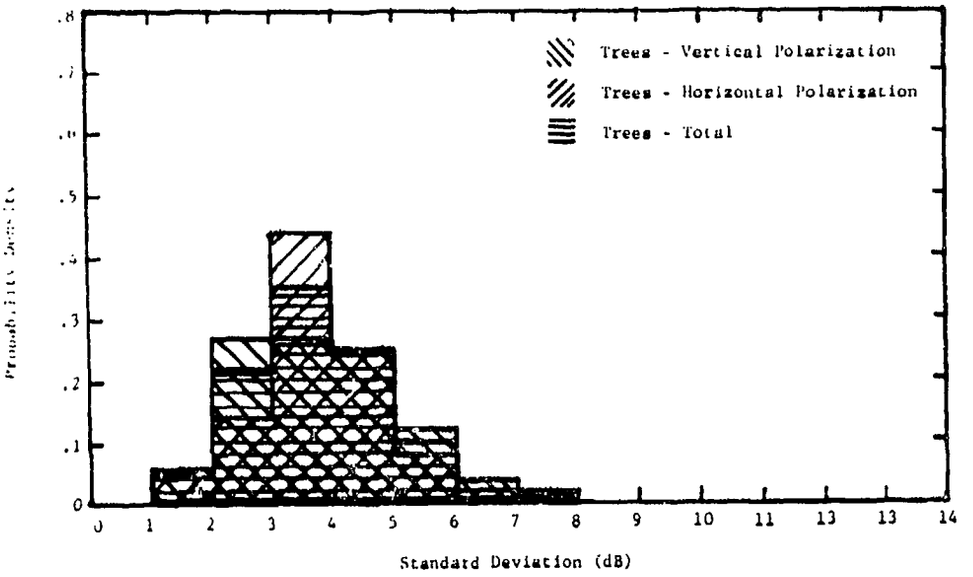

Figure 33. Probability density functions for the measured standard deviations of the amplitude distributions as a function of polarization; 9.5 GHz.

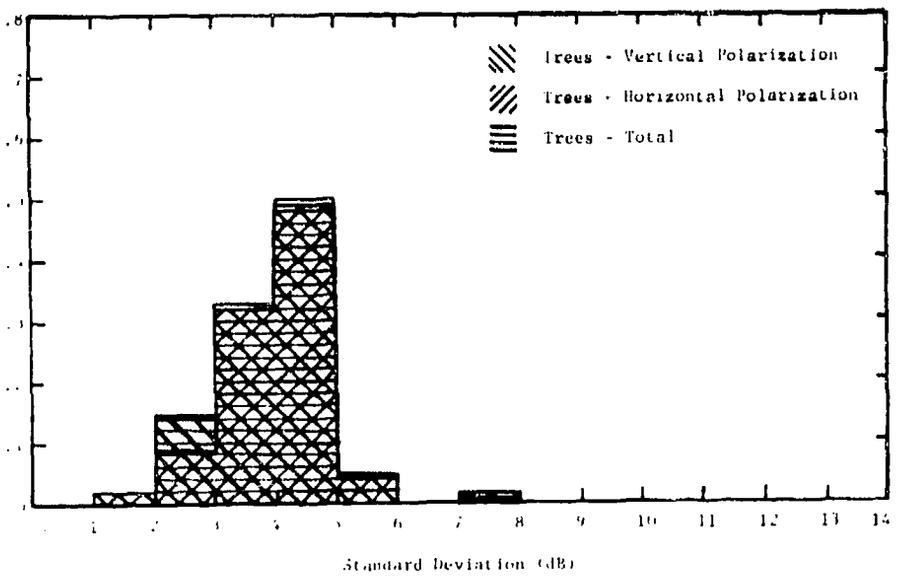

Figure 34. Probability density functions for the measured standard deviations of the amplitude distributions as a function of polarization; 16.5 GHz.

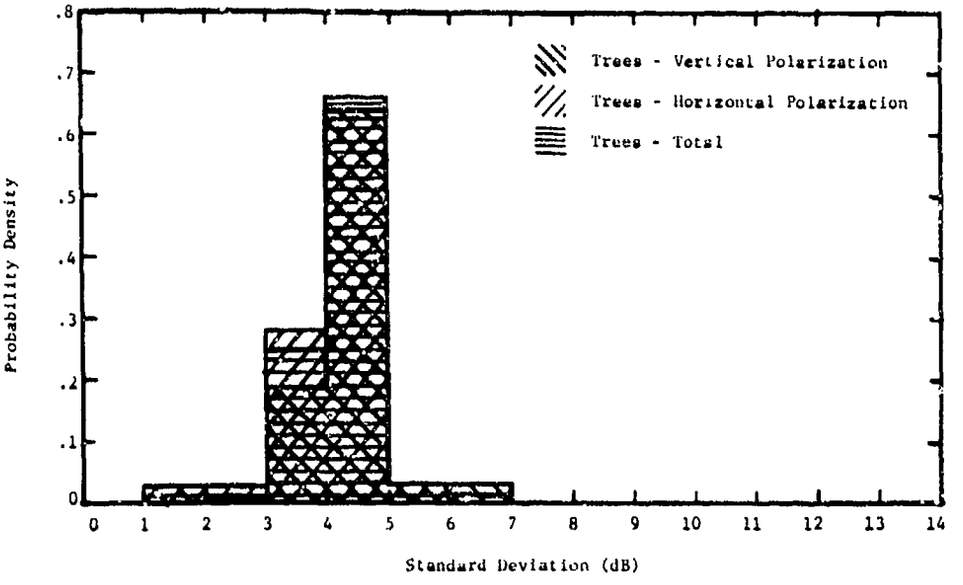

Figure 35. Probability density functions for the measured standard deviations of the amplitude distributions as a function of polarization; 35 GHz.

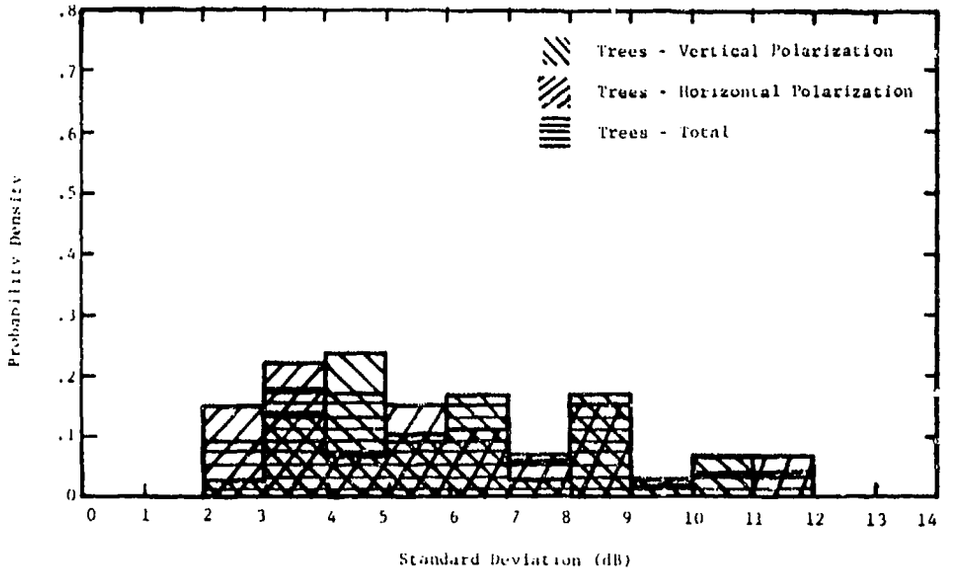

Figure 36. Probability density functions for the measured standard deviations of the amplitude distributions as a function of polarization; 95 GHz.

4. Spectral Distributions

All the radars employed in these tests were incoherent systems so that it was not possible to obtain the coherent Doppler frequency spectrum of the return signals from the land clutter. However, it was possible to determine the frequency components without coherent phase relationship in the power spectrum. The equipment and data-processing techniques for obtaining the spectra are presented in a previous section of this report.

For the purpose of comparing data from this project to that obtained by previous investigators, it is important to note differences in the measurement radars employed as compared with those used by previous investigators. All of the radars used in this investigation employed log-if amplifiers. Previous investigators have used linear receiver systems. Thus, in order to obtain the linear frequency spectrum from the logarithmic signals so as to be directly comparable to previous results, the signals must be properly formated prior to computation of the fast Fourier transform. However, since many radar systems are currently designed with logarithmic receivers, it was decided to also process the data in the same form as they were recorded, i.e. as the output of a logarithmic receiver. This will allow system designers to use the final results directly. Thus, if a Doppler processor is used with linear receivers, the spectral width expected from deciduous trees will be as shown in Figures 37 through 40 for vertical polarization, and for a log receiver the spectral widths will be as shown in Figures 41 through 44. Horizontal polarization is not shown as the spectra are similar to the vertical distributions.

Figures 37 through 40 indicate that the frequency spectra slopes can be fit well by a cubic function at 9.5 GHz and 16.5 GHz and by a quadratic function at 95 GHz, with 35 Ghz being fit best by a power function with a 2.5 power exponent. Many investigators are currently using Gaussian shaped slopes for clutter spectra rolloff which could lead to large errors between predicted and actual MTI performance. The corner frequencies can be seen to be both windspeed and transmitted frequency dependent increasing with increasing windspeed and increasing frequency. A dependence of the corner frequencies on the wind direction, i.e., parallel or perpendicular to the radar line-of-sight direction, appears to exist; although the data were scattered, it appears that the

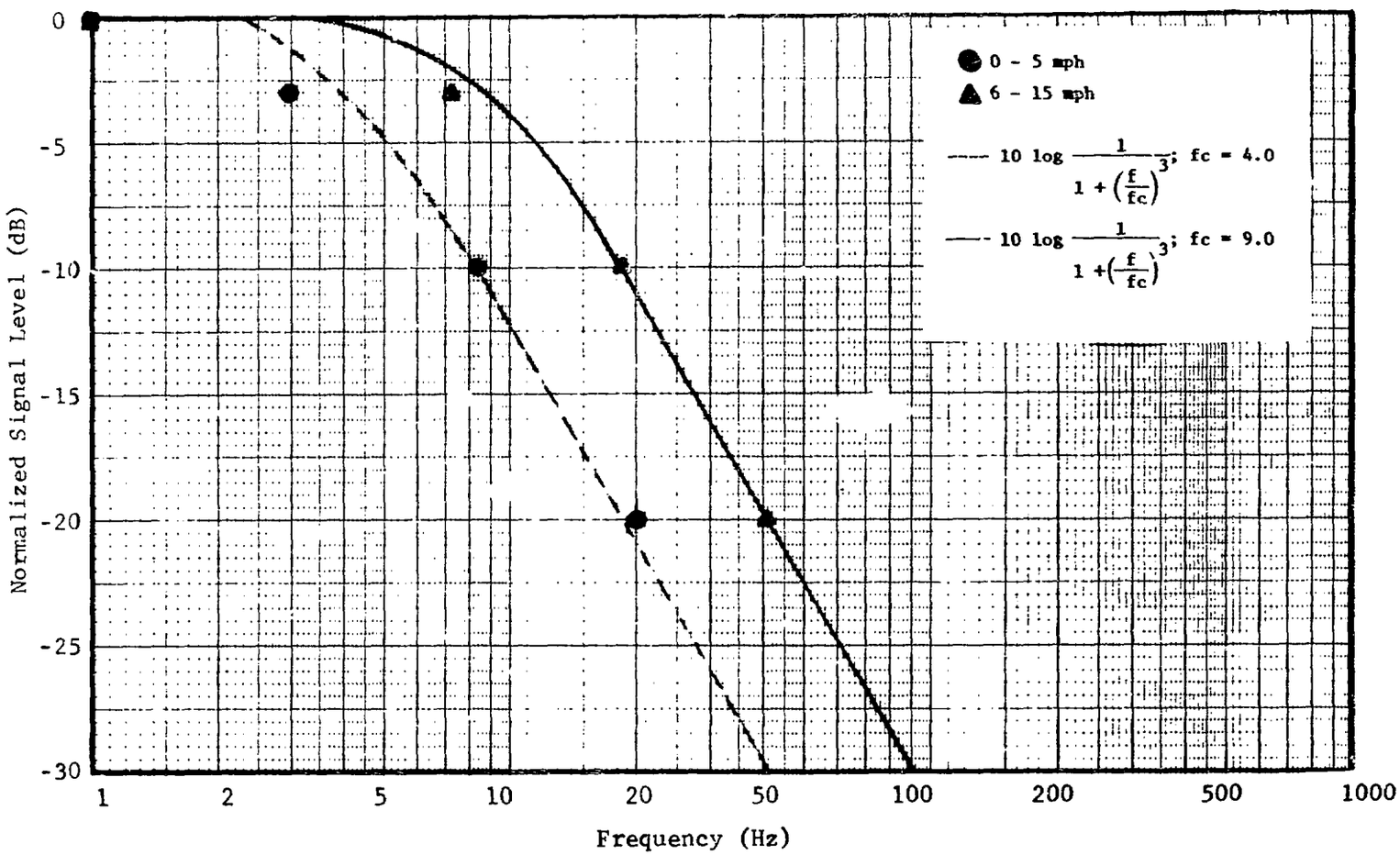

Figure 37. Normalized frequency spectrum of the return from deciduous trees for two ranges of wind speed; 9.5 GHz, vertical polarization (linear receiver).

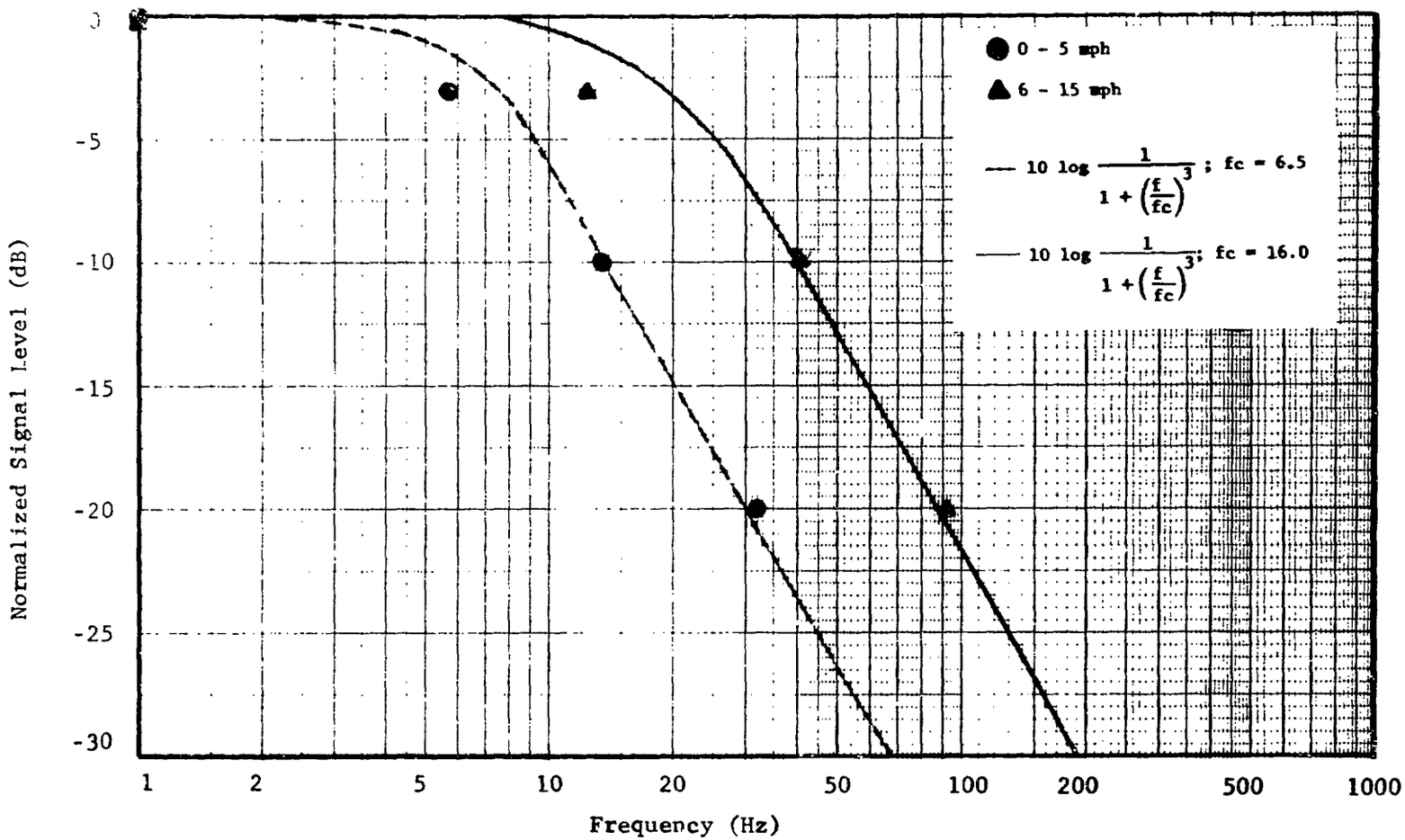

Figure 38. Normalized frequency spectrum of the return from deciduous trees for two ranges of wind speed; 16.5 GHz, vertical polarization (linear receiver).

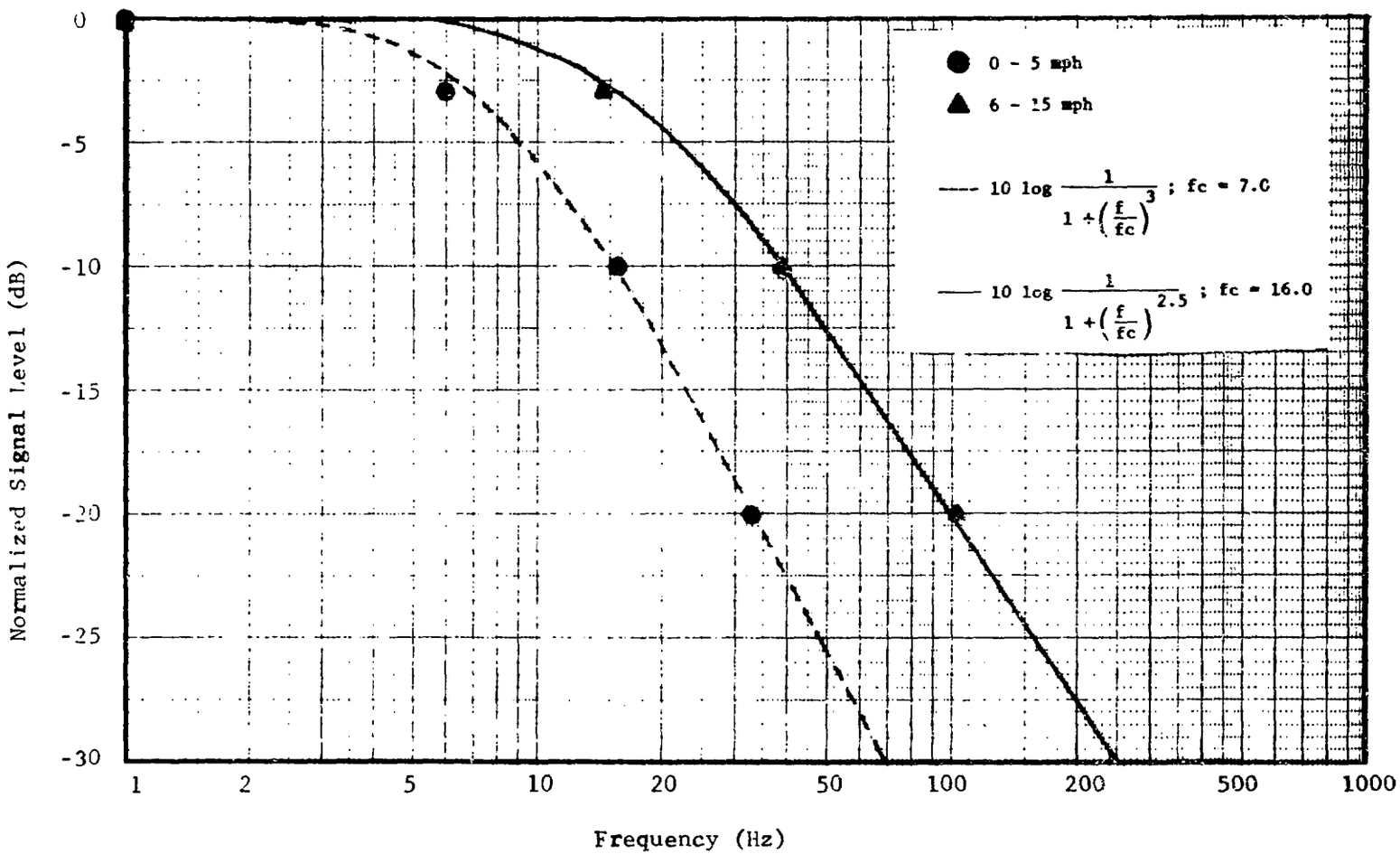

Figure 39. Normalized frequency spectrum of the return from deciduous trees for two ranges of wind speed; 35 GHz, vertical polarization (linear receiver).

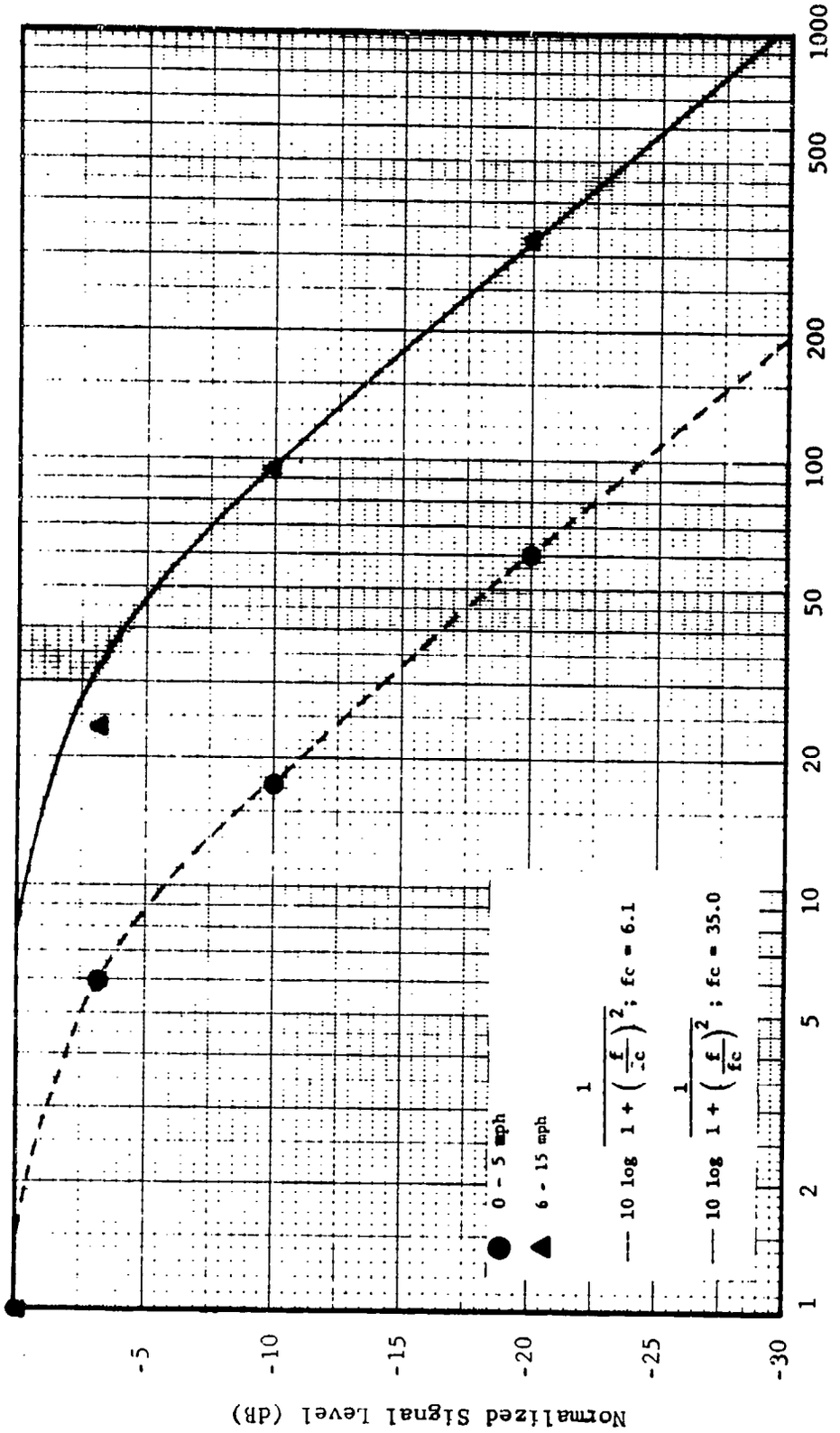

Figure 40. Normalized frequency spectrum of the return from deciduous trees for two ranges of wind speed; 95 GHz, vertical polarization (linear receiver).

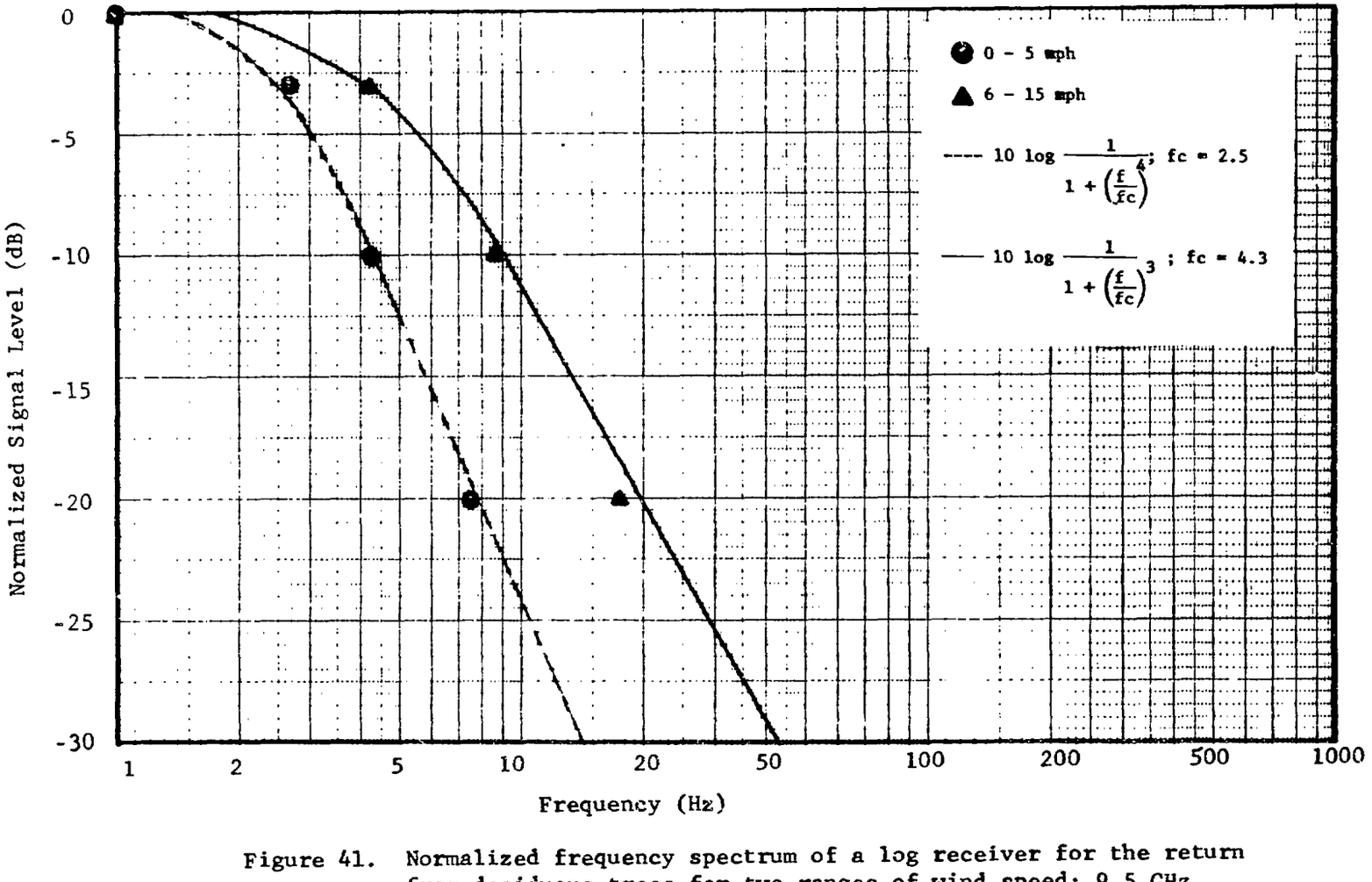

Figure 41. Normalized frequency spectrum of a log receiver for the return from deciduous trees for two ranges of wind speed; 9.5 GHz. vertical polarization.

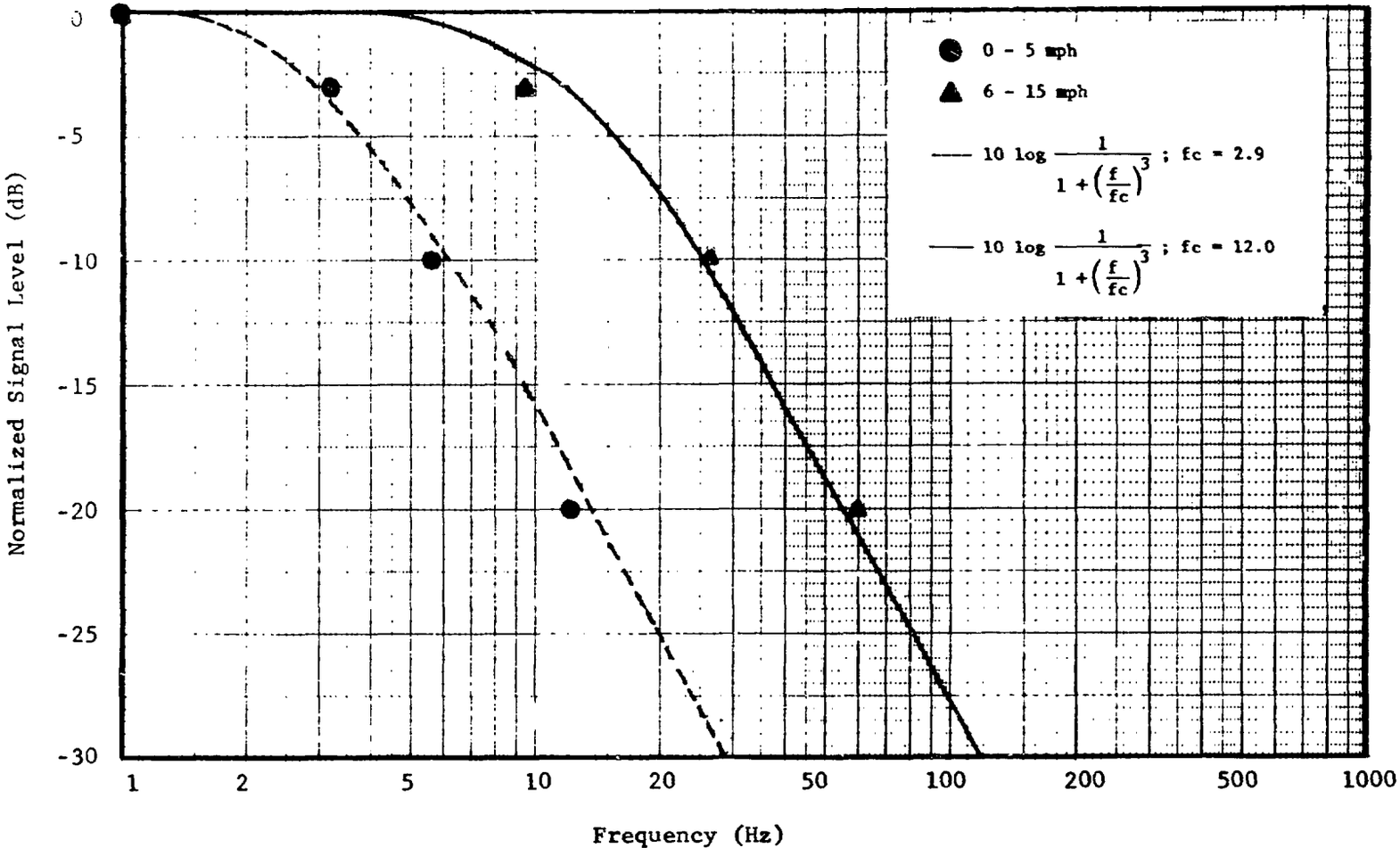

Figure 42. Normalized frequency spectrum of a log receiver for the return from deciduous trees for two ranges of wind speed; 16.5 GHz, vertical polarization.

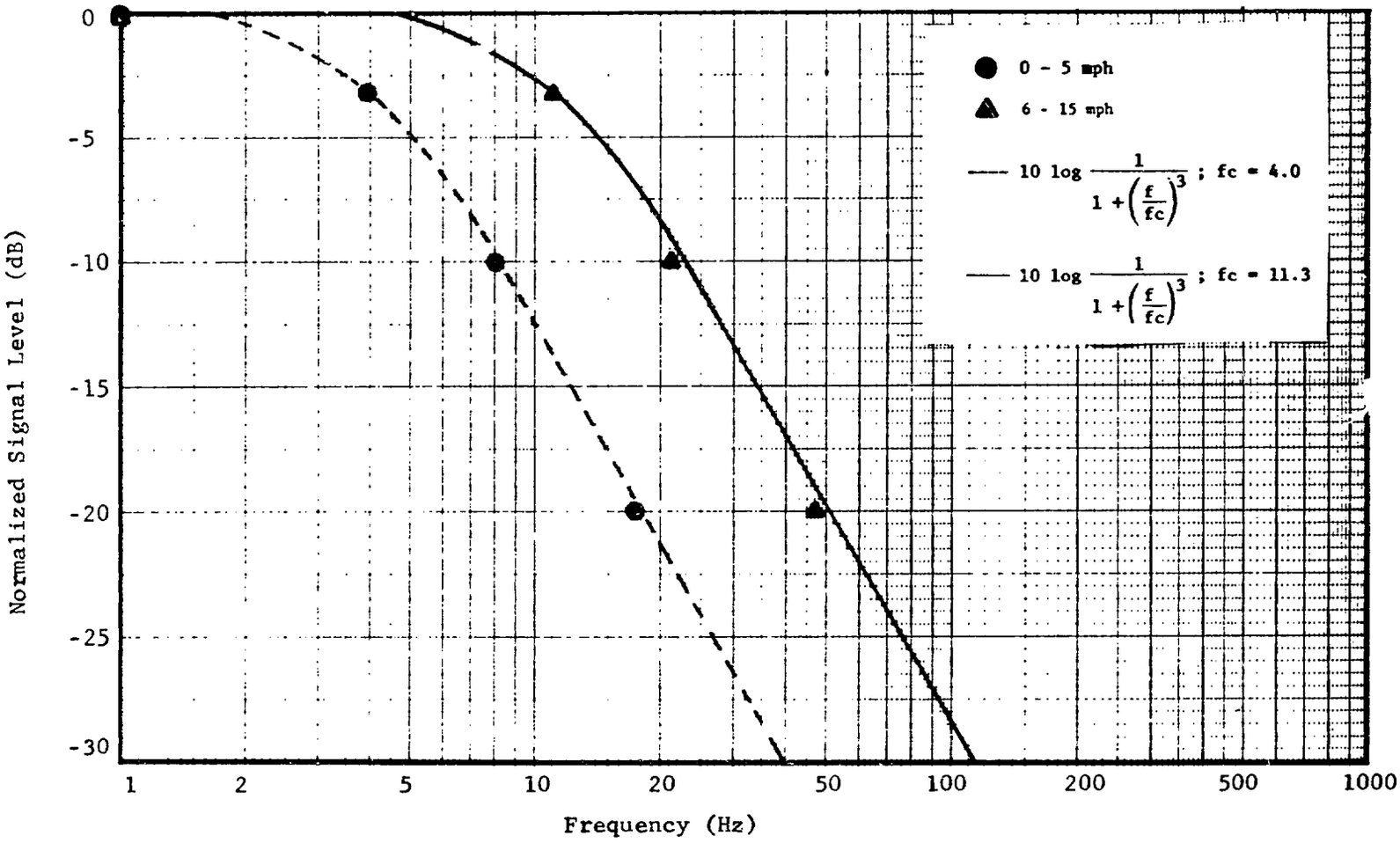

Figure 43. Normalized frequency spectrum of a log receiver for the return from deciduous trees for two ranges of wind speed; 35 GHz, vertical polarization.

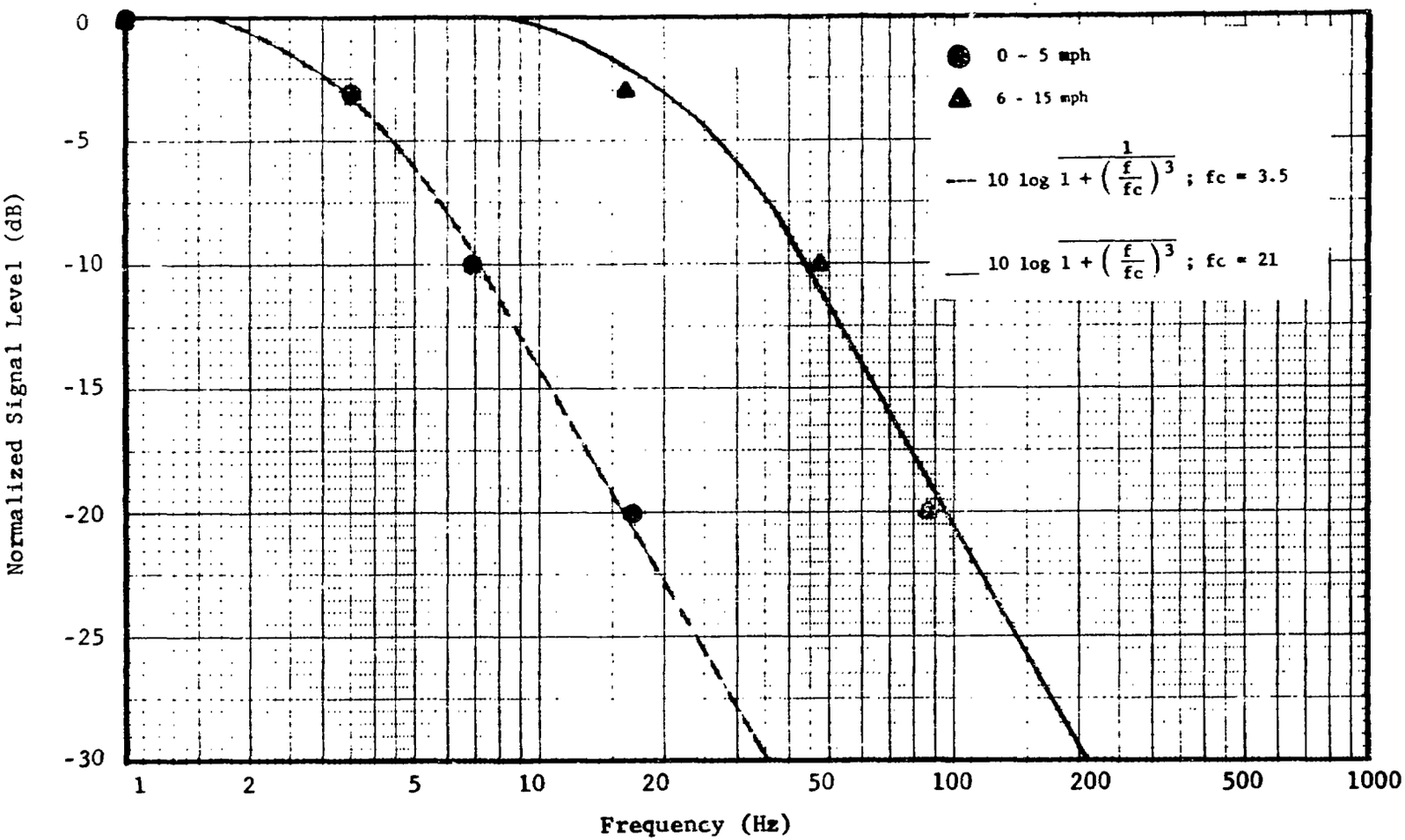

Figure 44. Normalized frequency spectrum of a log receiver for the return from deciduous trees for two ranges of wind speed; 95 GHz, vertical polarization.

corner frequencies for individual data runs tended to be larger when the wind direction was parallel to the radar line-of-sight.

It should be noted that the results of the 9.5 GHz data given here compare favorably with results obtained by Fishbein [9] for X-band and windspeeds of 10 to 15 mph. He determined that land clutter could be fitted with a cubic function with a corner frequency of 6.7 Hz, whereas the data obtained at 9.5 GHz shown in Figure 37 is best fitted by a cubic function with a corner frequency of 9.0 Hz. The excellent agreement of the data presented here at X-band with previous data obtained by Fishbein serves to reinforce the validity of the results at the higher frequencies where no previous data have been obtained.

Figures 41 through 44 give the frequency spectra from deciduous trees for a system with a logarithmic receiver. By comparing these spectra for log receivers with the previously discussed spectra for linear receivers, the differences in the spectral characteristics can be determined. If the linear and logarithmic spectra for each transmitted frequency are compared it can be seen that the slopes are steeper for the log receiver case than for the linear receiver. The log spectra have a fourth power roll-off characteristic at 9.5 GHz and a cubic characteristic at 95 GHz as opposed to cubic and quadratic roll-offs for the two respective frequencies for the linear case. Furthermore the break frequencies are lower for the log receiver case. Thus, it can be seen that use of logarithmic receiver will reduce the clutter spectral widths appreciably. However, the target-to-clutter amplitude ratios will also be reduced so that the beneficial effects of the narrowing of the clutter spectrum by the use of a log receiver may be cancelled out.

5. Correlation Functions

The time required to obtain independent samples of radar returns from clutter is of concern to the designer of radars used in a space scanning mode. Since the auto-correlation function provides this basic information, the

radar backscatter data from trees were processed to obtain the linear correlation functions. The results of this investigation are shown in Figure 45. Each point on this figure is the result of an average of a number of data runs each consisting of 8 data samples lasting approximately 0.5 seconds. It is noted that in general as the windspeed increases and/or the radar frequency is increased, the decorrelation time decreases. This is consistent with the observation that the power spectrum distribution becomes wider as the windspeed and/or the radar frequency is increased.

It should be noted that in some cases where the windspeed was very low i.e., $\sim$ 2 mph, the decorrelation time was extremely long, i.e. several thousand milliseconds, at 9.5 GHz. This probably occurred when the major scatterers in the resolution cell were essentially at rest for a few seconds, so that their respective phases remained relatively constant. An example of this phenomenon is given in Appendix B. The conclusions to be [illegible] from the measured decorrelation time are that returns from trees will always be correlated on a pulse-to-pulse basis, and sometimes will be correlated over several scan periods, particularly for a rapid scan radar.

[illegible] correlation functions were obtained between the signals from the [illegible] radar systems when operating at exactly the same time. The 9.5 GHz [illegible] was used as the reference system and correlation functions between [illegible] systems, 9.5 and 35 GHz systems, and 9.5 and 95 GHz systems were computed.

Figures 50 through 51 give examples of the cross-correlation functions for two windspeeds, 2 mph and 8 mph. It should be noted that the dc levels of the signals have been suppressed so that these figures give only the correlation of the varying components of the respective returns.

As can be seen from the figures, the cross-correlations are quite low, typically less than 0.3. However, a periodic component does appear evident in the correlation functions; the frequency and amplitude of this periodic component increase with increasing wind speed and transmitted frequency. Since a 0.3 correlation coefficient or less between two signals is generally considered to indicate linear independence, the radar returns are

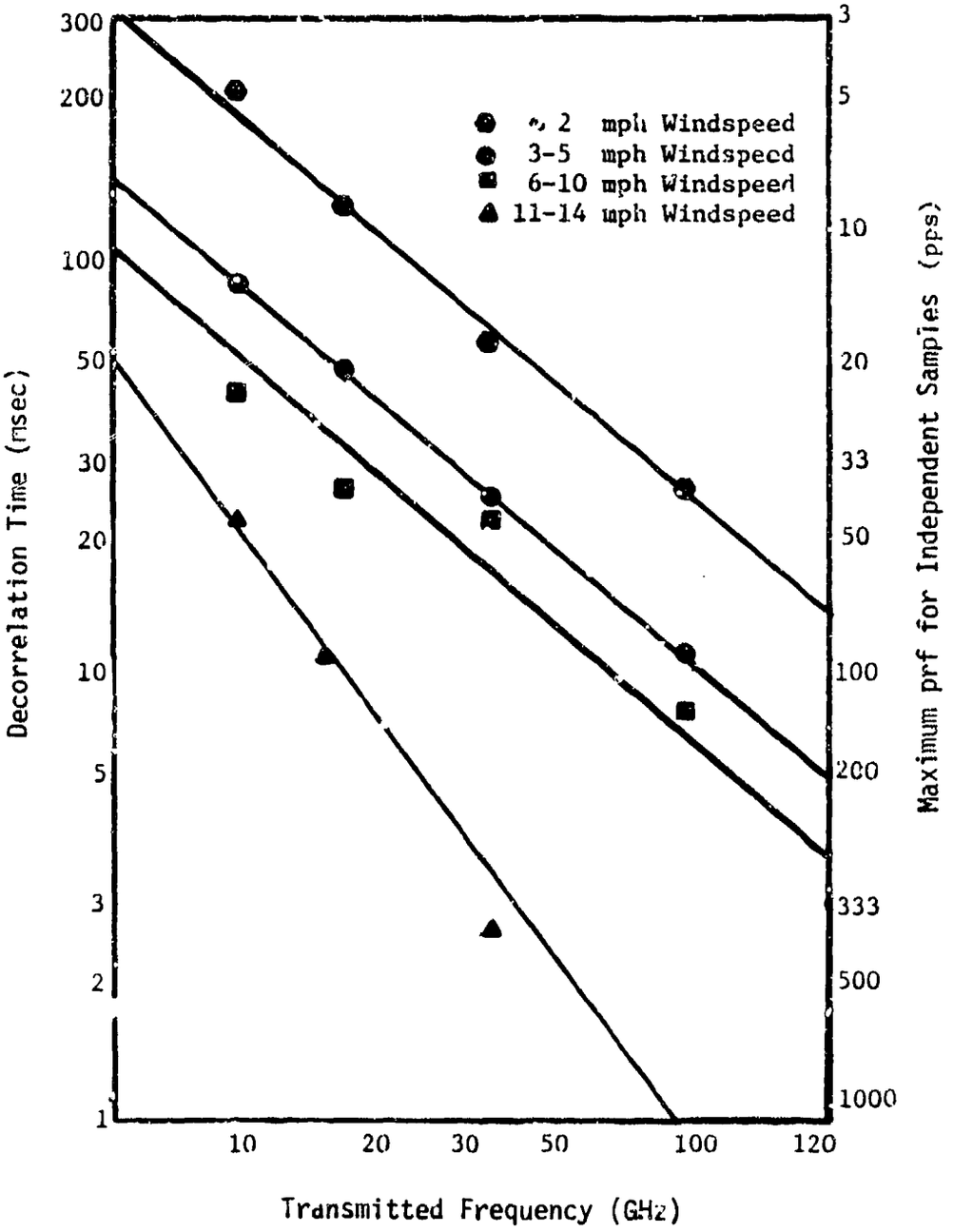

Figure 45. Decorrelation time versus frequency and windspeed for return from deciduous trees.

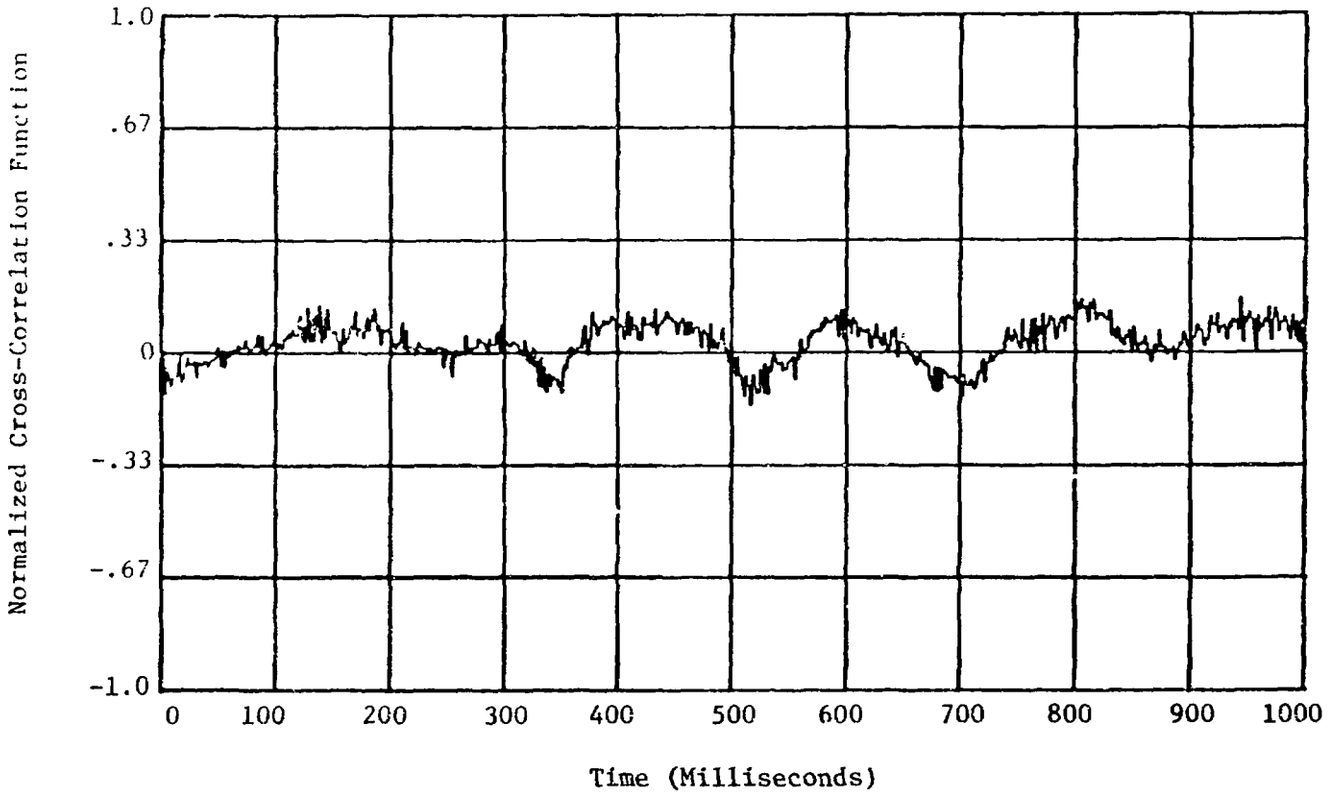

Figure 46. Normalized cross-correlation function for return from deciduous trees for 9.5 GHz and 16.5 GHz (9.5 x 16.5): 2 mph windspeed.

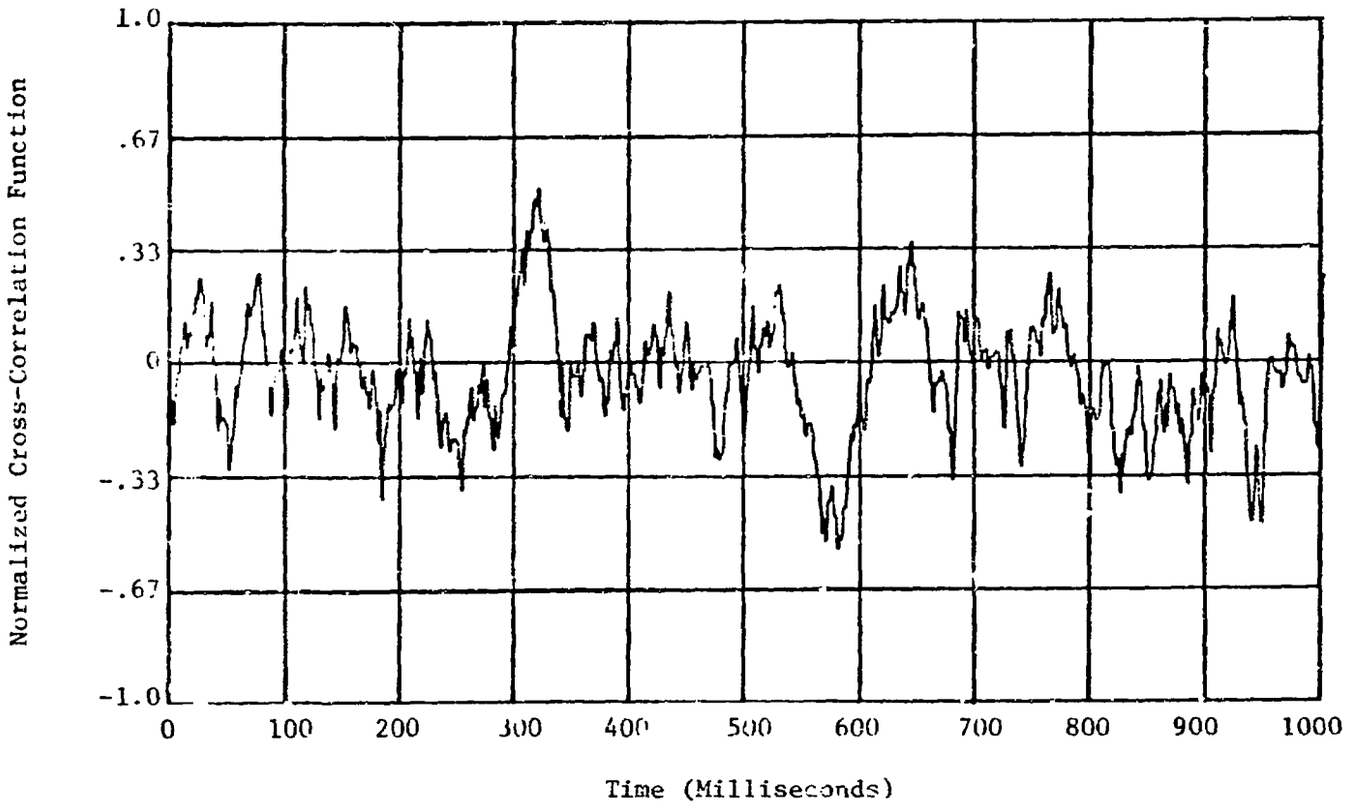

Figure 47. Normalized cross-correlation function for return from deciduous trees at 9.5 GHz and 16.5 GHz (9.5 x 16.5); 8 mph windspeed.

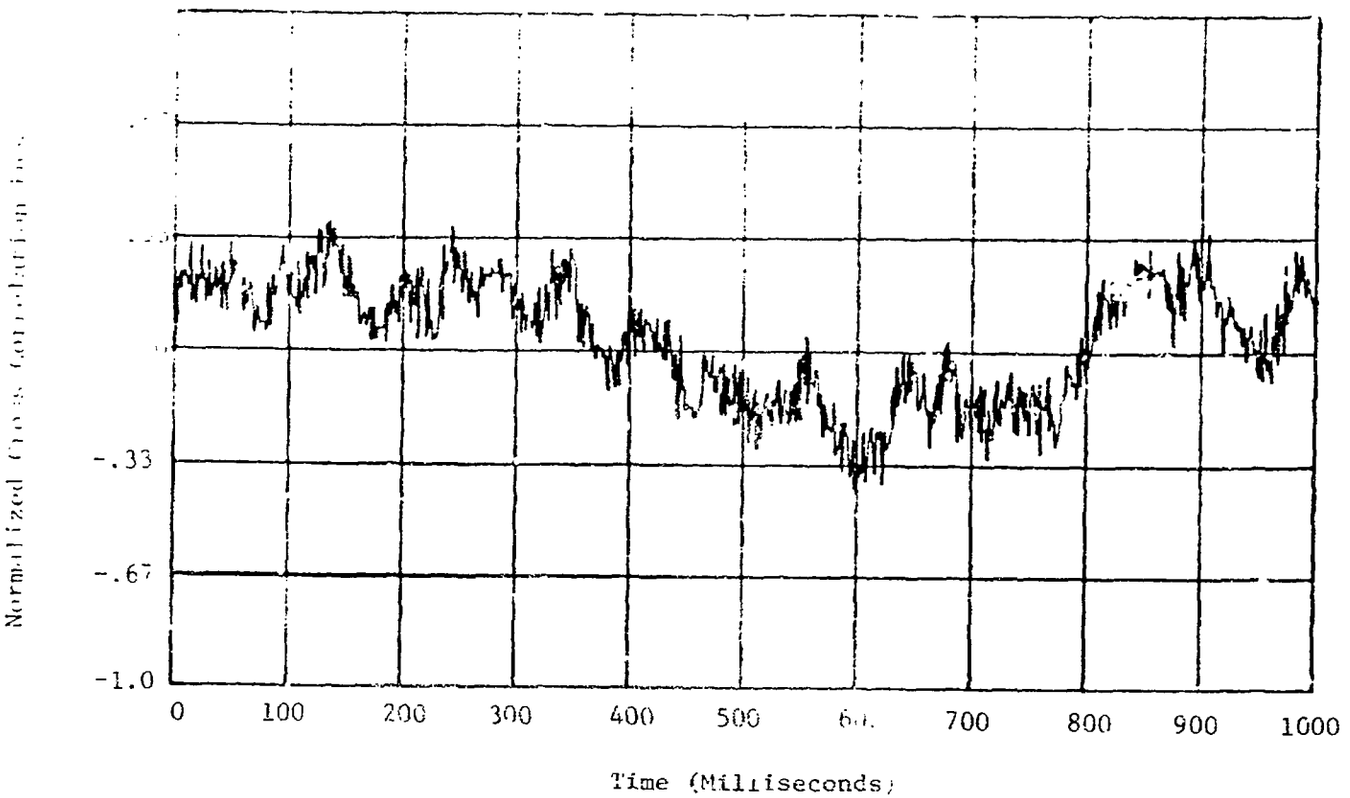

Figure 48. Normalized cross-correlation function for return from deciduous trees for 9.5 GHz and 35 GHz (9.5 x 35); 2 mph wind speed.

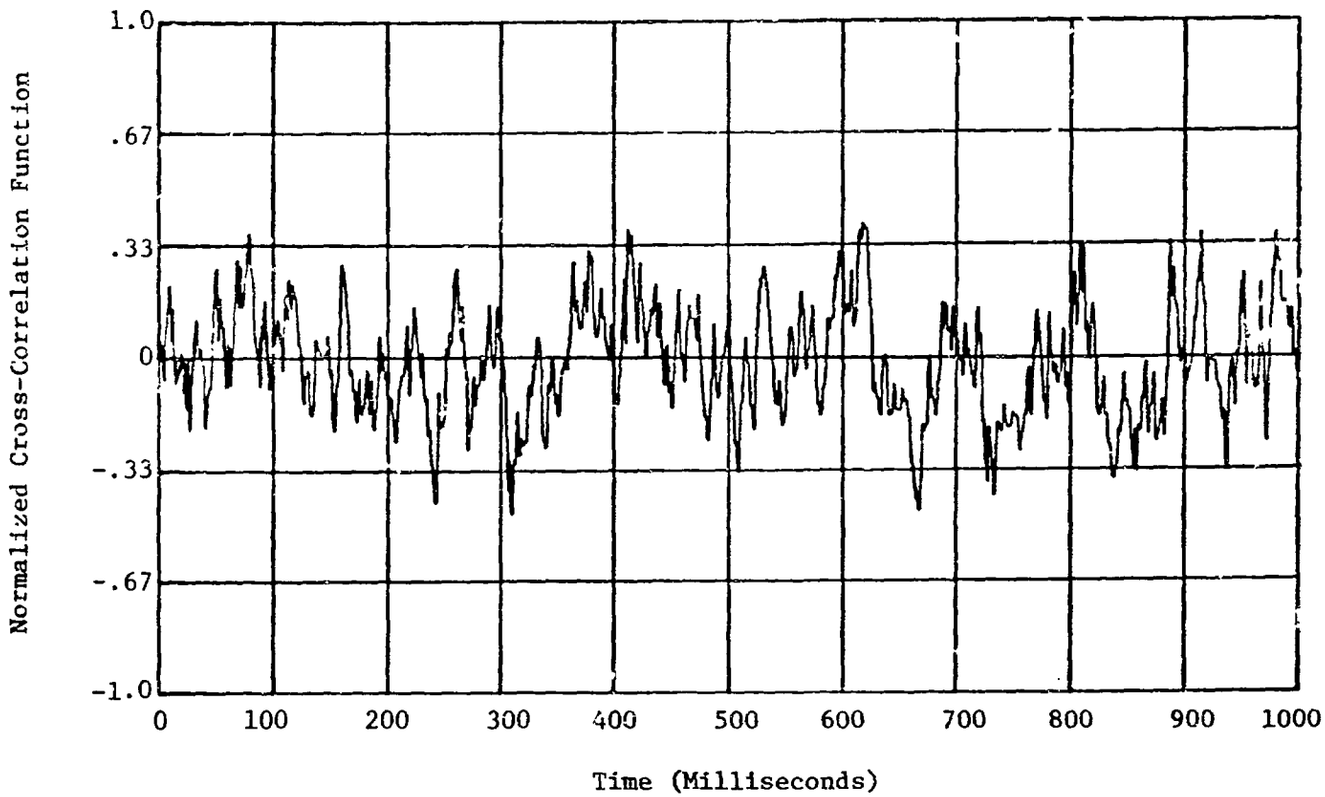

Figure 49 . Normalized cross-correlation function for return from deciduous trees for 9.5 GHz and 35 GHz (9.5 x 35); 8 mph windspeed.

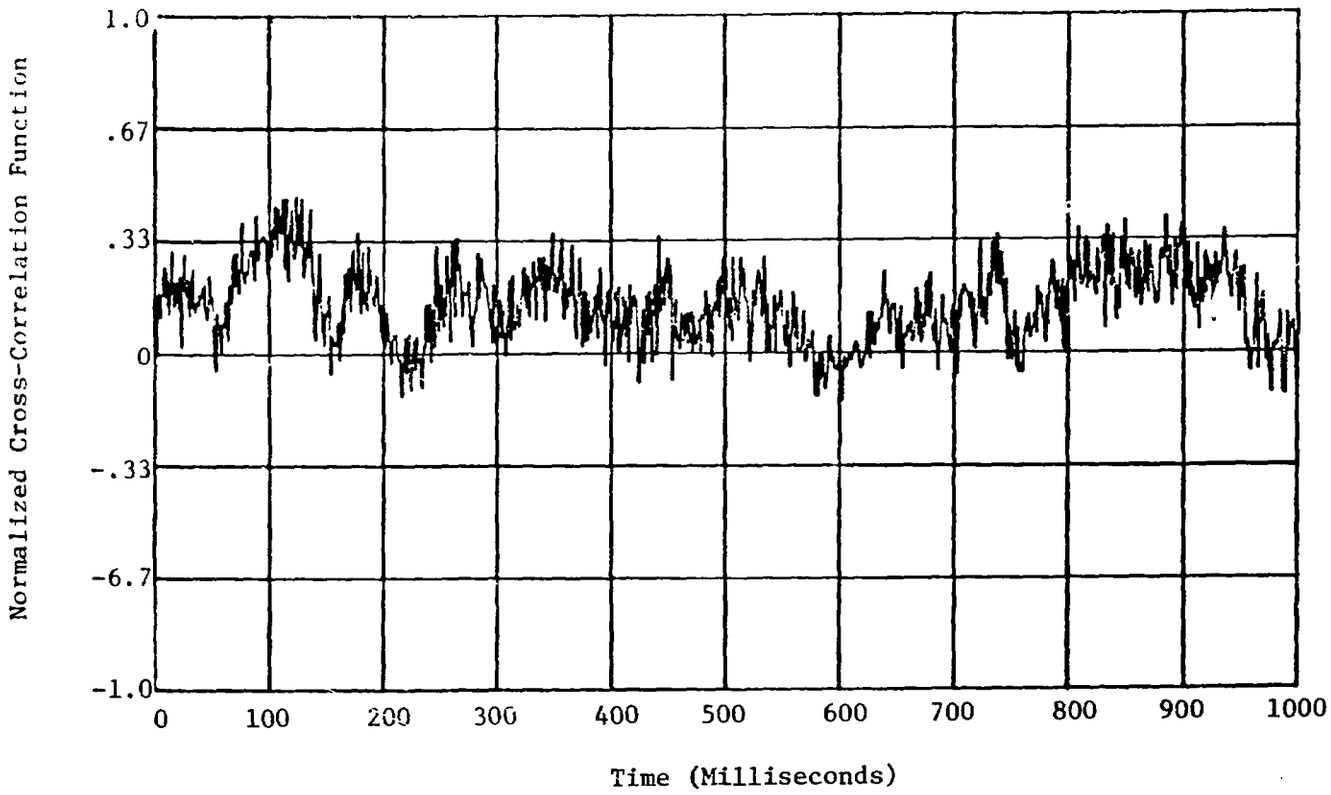

Figure 50. Normalized cross-correlation function for return from deciduous trees for 9.5 GHz and 95 GHz (9.5 x 95); 2 mph windspeed.

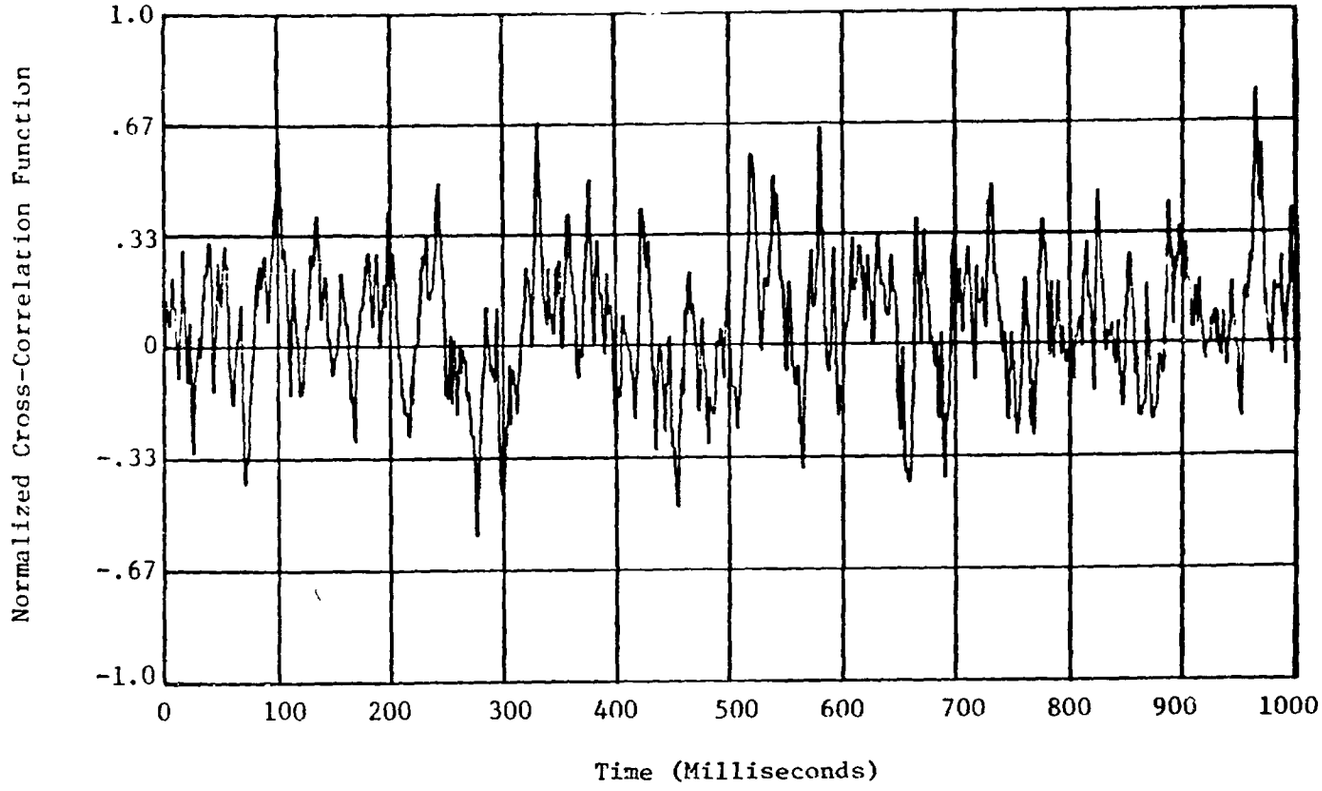

Figure 51. Normalized cross-correlation function for return from deciduous trees for 9.5 GHz and 95 GHz (9.5 x 95); 8 mph windspeed.

essentially independent when averaged over the 15 second interval required to obtain the calculated results shown in the figures. (See Section II-A for a discussion of how the cross-correlation functions were computed.)

III. CONCLUSIONS AND RECOMMENDATIONS

The design of the experiments described here was based on the recognition of a number of deficiencies in the knowledge of the radar backscatter from foliage and other natural objects at millimeter wavelengths [1]. The experiments were structured to obtain detailed data on the nature of the backscatter at a variety of grazing angles between 2 degrees and 20 degrees, for approximately octave steps in frequency between 9.5 GHz and 95 GHz.

Due to funding and time limitations, as much as for technical reasons, the results reported here are primarily for scattering from foliage. The emphasis on foliage is not necessarily an undue restriction at this time, since the properties of the scattering from foliage are critically needed in the design of signal-processing schemes and may actually represent the most important single case in this respect, especially for the development of MTI and related techniques. Further investigation of discrete scatterers should, of course, be undertaken to complement the data reported here.

The major results of the summaries of the average backscatter characteristics (σ^o) were as follows.

(1) The scattering was found to be weakly dependent upon frequency.

(2) The average polarization effects were less at the higher frequencies and generally less than the total variability due to other causes.

(3) The scattering was approximately independent of angle of arrival, for angles above 5 degrees for all frequencies.

(4) The variance of the data was approximately independent of frequency polarization and angle.

(5) The spread of the observed values of σ^o is almost certainly due to real variations of the scattering objects.

(6) The median value and spread of the resulting data are remarkably consistent with those data previously available.

The major results of the investigations of the amplitude statistics of the backscatter are as follows.

(1) The observed amplitude distributions were generally well represented by the log normal function.

(2) The general behavior of the observed amplitude distributions was essentially independent of frequency above 9.5 GHz.

(3) The observed amplitude distributions were more regular at the higher windspeeds and appeared to be weakly dependent upon windspeed at the higher frequencies.

(4) The amplitude statistics appear to be weakly dependent upon the type of tree for fall or summer conditions.

The investigations of the temporal and spectral properties of the backscatter from foliage were limited to observations of the incoherent properties, since only incoherent pulse radars were available. The principal results were as follows.

(1) The normalized frequency spectra were dependent on windspeed and frequency, with the corner frequency observed to be higher for the higher windspeeds and/or higher frequencies.

(2) The slopes of the linear frequency spectra were observed to vary inversely with frequency and could be fitted with power laws ranging from cubic at 9.5 GHz to quadratic at 95 GHz.

(3) The decorrelation times of the returns (as obtained from the autocorrelation function) varied with transmitted frequency and windspeed in the expected manner and had values consistent with generally accepted theories; however, the effects of motions of individual leaves and other small scattering elements were observed to be quite important at 95 GHz, especially at low wind speeds.

(4) Returns at different transmitted frequencies appeared to be only weakly correlated (as obtained from the cross-correlation functions) for most observations; however, at very low windspeeds the degree of correlation was significant.

The temporal and spectral behavior of the observations made of rocky terrain, corner reflectors, etc., was also as anticipated, with the characteristics somewhat a function of signal-to-background ratio (i.e., fixed target-to-foliage and/or -noise) and exhibited similar values at all frequencies for high signal-to-background ratios.

It is to be concluded that, while much new information has been obtained as a result of this investigation, a number of important questions remain to be answered and should be the subject of future investigations. Specifically, the main emphasis of the work reported herein was on investigation of returns from foliage; however, this work represents only one step towards the identification of the characteristics of returns from targets immersed in clutter. Since the crucial questions concerning application of millimeter frequencies to radars for the detecting and identifying targets in clutter involve specification of target-to-background ratios, target/clutter signatures, and the general reliability of the specification of "standard" values of target and clutter properties for design purposes, a much more extensive program of investigation is needed. Specific data are needed on the characteristics of target returns in clutter, including especially polarization behavior, spectral characteristics, and amplitude statistics. In addition, the foliage penetration capability needs to be determined as a function of frequency to assist in scaling the measured target-to-background ratios. A commitment should be made to the development of the necessary tools and techniques for obtaining both coherent data and bistatic data for frequencies at least as high as 95 GHz. In addition, future planning should include the development of the necessary supporting instrumentation (both meteorological and signal calibration) and measurement standards to facilitate comparison of data from successive experiments, especially from different geographic and climatic regions.

IV. REFERENCES

1. R. D. Hayes and F. B. Dyer, "Land Clutter Characteristics For Computer Modeling of Fire Control Radar Systems," Technical Report No. 1 on Contract DAAA 25-73-C-0256, Engineering Experiment Station, Georgia Institute of Technology, 15 May 1973.

2. F. B. Dyer, "Engineering Services in Support of Millimeter Rain Clutter Experiment," Final Letter Report on Contract DAAA 25-73-C-0256, Mod. P00002, Engineering Experiment Station, Georgia Institute of Technology, 25 October 1973.

3. N. C. Currie, F. B. Dyer, and R. D. Hayes, "Analysis of Radar Rain Return at Frequencies of 9.375, 35, 70, and 95 GHz," Technical Report No. 2 on Contract DAAA 25-73-C-0256, Engineering Experiment Station, Georgia Institute of Technology, 1 February 1975.

4. Louis N. Ridenour, Radar System Engineering, Vol. 1 of the M.I.T. Radiation Laboratory Series, Dover Publications, Inc., New York, 1947, p. 21.

5. D. E. Wrege and D. S. Harmer, "FOCAL/F An Extended Version of 8-K FOCAL 69$_{TM}$," School of Nuclear Engineering, Georgia Institute of Technology, 1 June 1972.

6. W. Rivers, "Low-Angle Radar Sea Return at 3 mm Wavelength," Final Technical Report on Contract N62269-70-C-0489, Engineering Experiment Station, Georgia Institute of Technology, 15 November 1970.

7. C. M. Close, The Analysis of Linear Circuits, Harcourt, Brace, and World, Inc., 1966.

8. David K. Barton, Radar System Analysis, Prentice-Hall, Inc., Englewood Cliff, N.J., 1964, p. 96-97.

9. W. Fishbein et al., "Clutter Attenuation Analysis," Technical Report No. ECOM-2808, U.S. Army Electronics Command March 1967.

V. APPENDICES

APPENDIX A

Selected Spectral Distributions

This appendix contains examples of computer generated x-y plots of the noncoherent spectra of returns from deciduous trees for windspeeds of 5 mph and 10 mph at 9.5, 16.5, 35, and 95 GHz. Each plot represents about 5 seconds of data, and the data for each frequency were processed for the same time interval so that direct comparisons can be made. The odd numbered figures give the normalized linear frequency spectra for the returns. That is, the recorded logarithmic data were exponentiated prior to computation of the Fourier transform so as to obtain the linear frequency spectra as discussed in Section II-A-1-b. The even numbered figures represent the spectra obtained by processing the same data as for odd numbered figures without exponentiating the data prior to calculation of the Fourier transform, and thus represent the normalized frequency spectrum of a logarithmic receiver.

Looking at the figures, it can be seen that the logarithmic frequency spectra always have lower cutoff frequencies and a steeper roll-off characteristics than the corresponding linear frequency spectra runs. In general the corner frequencies of the spectra increase with increasing transmitted frequency and windspeed. It should be noted that the linear spectra appear noisier than the logarithmic spectra because the exponentiation process greatly increased the dynamic range of the data, and to prevent overflow in the computer, the data had to be "clipped" on the low end. Thus the "spikes" which appear on some of the spectra in the 100 Hz to 1000 Hz region are due to noise resulting from this problem.

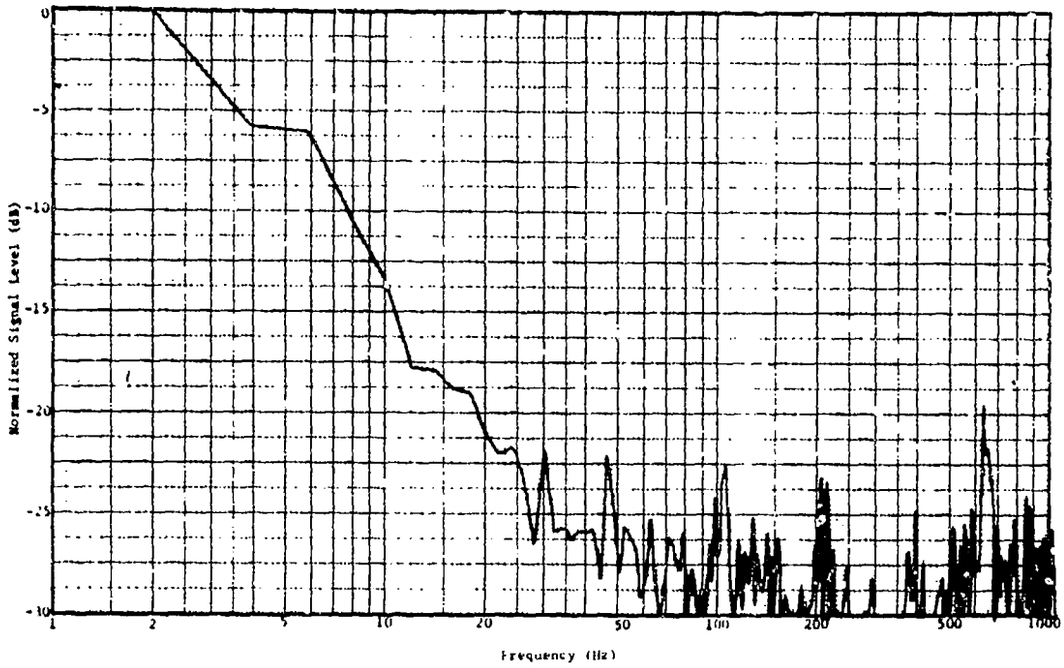

Figure A-1. Example of the frequency spectrum of the return from deciduous trees; 9.5 GHz, vertical polarization, and 5 mph wind speed (linear detector).

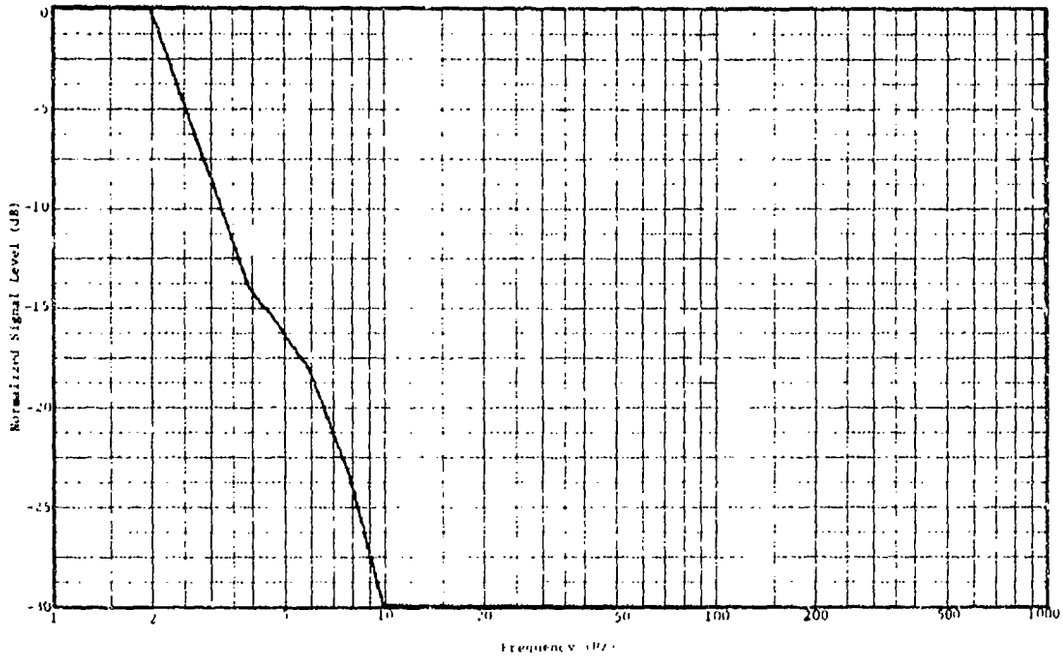

Figure A-2. Example of the frequency spectrum from a logarithmic receiver of the return from deciduous trees; 9.5 GHz, vertical polarization, and 5 mph wind speed.

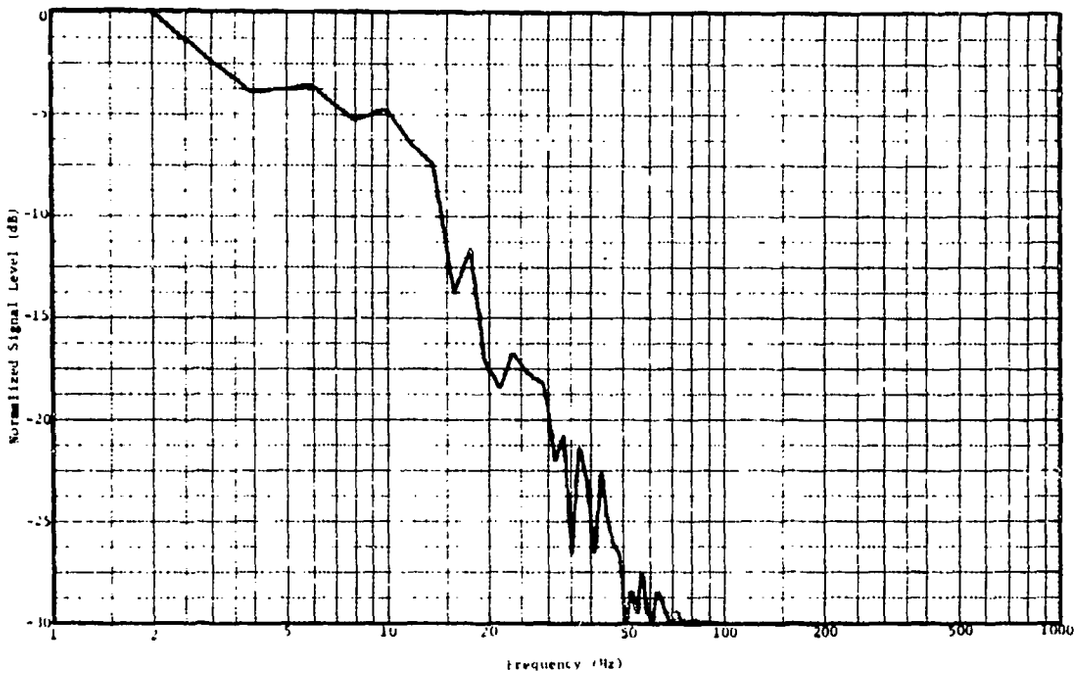

Figure A-3. Example of the frequency spectrum of the return from deciduous trees; 16.5 GHz, vertical polarization, and 5 mph wind speed (linear receiver).

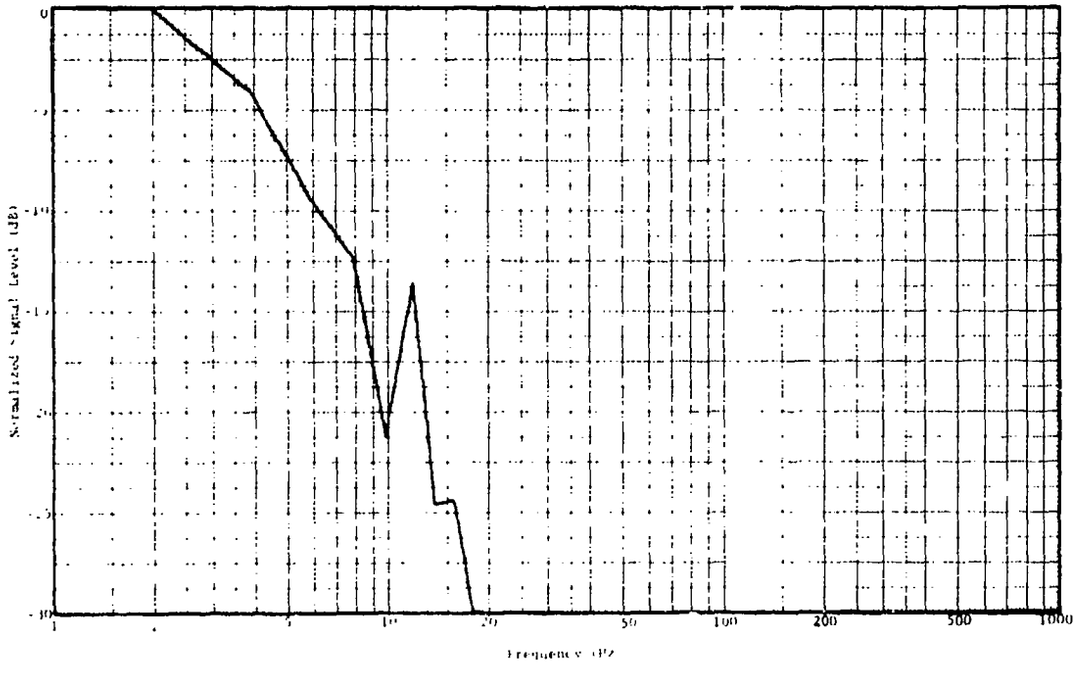

Figure A-4. Example of the frequency spectrum from a logarithmic receiver of the return from deciduous trees; 16.5 GHz, vertical polarization, and 5 mph wind speed.

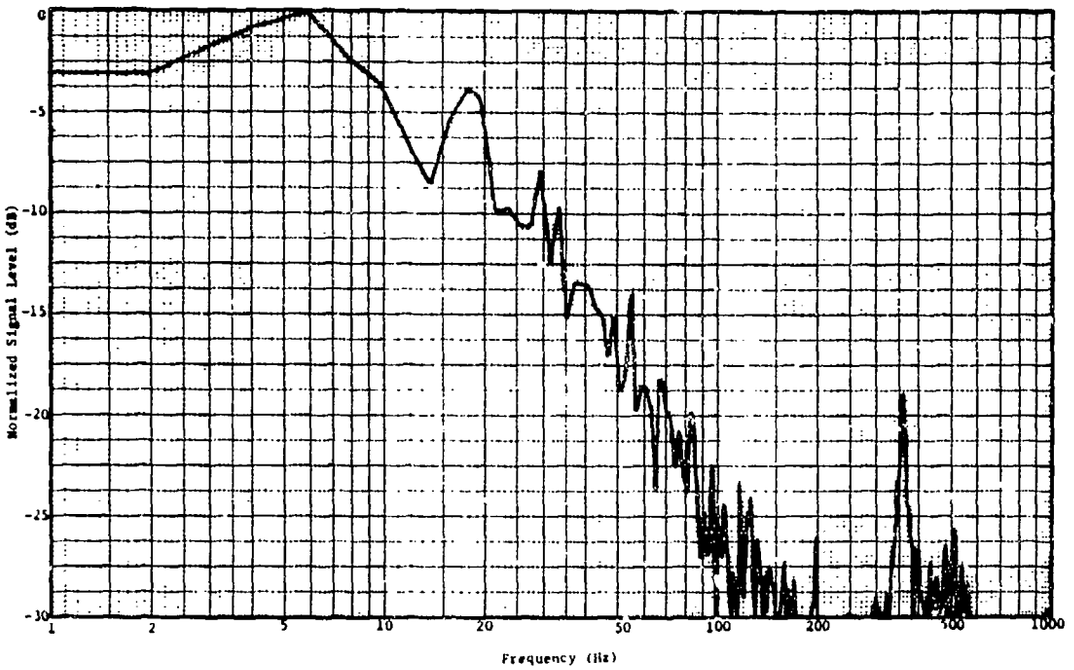

Figure A-5. Example of the frequency spectrum of the return from deciduous trees; 35 GHz, vertical polarization, and 5 mph wind speed (linear receiver).

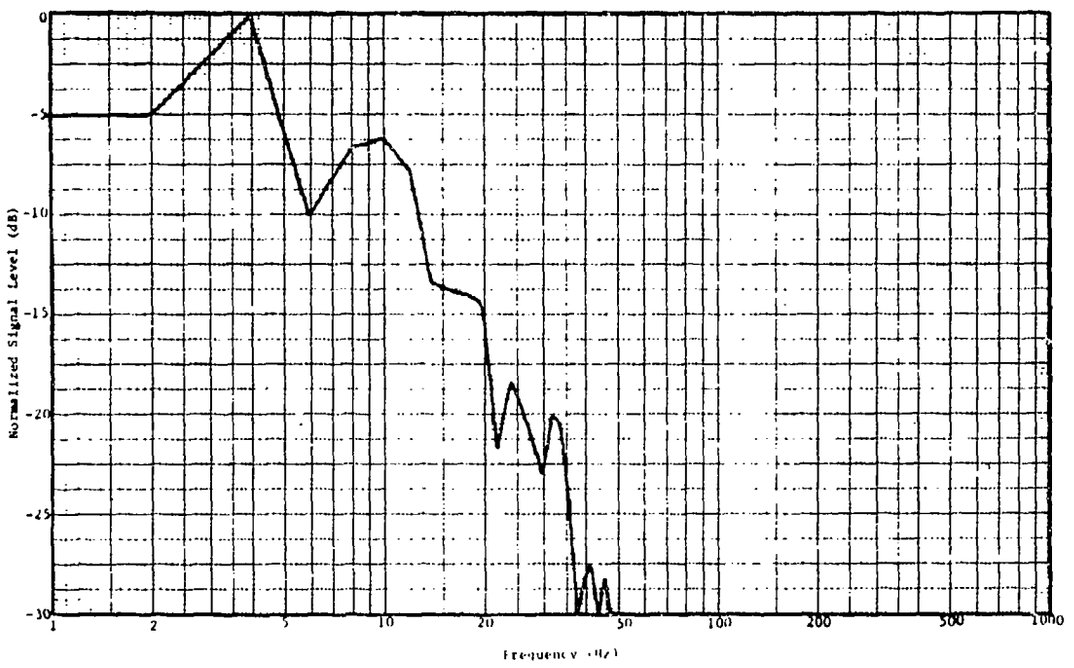

Figure A-6. Example of the frequency spectrum from a logarithmic receiver of the return from deciduous trees; 35 GHz, vertical polarization, and 5 mph wind speed.

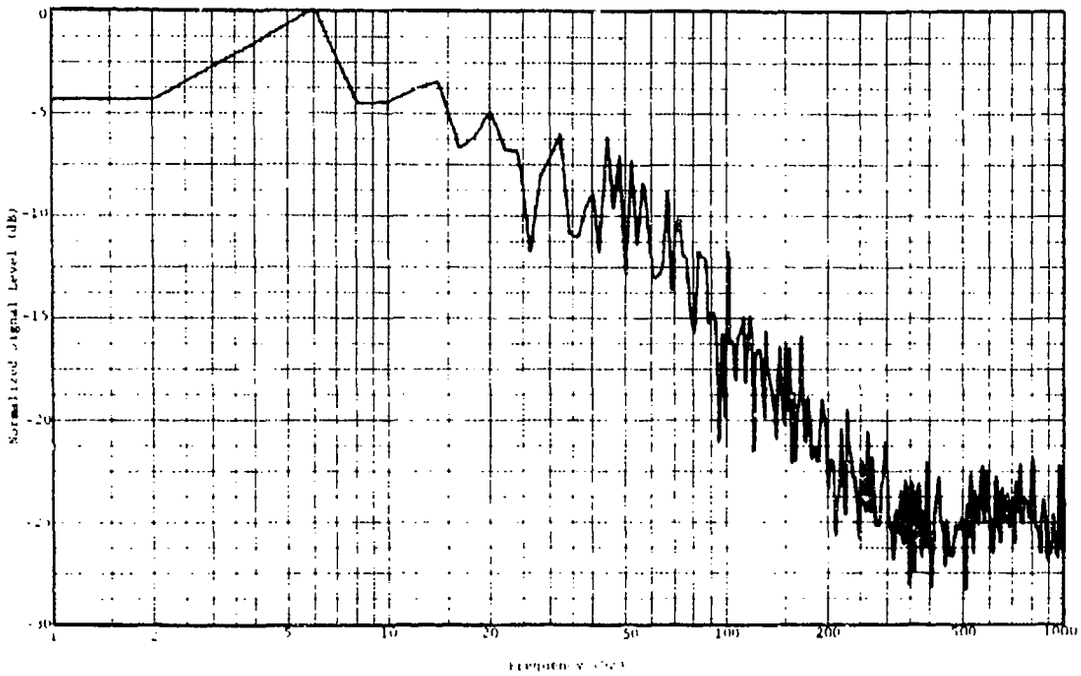

Figure A-7. Example of the frequency spectrum of the return from deciduous trees; 95 GHz, vertical polarization, and 5 mph wind speed (linear receiver).

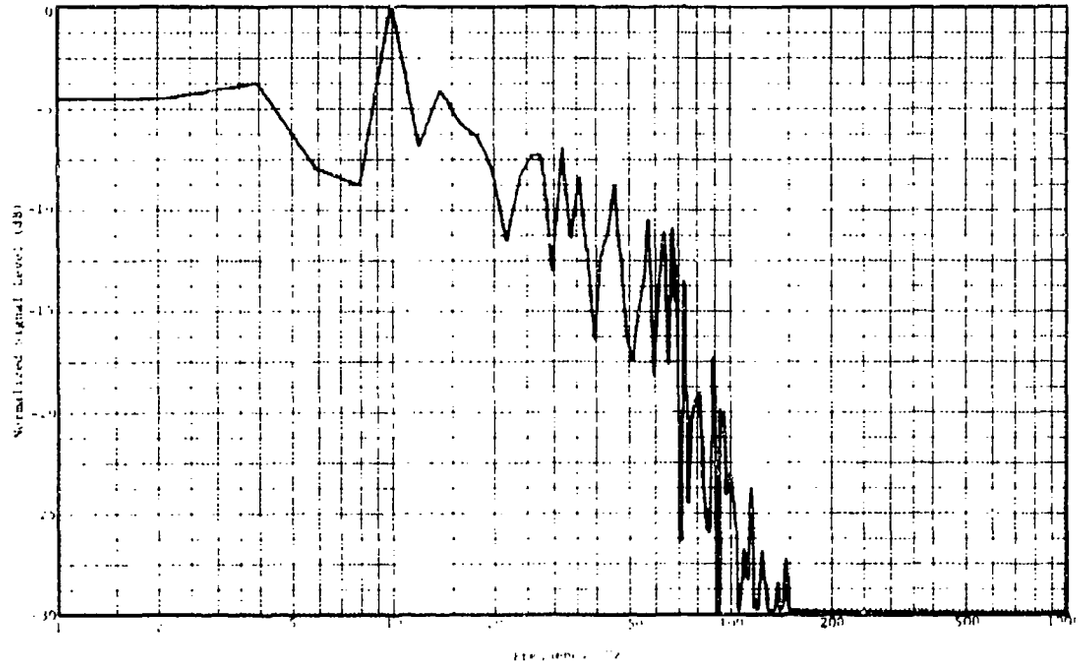

Figure A-8. Example of the frequency spectrum from a logarithmic receiver of the return from deciduous trees; 95 GHz, vertical polarization, and 5 mph wind speed.

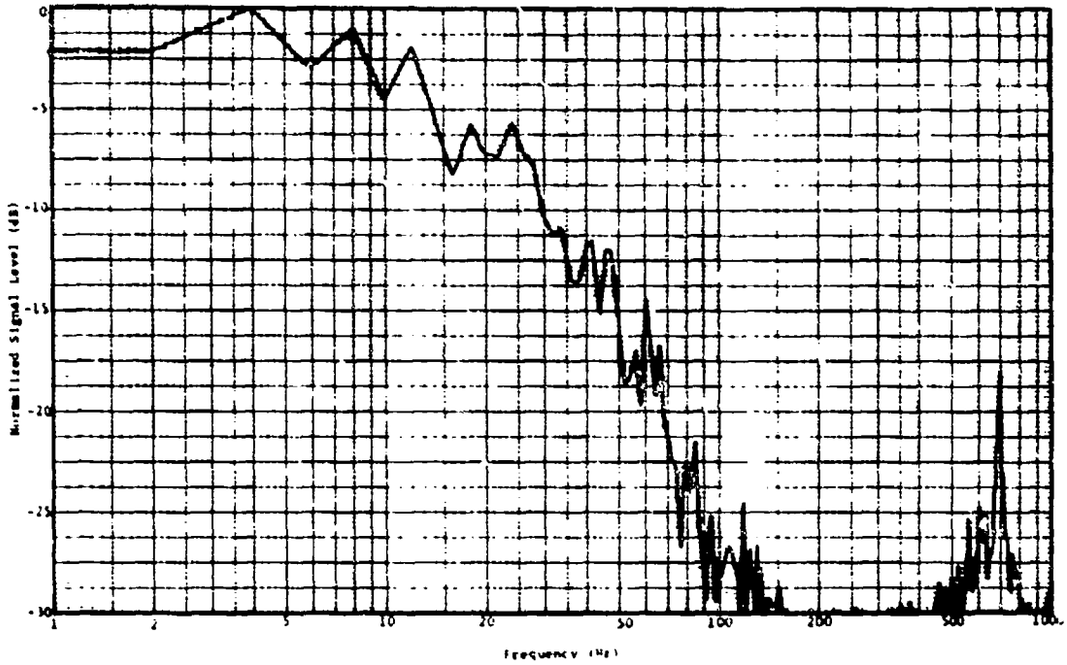

Figure A-9. Example of the frequency spectrum of the return from deciduous trees; 9.5 GHz, vertical polarization, and 10 mph wind speed (linear receiver).

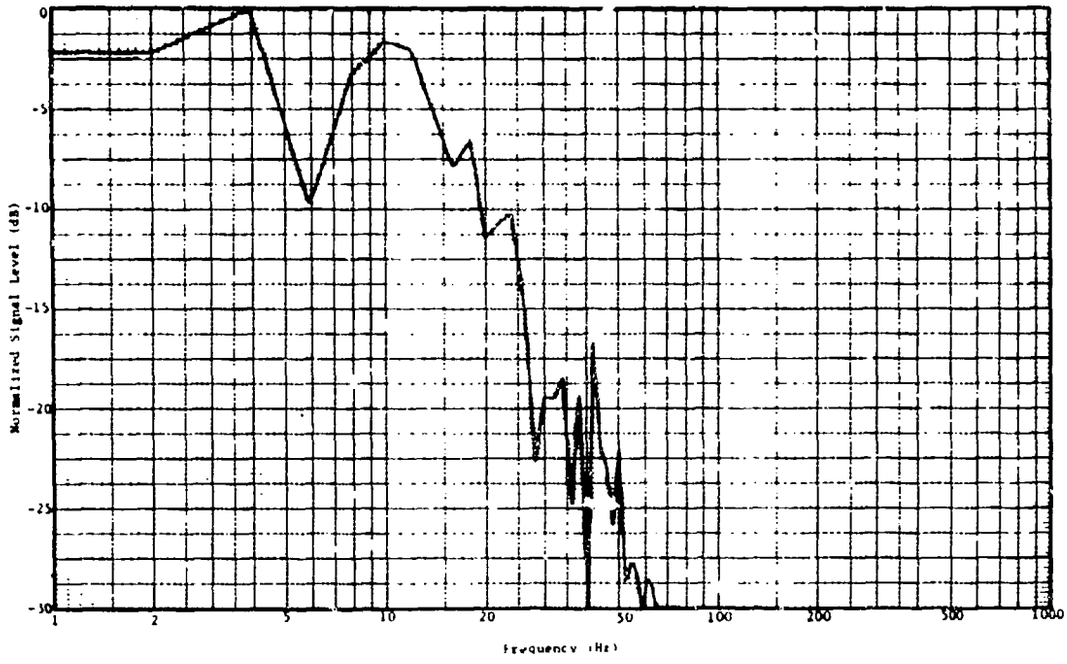

Figure A-10. Example of the frequency spectrum from a logarithmic receiver of the return from deciduous trees; 9.5 GHz, vertical polarization, and 10 mph wind speed.

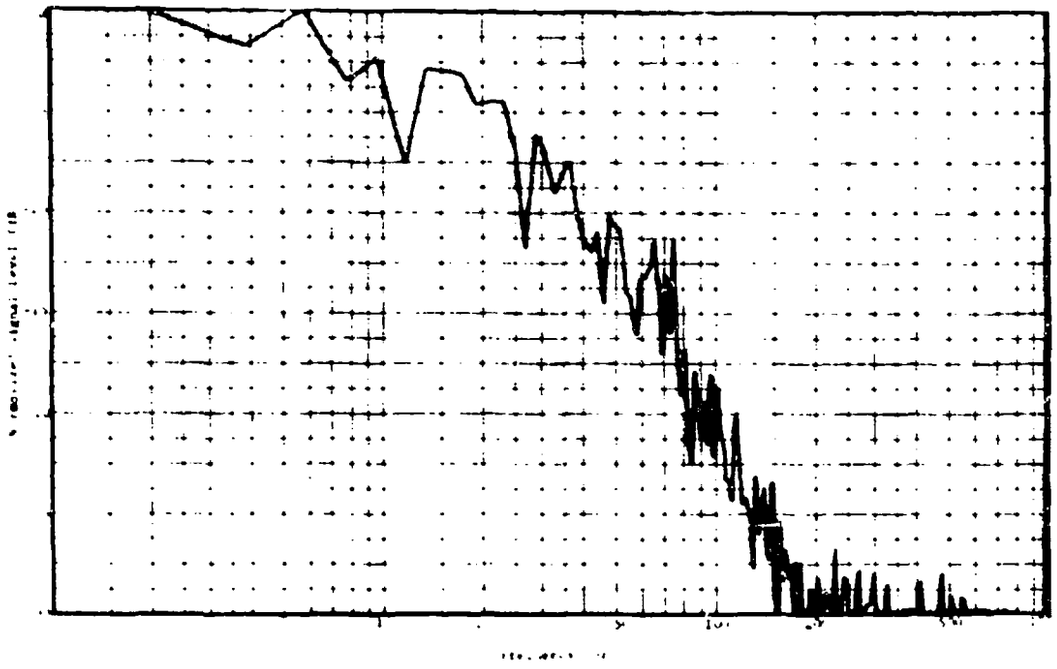

Figure A-11. Example of the frequency spectrum of the return from deciduous trees; 16.5 GHz, vertical polarization, and 10 mph wind speed (linear receiver).

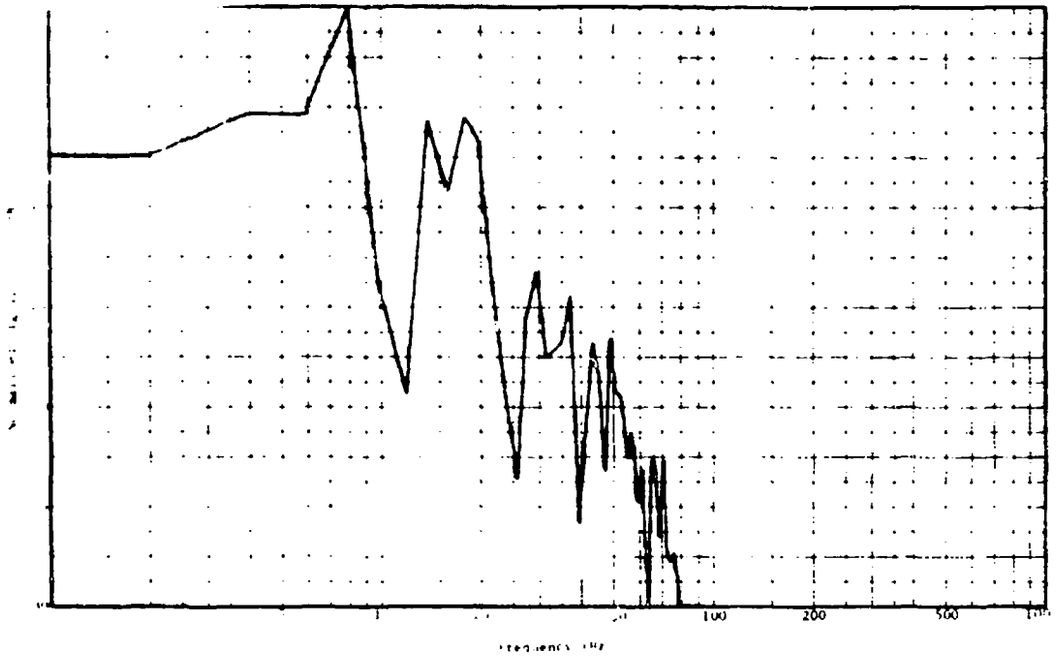

Figure A-12. Example of the frequency spectrum from a logarithmic receiver of the return from deciduous trees; 16.5 GHz, vertical polarization, and 10 mph wind speed.

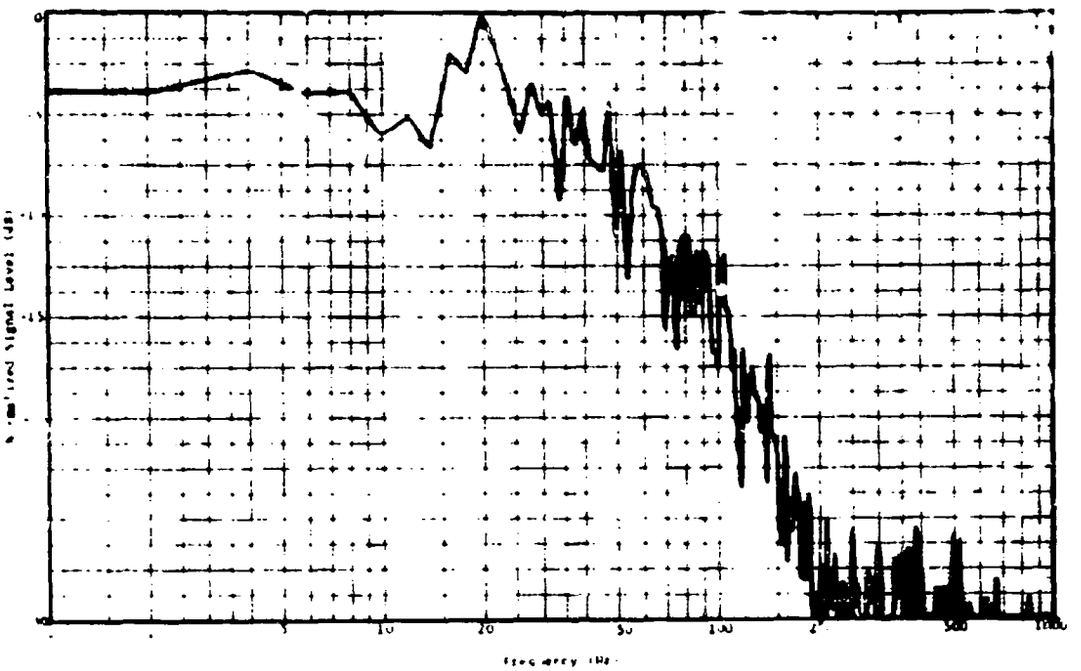

Figure A-13. Example of the frequency spectrum of the return from deciduous trees; 35 GHz, vertical polarization, and 10 mph wind speed (linear receiver).

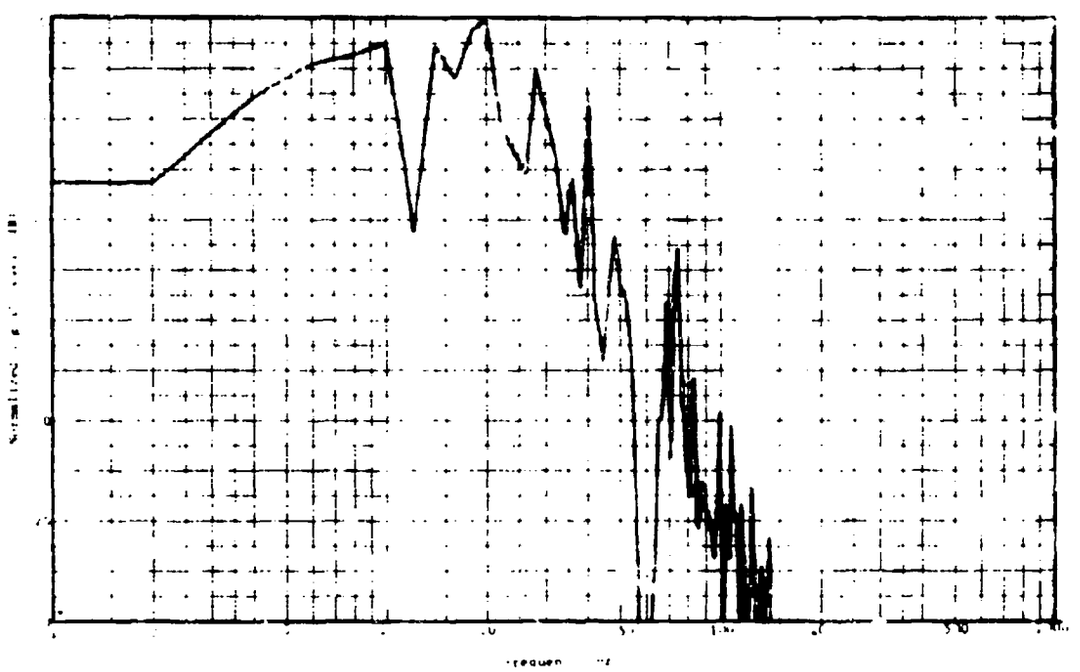

Figure A-14. Example of the frequency spectrum from a logarithmic receiver of the return from deciduous trees; 35 GHz, vertical polarization, and 10 mph wind speed.

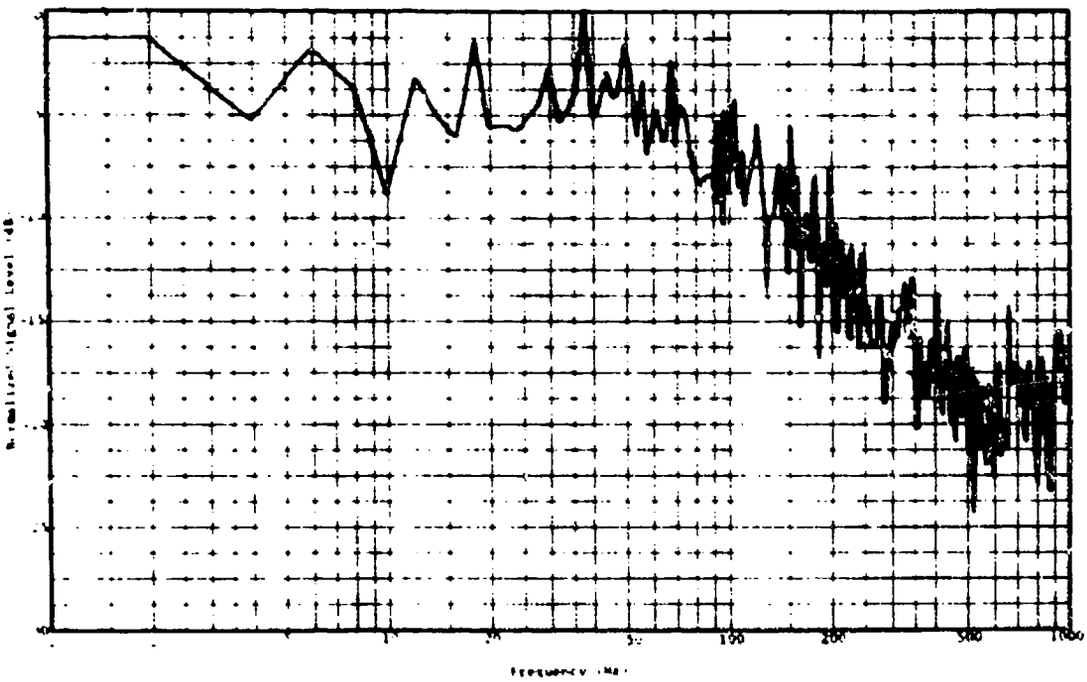

Figure A-15. Example of the frequency spectrum of the return from deciduous trees; 95 GHz, vertical polarization, and 10 mph wind speed (linear receiver).

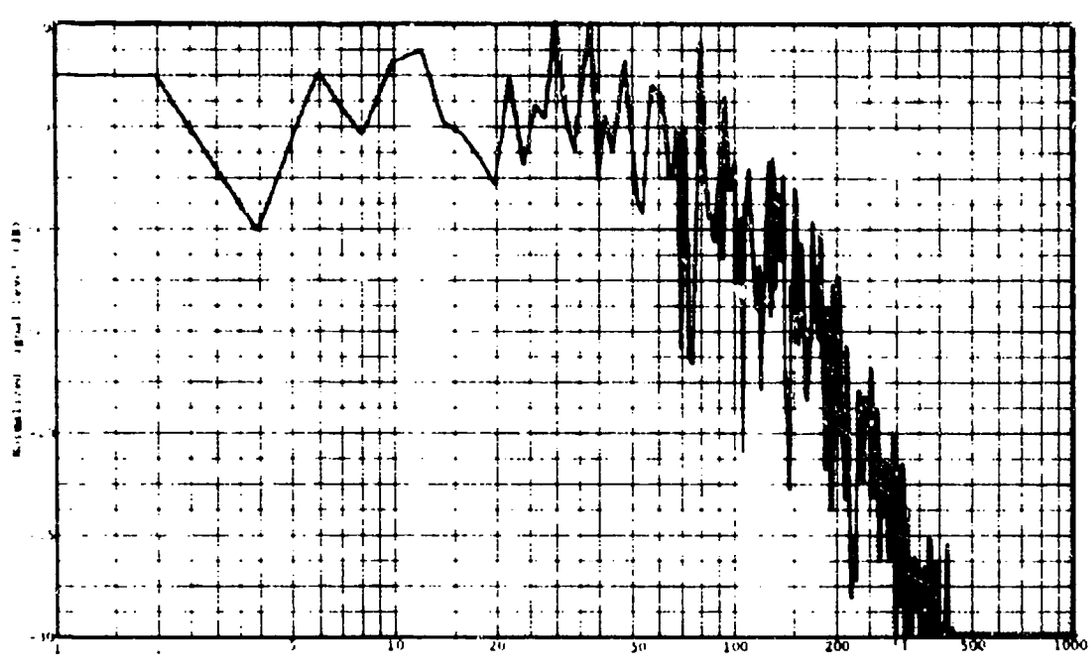

Figure A-16. Example of the frequency spectrum from a logarithmic receiver of the return from deciduous trees; 95 GHz, vertical polarization, and 10 mph wind speed.

APPENDIX B

Auto-Correlation Functions for Selected Data Runs

This appendix contains selected examples of the computer generated auto-correlation functions for the returns from deciduous trees for wind speeds of 2, 5, 8, and 10 mph. The horizontal axis represents a maximum delay time of 250 milliseconds determined by the sample rate.

Figures B-1 through B-4 represent a data run for which the indicated windspeed was 2 mph, however it is obvious that, at the instant that these data were processed, the wind was essentially calm. This accounts for the extremely long decorrelation times for 9.5 and 16.5 GHz. Note that the 35 GHz and 95 GHz runs still decorrelate fairly rapidly, probably due to leaf flutter which is not resolved at the lower frequencies.

In general these examples show that the decorrelation time decreases with increasing transmitted frequency and increasing windspeed.

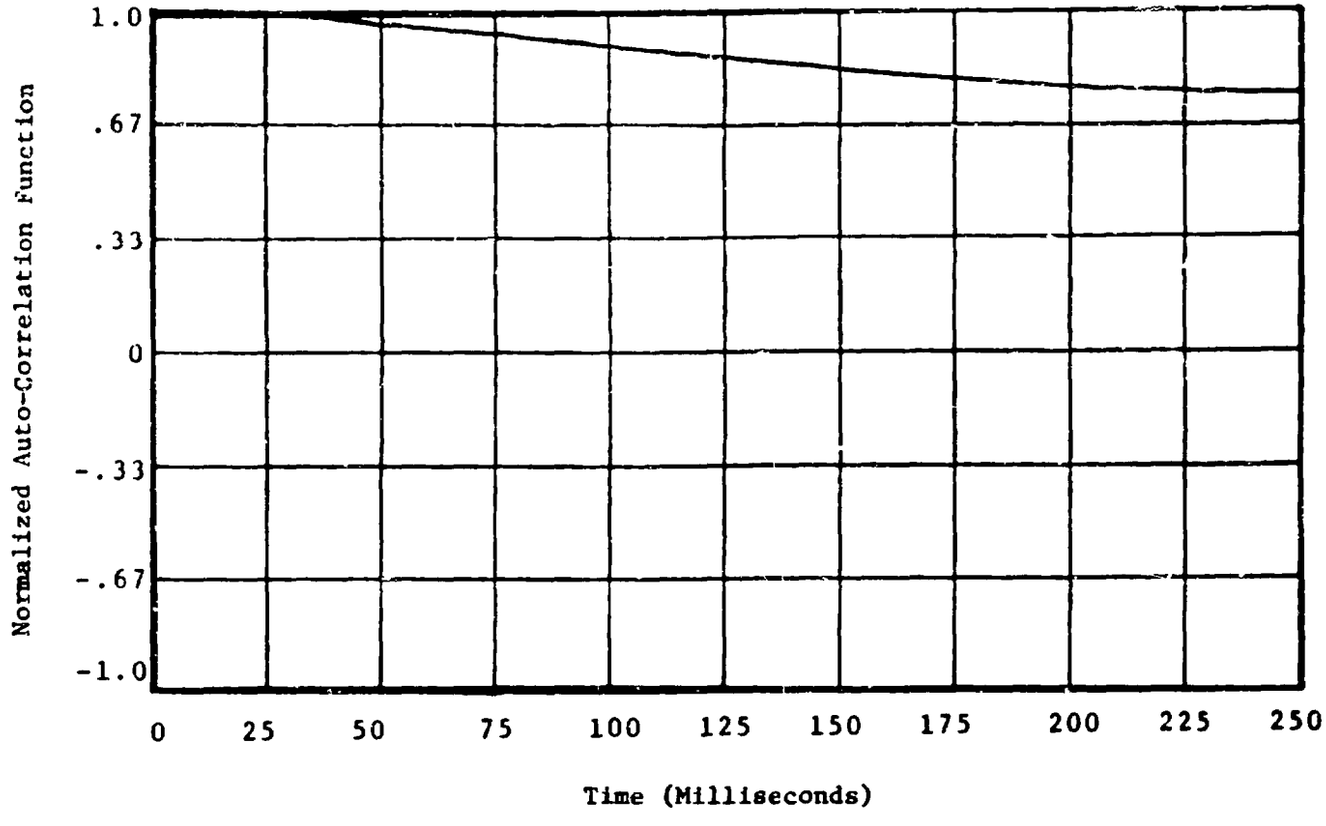

Figure B-1. Normalized auto-correlation function for the return from deciduous trees; 9.5 GHz, 2 mph windspeed.

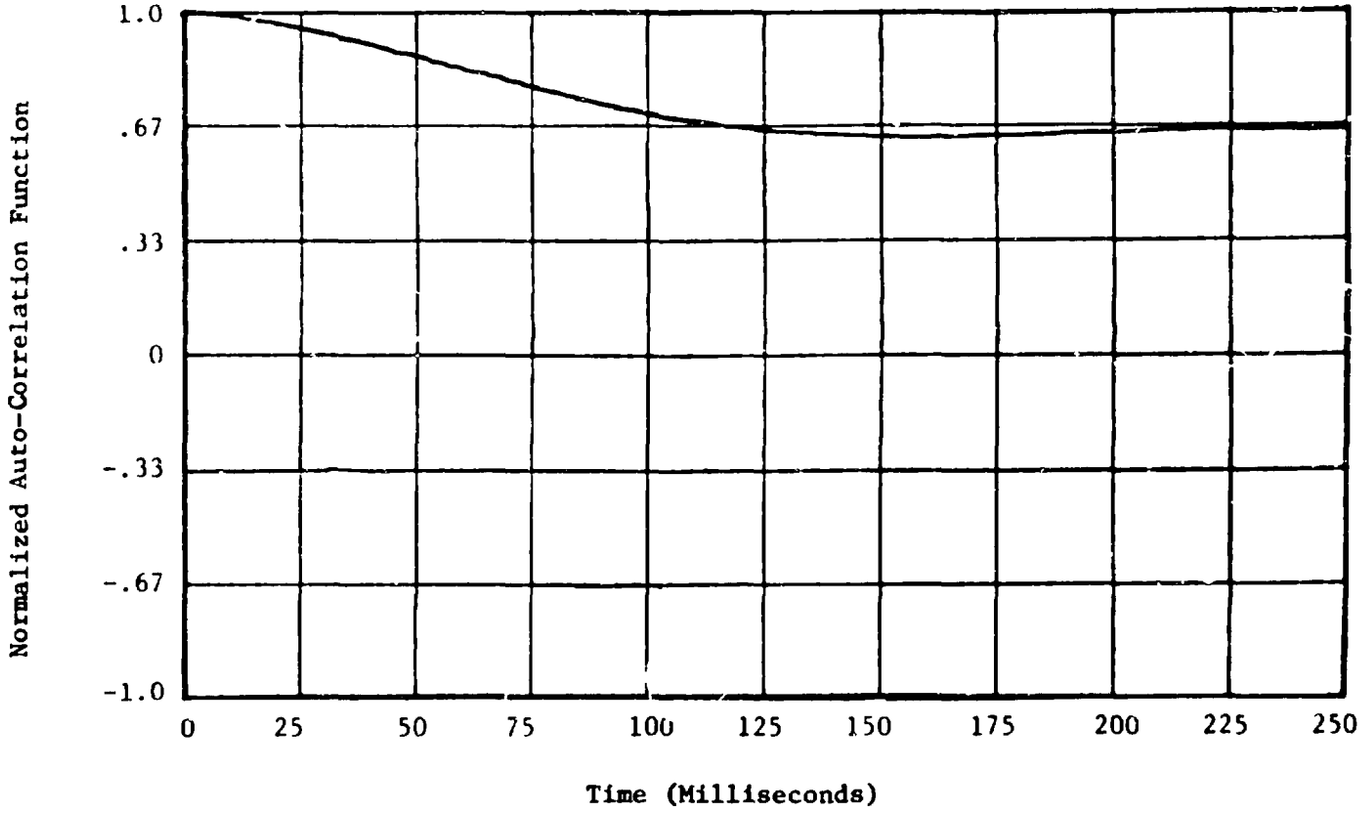

Figure B-2. Normalized auto-correlation function for the return from deciduous trees; 16.5 GHz, 2 mph windspeed.

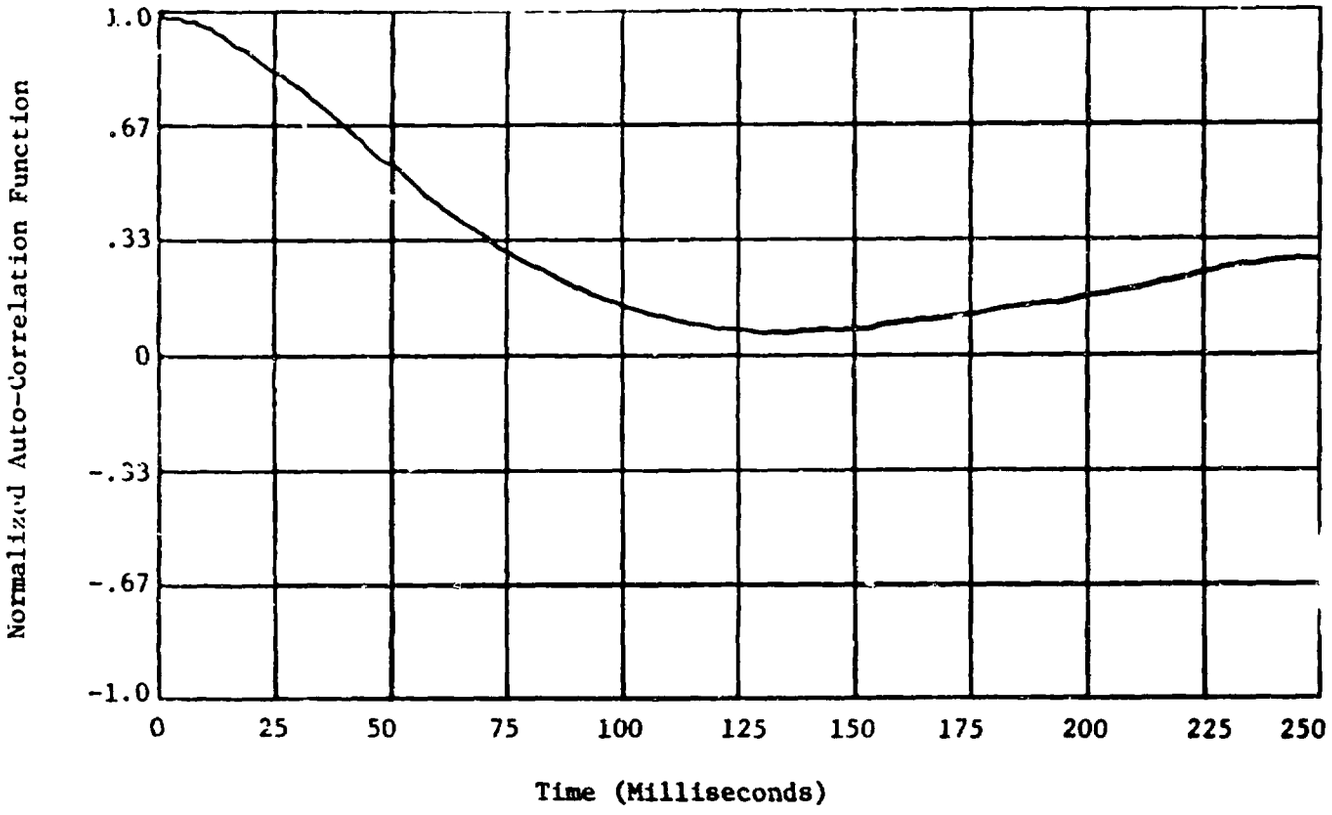

Figure B-3. Normalized auto-correlation function for the return from deciduous trees; 35 GHz, 2 mph windspeed.

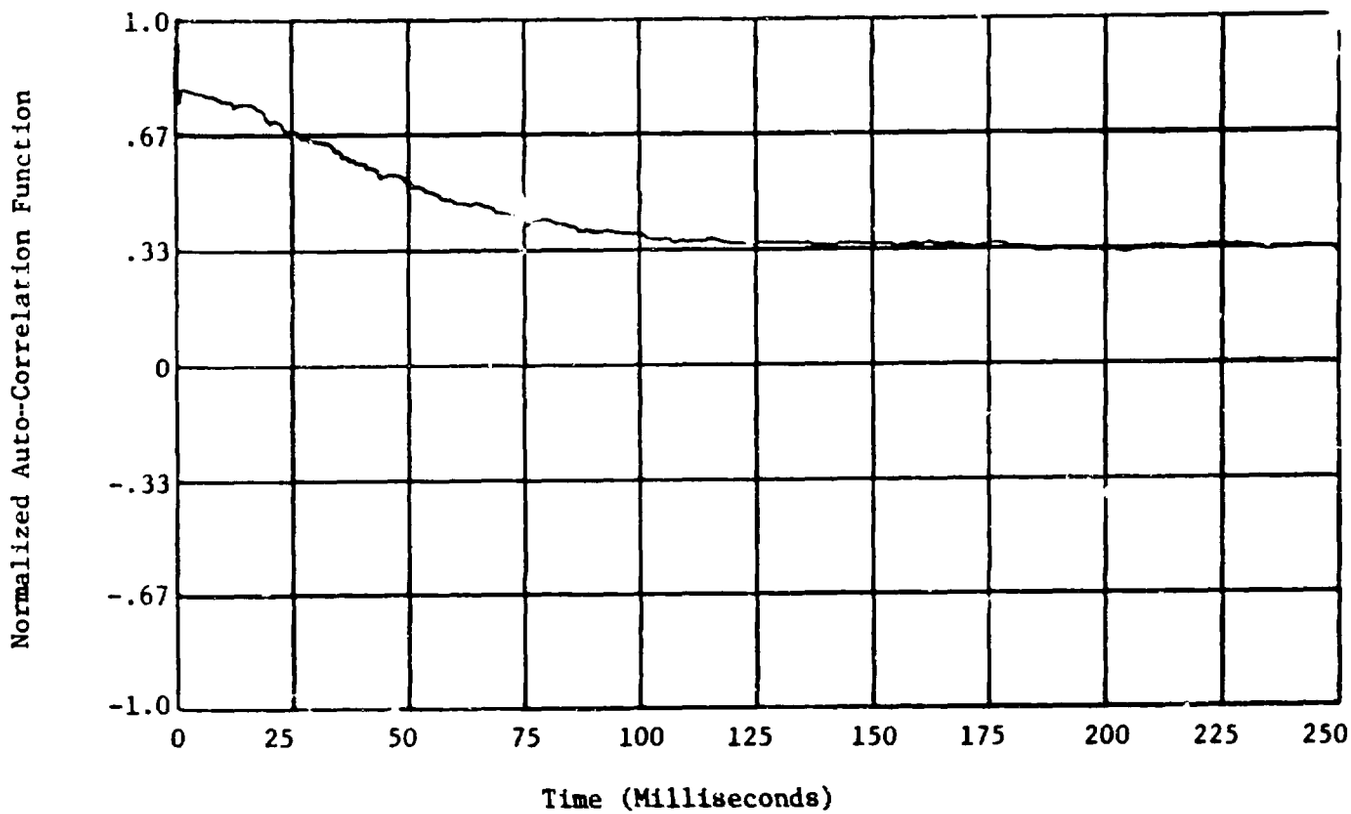

Figure B-4. Normalized auto-correlation function for the return from deciduous trees; 95 GHz, 2 mph windspeed.

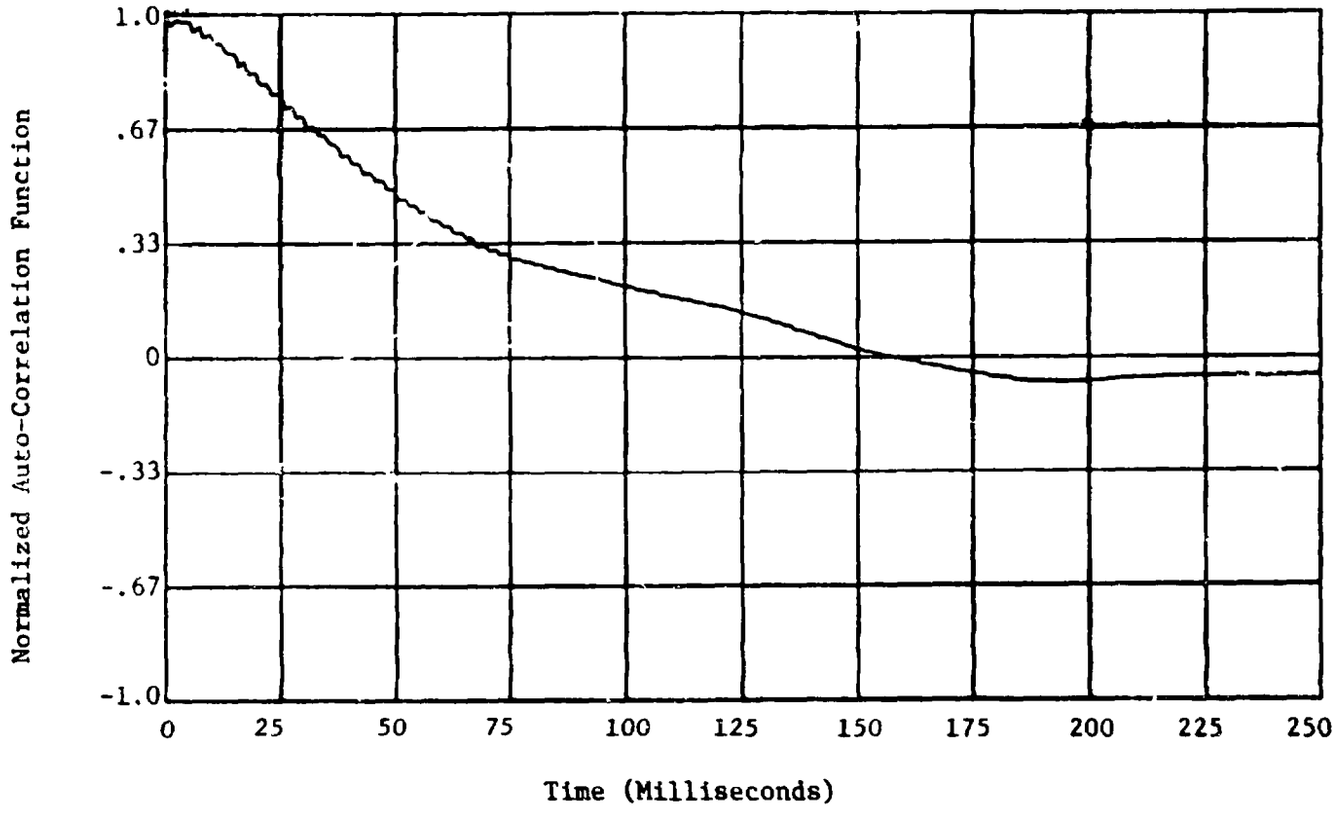

Figure B-5. Normalized auto-correlation function for the return from deciduous trees; 9.5 GHz, 5 mph windspeed.

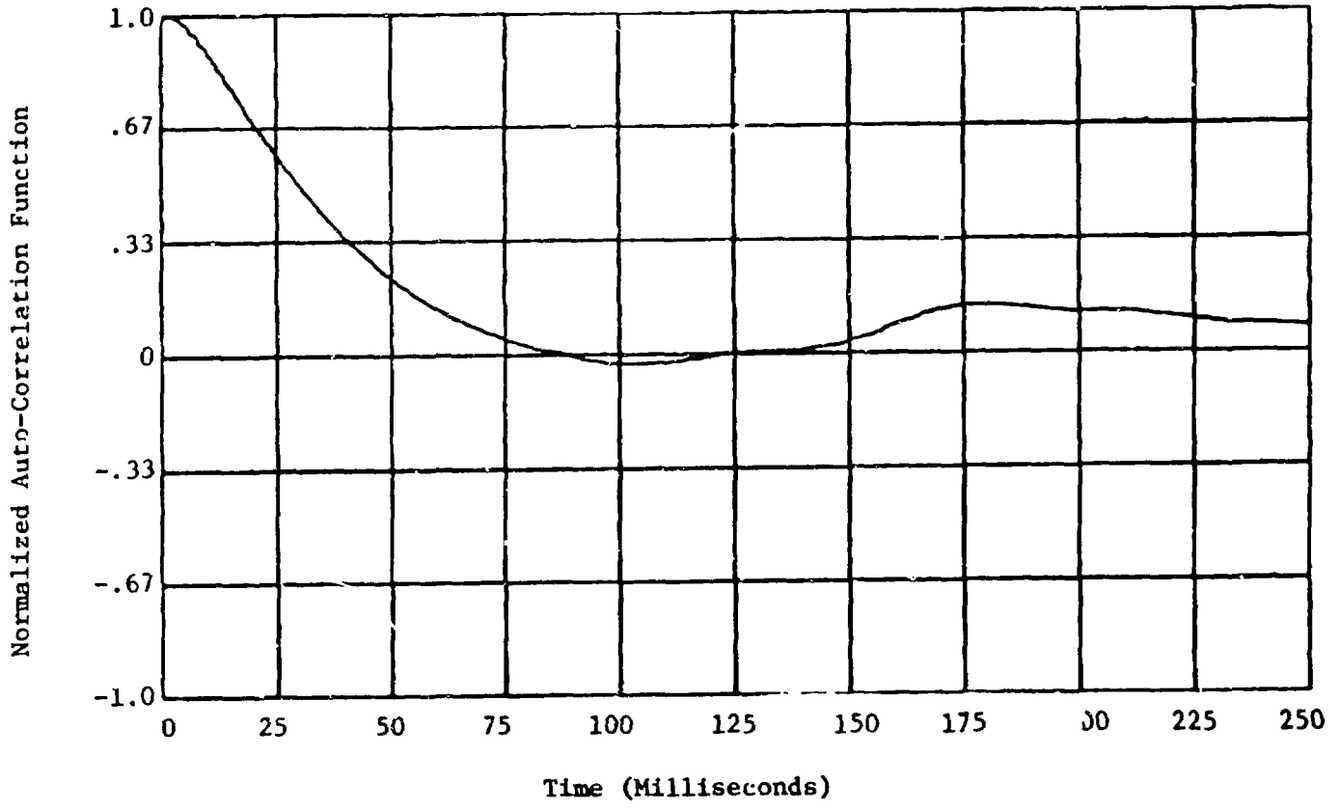

Figure B-6. Normalized auto-correlation function for the return from deciduous trees; 16.5 GHz, 5 mph windspeed.

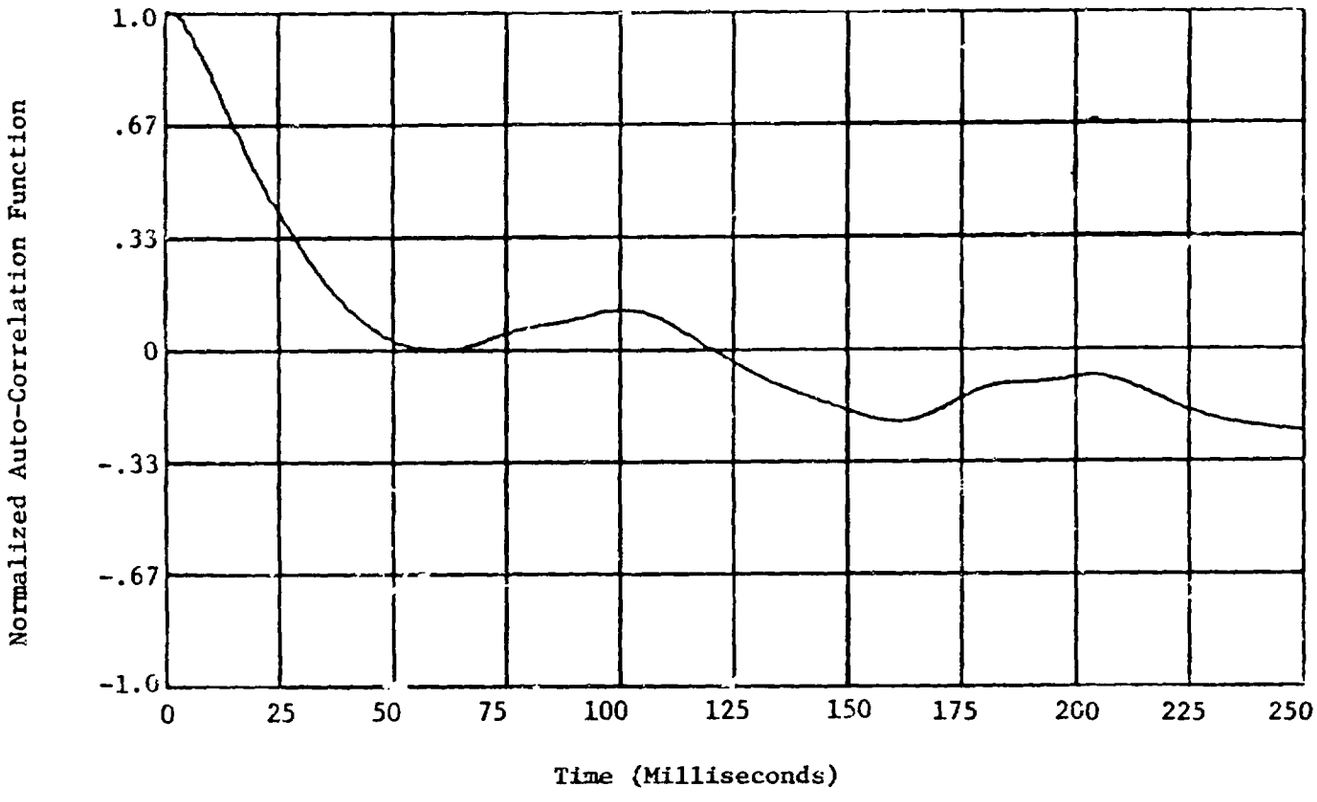

Figure B-7. Normalized auto-correlation function for the return from deciduous trees; 35 GHz, 5 mph windspeed.

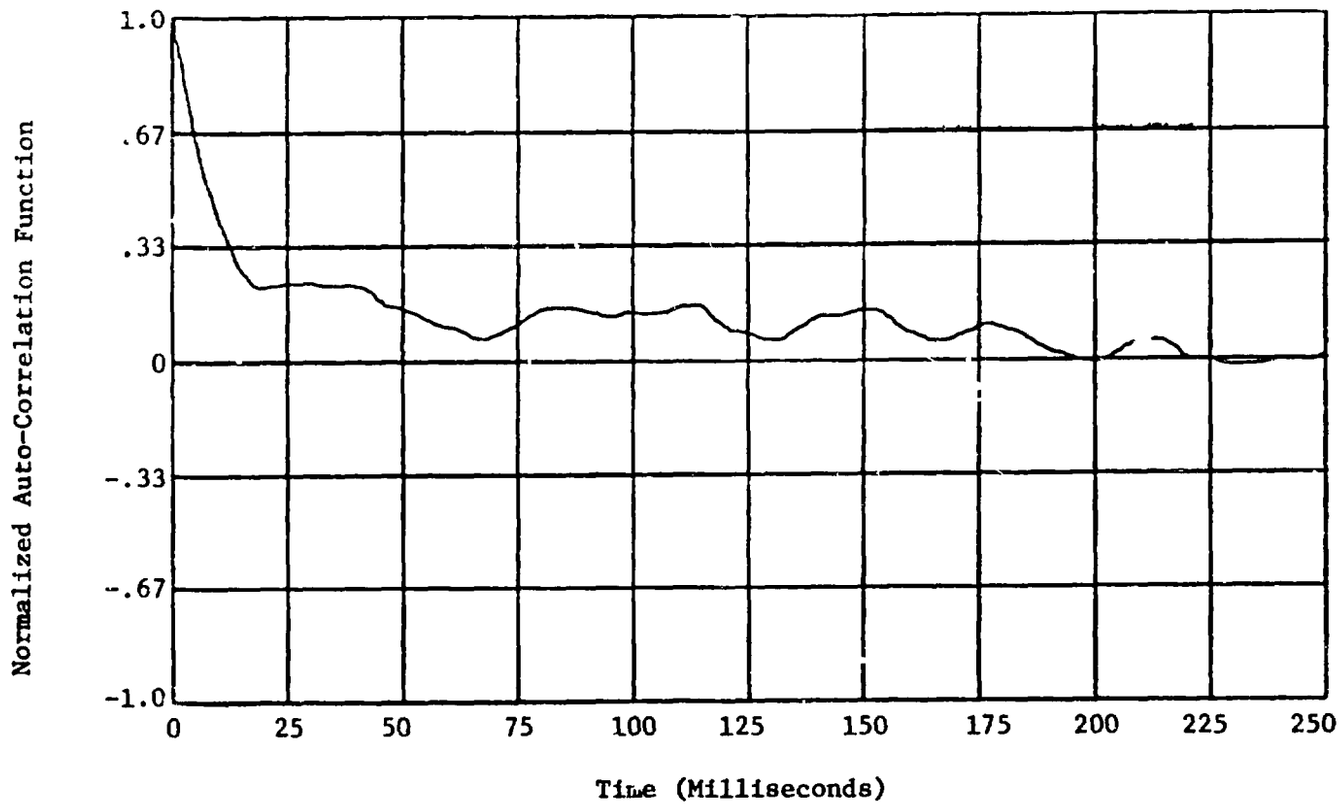

Figure B-8. Normalized auto-correlation function for the return from deciduous trees; 95 GHz, 5 mph windspeed.

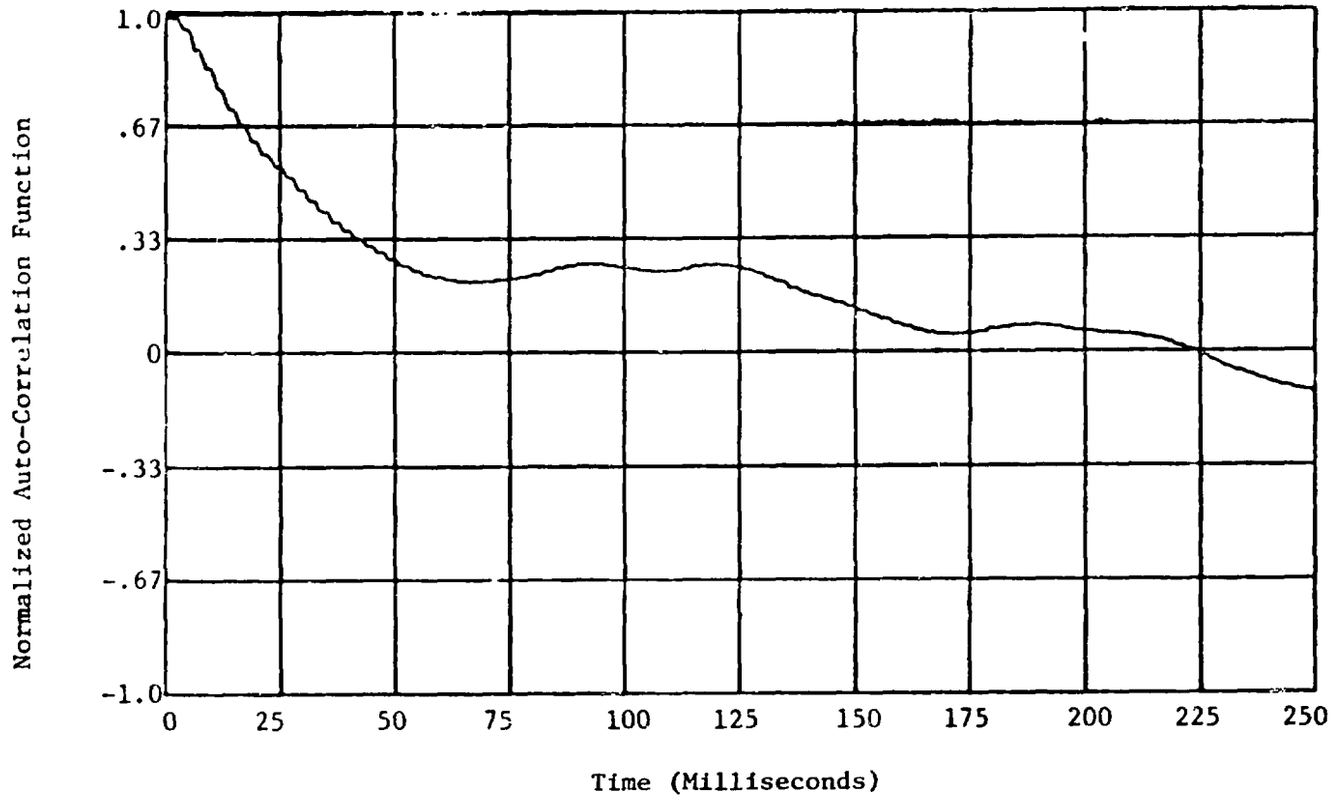

Figure B-9. Normalized auto-correlation function for the return from deciduous trees; 9.5 GHz, 8 mph windspeed.

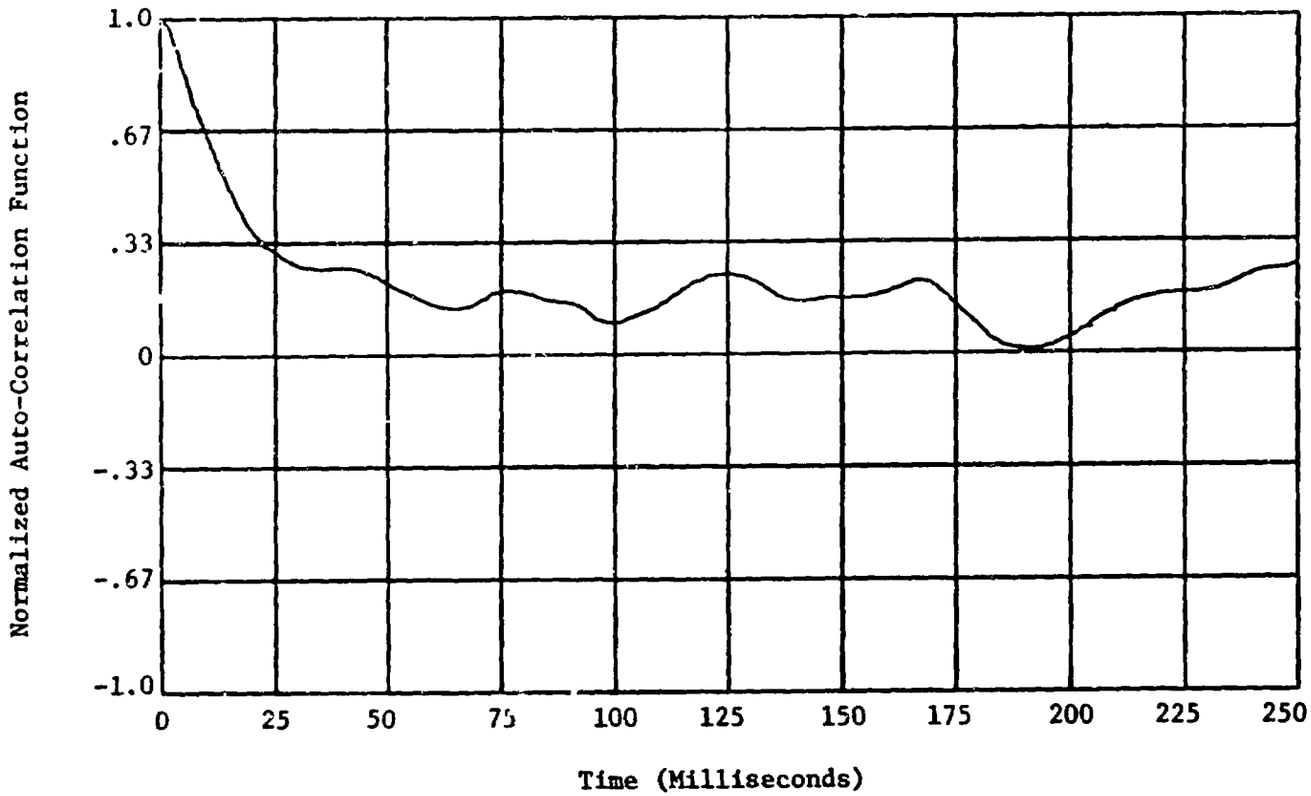

Figure B-10. Normalized auto-correlation function for the return from deciduous trees; 16.5 GHz, 8 mph windspeed.

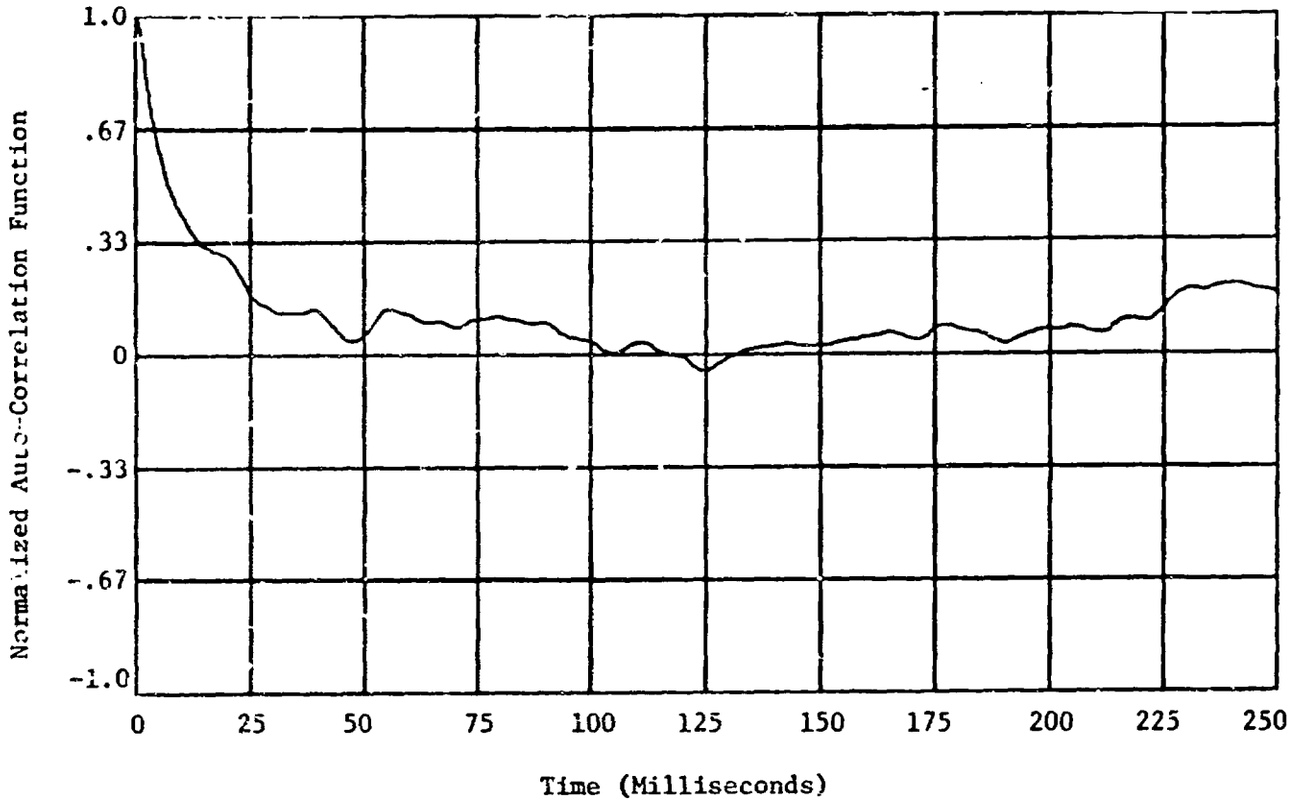

Figure B-11. Normalized auto-correlation function for the return from deciduous trees; 35 GHz, 8 mph windspeed.

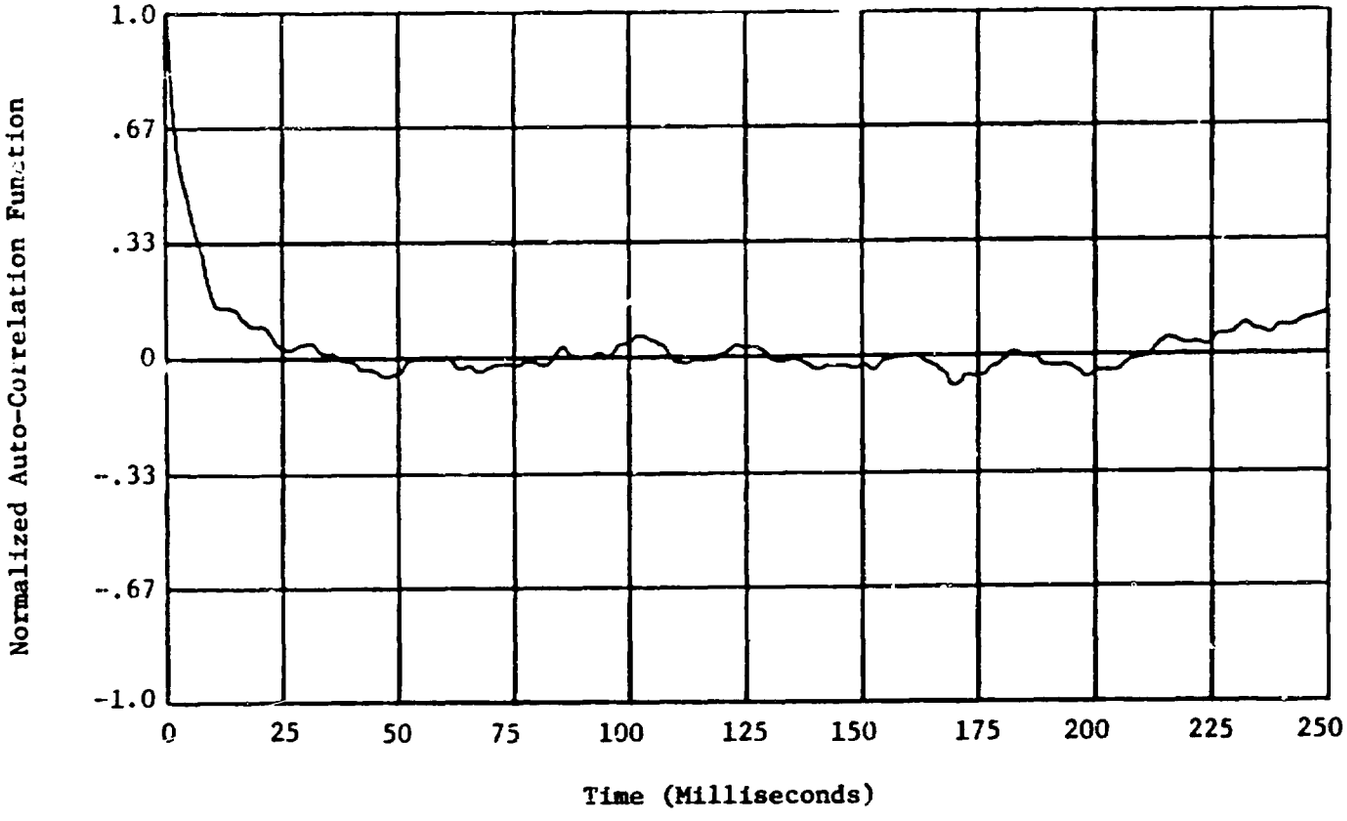

Figure B-12. Normalized auto-correlation function for the return from deciduous trees; 95 GHz, 8 mph windspeed.

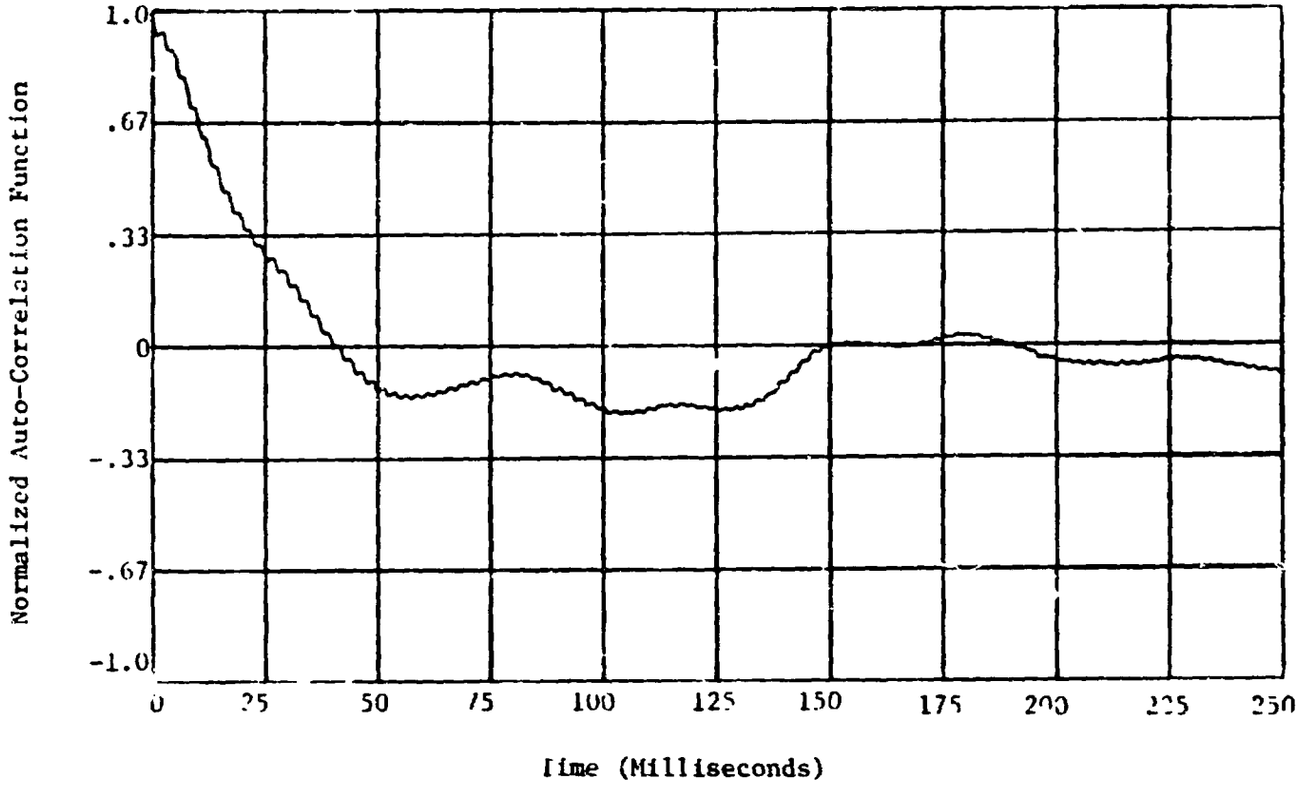

Figure B-13. Normalized auto-correlation function for the return from deciduous trees; 9.5 GHz, 10 mph windspeed.

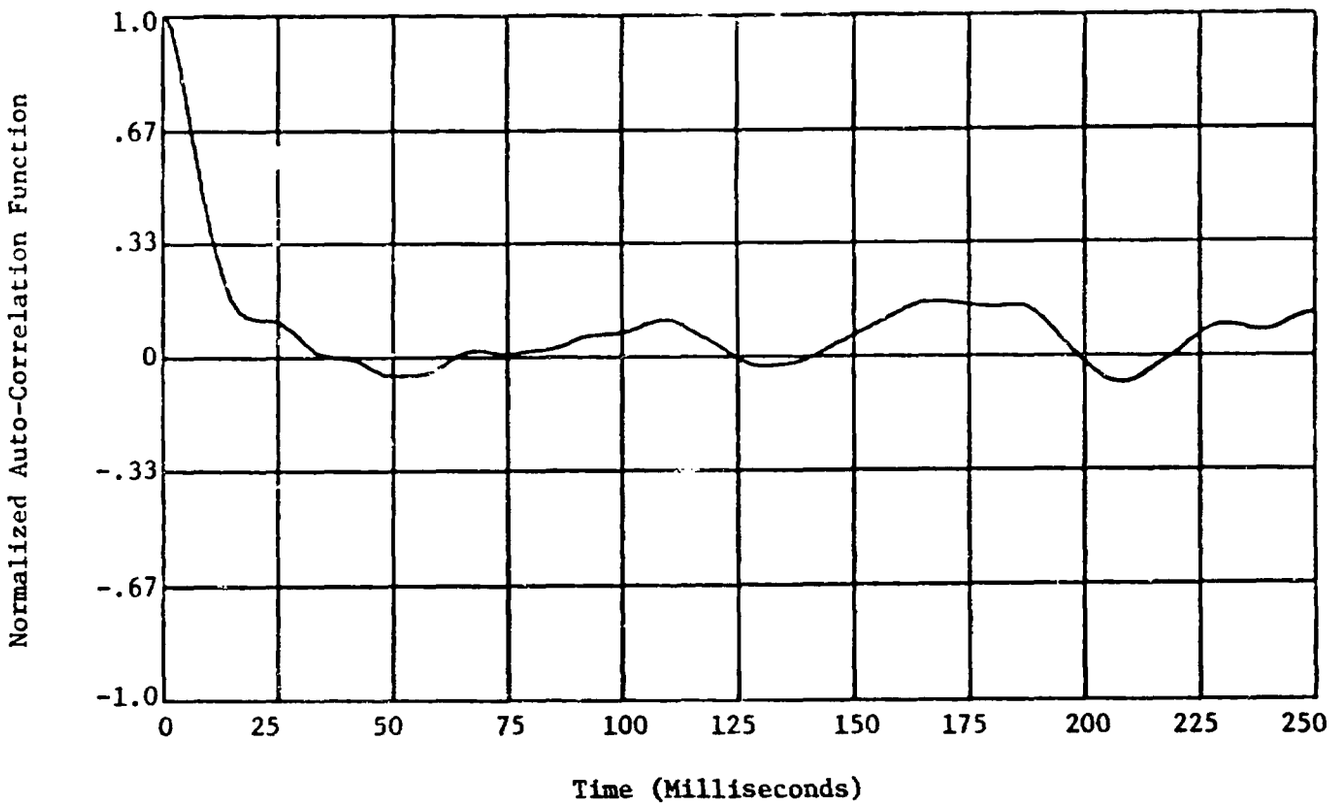

Figure B-14. Normalized auto-correlation function for the return from deciduous trees; 16.5 GHz, 10 mph windspeed.

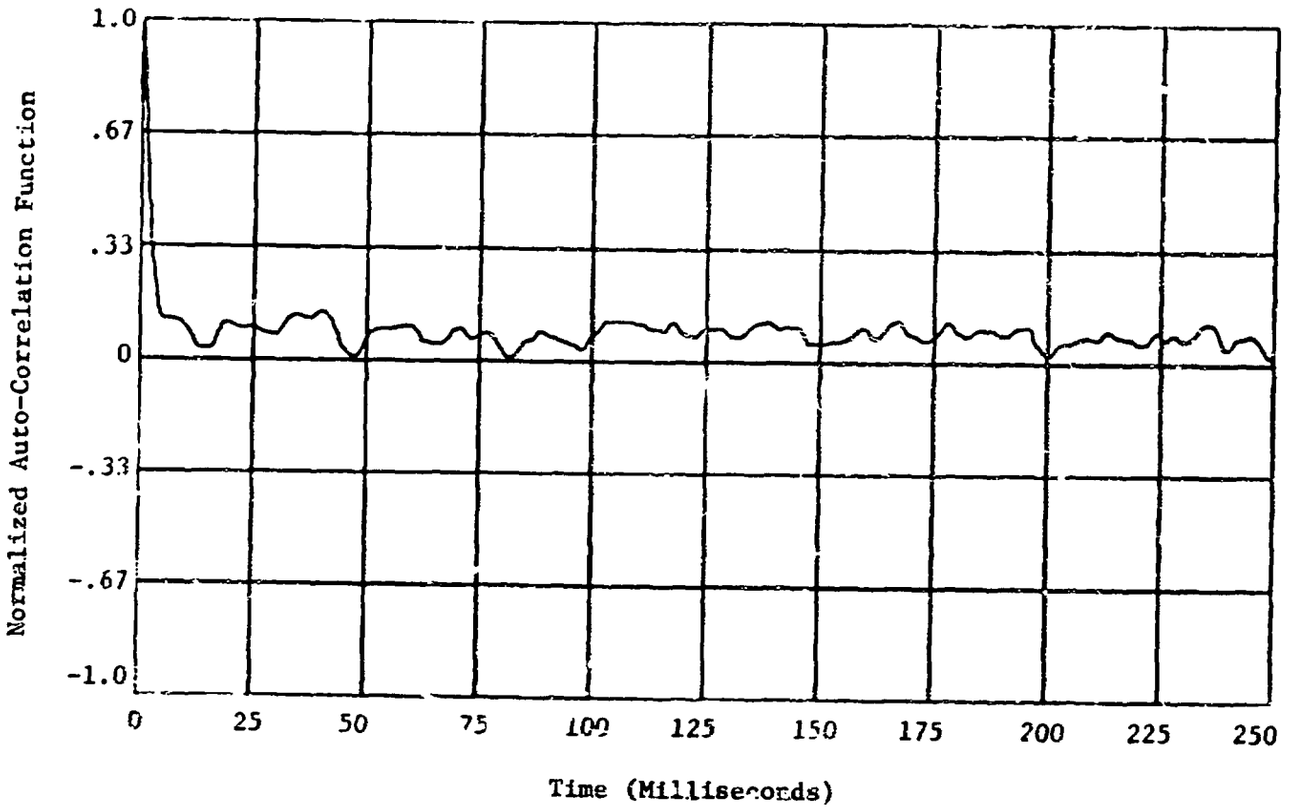

Figure B-15. Normalized auto-correlation function for the return from deciduous trees; 35 GHz, 10 mph windspeed.

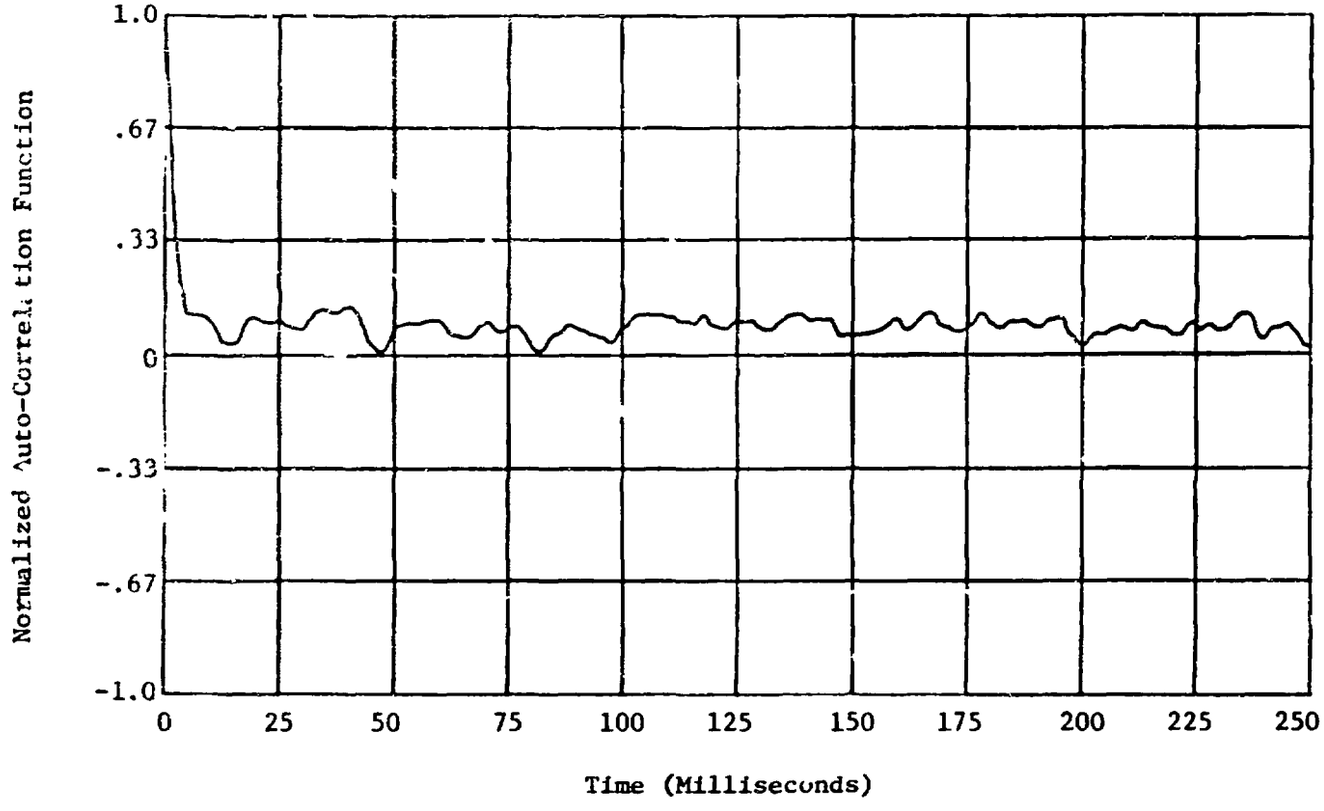

Figure 8-16. Normalized auto-correlation function for the return from deciduous trees; 95 GHz, 10 mph windspeed.